Generalized Motion Planning for Underactuated Mechanical Systems

Thesis by
Elie A. Shammas

Thesis Advisor
Howie Choset

Committee Members
Cristina Amon
Philip LeDuc
Matt Mason
Alfred A. Rizzi

In Partial Fulfillment of the Requirements
for the Degree of
Doctor of Philosophy

Carnegie Mellon University
Pittsburgh, Pennsylvania

2006

(Defended March 20, 2006)

© 2006
Elie A. Shammas
All rights Reserved

Carnegie Mellon University
Carnegie Institute of Technology

THESIS

Submitted in Partial Fulfillment of the Requirements
For the Degree of Doctor of Philosophy

TITLE

Generalized Motion Planning for Underactuated Mechanical Systems

Presented By

Elie A. Shammas

Accepted by the Department of Mechanical Engineering

Major Professor Date

Department Head Date

Approved by the College Council

Dean Date

To my dad and mom, Ayoub and Fadwa Shammas

Abstract

For mechanical systems, it is straight forward to compute the dynamic equations of motion which govern the evolution of the systems' configuration variables as the system is subjected to set of input forces. Solving the "reverse" problem or the motion planning problem, that is, finding the input forces that cause the system variables to move from a start to a goal configuration is a more challenging problem.

Researchers have successfully tackles particular flavors of this challenging problem. In fact, trajectory tracking controllers were defined in a coordinate free way for fully actuated mechanical systems, that is, systems that have as many input forces as the systems' degrees of freedom. On the other hand, motion planning for underactuated mechanical systems is still an ongoing research. In this dissertation, we approach this specific problem and present our preliminary results.

Motion planning for underactuated mechanical systems is particularly hard due to the nonlinearity of equations of motion and additionally due to their complex expressions. We express the same governing equations of motion in a simplified and reduced form for a large family of locomotion systems. Utilizing these reduced forms we develop intuitive evaluation tools that relate the evolution of the unactuated degrees of freedom to the actuated ones. Then, we utilize these evaluation tools to actually generate gaits that locomote a large class of mechanical systems along a desired direction. In other words, we design curves in the actuated subspace of the configuration space that will cause a desired change in unactuated degrees of freedom.

Acknowledgement

First and foremost, I would like to thank my official and non-official advisors, Howie Choset and Alfred Rizzi. This work would have never seen the light if it was not for both of these excellent scholars. Howie has sculpted me into a better learner and communicator while Al chiseled me into a better applied mathematician. Often these roles were interchanged, however, the respective roles of my advisors were always complementary, supportive, and enlightening.

During my stay at Carnegie Mellon, I was always fascinated by the collaboration between graduate students and professors. Through this, I had chance to work with and learn from several of many amazing professors. In particular, I would like to thank Matt Mason, whose vision and ability to always see the big picture has always been an inspiration to me. I also would like to thank William Hrusa in the Mathematics department who through his teaching style helped me develop an interest and appreciation of mathematics. My thanks also extends to many other professors in the Robotics Institute who always genuinely showed interest in my work and never failed to give me motivation and technical support. I would like to extend my thanks to the rest of advisory committee members, Cristina Amon, Philip LeDuc, whose feedback and input had improved my dissertation.

My graduate school experience would have never been complete without the help and support of all my lab member and friends. Especially, I would like to thank, in no particular order, Giacomo Zambelli, Ercan Acar, Ji Yeong Lee, Prasad Atkar, David Conner, Sarjoun Skaff, Ravi Balasubramanian, Klaus Schmidt, Alon Wolf, Amir Degani, and Peggy Martin. I also would like to thank the army of undergraduates that worked in the lab throughout the years.

Finally, I would like to thank my family back in Lebanon. My parents, Ayoub and Fadwa, thanks for your endless support and unconditional love. My three sisters, Mireille, Cosette, and Manal, thanks for being there for me and putting a smile on my face whenever times were rough. I would like to thank the rest of my family for letting me know the

feeling of a belonging, and special thanks goes to my grandmother Hanneh and my aunts Zaher and Therese.

Last but never least, I would like to thank my wife Magguie. She has always believed in me and supported me all through graduate school. She fills my day to day life with joy and the will to keep going. To Magguie I say, thanks and I love you.

Contents

List of Figures

List of Tables

List of Theorems.

List of Assumptions.

List of Definitions.

Chapter 1

Introduction

Locomotion is all around us, be it in animals running, swimming, flying, slithering, etc. or be it in us humans walking, running, or even astronauts reorienting themselves in space. Locomotion is such a broad term, however, one can simply think about it as an organism or a robot actively being able to change its position or orientation in the ambient space. Early locomotion ideas in the robotics field were along to main streams, legged locomotion which is biologically inspired and wheeled locomotion. Recently, robotics researchers addressed new types of locomotion such as underwater locomotion and slithering of snake-like robots. In this dissertation we present a unifying understanding of the locomotion problem such that it governs several seemingly different locomotion modes. Specifically, we seek to unify the analysis of locomotion to understand systems ranging from slithering of snake-like robots to cats orienting their bodies in mid-air, and additionally novel locomoting robots that do not have any biological counterparts.

While legged and wheeled locomotion can be thought of as "direct" modes of locomotion where the legs or wheel directly apply traction forces to the environment, snakes slithering and cats reorienting their bodies in flight seem to be un-intuitive due to what believe is their "indirect" modes of locomotion. Nonetheless, what is common to the latter modes of locomotion is the fact that position or orientation change is accomplished through repetitive body-shape changes. In fact, studying how internal shape motions affect the position and orientation of a mechanical system constitutes a main research body in robotic locomotion. This dissertation addresses this very problem but in a different approach.

As in the case of legged locomotion, where researchers analyzed how real legged animals locomote, analysis of locomoting snake-like robots had its bio-mimetic roots. For legged locomotion, understanding how animals locomote was documented by numerous

photographs by Muybridge in [37]. On the other hand, work done by Kumar and Waldron presents a survey of legged robotic locomotion in [29]. More legged locomotion can be found in [44, 53]. As for slithering snake locomotion, Hirose took a bio-mimetic approach, where here observed how real snakes locomote in [20]. In fact, Hirose was able to extract the geometric structure which the body of the snake cycles through as it slithers on the ground. He represented this geometric structure by what he terms as the *serponiod* curve which is dictated by the assumption that the forces in the contraction muscles along the body of the snake vary in a smooth sinusoidal transition as the snake undulates. These muscle forces can then be related to the curvature along the body length of the snake which defines the shape of the serponoid curve.

Hirose, then successfully demonstrated robotic locomotion on snake-like mechanical systems that have passive wheels on the bottom. These wheels provide high frictional forces against lateral motion while providing almost null friction along the forward and backward directions. In fact, Hirose replaced the wheels by mini-iceskates and demonstrated a snake-like robot undulating on an ice sheet. Thus, he performed robotic slithering of snake robot by forcing these structures to track various serpenoid curves whose parameters were empirically derived. As a side note, not only did Hirose study snake locomotion but also developed novel robotic joint designs that allowed the construction of snake-like robots [21]. We also have done extensive work in robotic joint designs suitable for snake-like robots [12, 48–50]. Actually, we improved upon robotic joint designs by increasing the joint's range of motion, strengthening the joint's resistive torque, and minimizing the joint's overall volume and weight.

Even though we designed our spatial snake-like robot with three-dimensional climbing in mind as an application, we had to consider much simpler mechanical systems to develop our theory. Similarly, Walsh, and Sastray, among other researchers who were motivated by how a cat changes its orientation in mid-air, considered and analyzed a simpler planar three link snake robot floating in space in [57]. Limiting the interlink angles to sinusoidal inputs and by varying the angle about which the outer two links oscillate, Walsh and Sastry were able to propose inputs, or gaits, that changed the global orientation of this planar robot after the completion of a cycle in the shape of the robot, that is, the robot retains its original shape after each cycle but its global orientation would have changed.

Even though we presented the above two locomotion modes, snake slithering and mid-air orientation as being similar, that is, locomotion is attained by the effect of internal body changes on the position and orientation of the robot, these two locomotion modes are

fundamentally different. In that, we mean that the laws of physics governing the motion of either mode are different. In the case of slithering snakes, the assumption that the body of the snake is not allowed to slip sideways completely specify the snakes' motion, while in the case of cat's the mid-air orientation change, the fact that angular momentum is being conserved is indeed what governs the motion of the falling cat and the above planar three link snake. Moreover, there are mechanical systems where none of the above governing laws exclusively specify the systems' motion, nonetheless, as we shall explain in this dissertation these two laws specify the systems' motion in a complementary way. Thus, one expects that the first governing laws, or what is referred to as non-holonomic constraints are, at a certain level, equivalent to momentum conservation.

In the previous paragraph, we casually mentioned terms like mechanical systems, non-holonomic constraint, and momentum conservation. Even though we define these terms later in the dissertation, we are introducing them here to help us formulate a bigger picture of the locomotion problem. The mechanical systems we are analyzing in this thesis, were first defined by Smale in [51, 52] for which a quantity termed the *Lagrangian* is defined as the difference between the systems' kinetic and potential energy. The configuration variables of such systems evolve in such a way that the integral of the Lagrangian is minimized according to the *principal of least action*, thus defining a variational problem. Recall that the *configuration variables* are a smallest set of numbers required to completely specify the location of each mass particle of the robot. Thus, for multi-rigid-bodied robot, configuration variables are naturally decomposed into position and shape variables. Non-holonomic constraints or non-integrable velocity constraints as well as external forces are easily incorporated into the above variational problem that depicts the evolution of a mechanical system.

Mechanics defines the analysis of motion of objects due to external fores acting on them. The variational problem we defined above is the Lagrangian formulation for mechanical systems as presented in classical mechanics by Goldstein in [17]. Using this formulation, it is straightforward to compute the dynamic equations of motion that govern the evolution of the systems' configuration variables. In fact, a solution to the above system of differential equation, a curve in the system's configuration space, is nothing but a minimized of the variational problem we introduced earlier. However, recent research in mechanics done mainly by Marsden and coworkers in [22, 32, 33] utilized geometric features of the configuration space of mechanical systems as well as symmetries in the laws of physics to simplify and reduce the dynamic equations of motion. This reduction proved to be quite

useful in approaching the motion planning problem.

Deriving the dynamic equations of motion can be thought of as the "forward" problem whose solution predicts how the configuration variables of a mechanical system evolve in time for a given set of input forces acting on the system. Motion planning, can be though of as the "reverse" problem, that is, finding a set of inputs forces that steer the configuration variables from a start to a goal configuration. In general the dynamic equations of motion are second order non-linear differential equations which render solving the reverse problem quite challenging. Thus one can clearly see the utility of simplifying these equations of motion which is exactly what Marsden *et al.* presented in there geometric mechanics approach to locomotion research [22, 32, 33].

Two main concepts allow for the simplification of the differential equations of motion of mechanical systems. First is the fact that the configuration space of mechanical systems has a *trivial principal fiber bundle structure* which can be decomposed into two subspaces: the base space which describes the internal shape changes of the system and the fiber space that represents the system's position and orientation with respect to a fixed inertial frame. This special structure of the configuration space endows mechanical systems with a special action, or map, due to the Lie group structure of their fiber space. Additionally, due to *symmetry* in the laws of physics, the placement of the inertial frame is redundant, thus, another order of simplification is done by representing the entire dynamic in a body-attached coordinate frame. Symmetry is then defined such that specific terms such as, kinetic energy and non-holonomic constraints, are invariant with respect to these actions. Both concepts, the structure of the configuration space as well as symmetry of the laws of physics, allow us to study the effect of body shape changes to position change by analyzing a first order differential equation usually termed as a *reconstruction equation*. The reader ir referred to work done by Bloch and Lewis [5, 30] for deeper explanation of reduction theory for mechanical systems.

Moreover, the same two concepts allow us to rewrite original equations of motion in reduced and decoupled forms. Specifically, the evolution of the base, or shape, variables is represented by a set of second order differential equation which are independent of the position and orientation of the robot, that is, the fiber variables. Additionally, the original second order differential equations describing the evolution of the fiber variables are reduced to be represented by a first order differential equation. This last set of differential equations is referred to as the *momentum evolution equations* since they are expressed in terms what is referred to as the generalized momentum rather than the original fiber

variables. In this dissertation we utilize both the reconstruction and momentum evolution equations to solve the gait generation for underactuated mechanical systems, thus solving a particular flavor of the motion planning problem. In other words, we will design curves in the actuated base space which will cause a desired motion in the unactuated fiber space.

We are not the first to utilize modern mechanics and its geometric intuition to address the locomotion problem. Ostrowski *et al.* in [40–43] deserve credit for applying geometric mechanics to mechanical system and utilizing the reduced forms of the equations of motion to actually approach the motion planning problem. Utilizing both the reconstruction and momentum evolution equations, Ostrowski *et al.* were able to represent the dynamic equations of motion as a linear affine control system. Then by taking recourse to controls theory and limiting the input forces to be sinusoidal, they were able to specify the frequencies of these sinusoidal inputs. In fact, these frequencies corresponded to the order of the non-trivial Lie bracket motions of the drift and control vector fields of the above control system. Thus, but studying the controllability of mechanical systems, Ostrowski specified the gait frequencies of the input forces, however, other gait parameters were empirically derived. Nonetheless, Ostrowski was successful in generating gaits for numerous mechanical system including the robotic snake robots analyzed by Hirose and novel mechanical systems like the Snakeboard©. Moreover, we would like to mention Chitta *et al.* who developed several unconventional locomoting robots, such as the rollerblader and the robo-trikke, [11,45] for which they used Ostrowski's techniques to generate sinusoidal gaits for these novel locomoting robots.

Another related work was done by Tsakiris *et al.* where they studied kinematic chains which they refer to as G-snakes in [26, 56]. These are snake-like structure with passive wheels on the bottom that are similar to the snake robots that Hirose built. Moreover, the shape actuation of the snake robot was done using parallel mechanism structure. They referred to these robots as "Variable Geometry Truss Assembly" in [25]. Tsakiris *et al.* intrigued by the geometric structure of the configuration space, worked on representing the fiber space using different group structures and computed their respective actions and lifted actions. Finally, they generated the gaits for several variants of the G-snakes where they associated the special Euclidean group to the system's fiber space in [27, 28, 56]. Tsakiris *et al.* applied his theory by generating gaits for the roller racer in [56] by limiting themselves to sinusoidal gaits. This robot is similar to the robot-Trikke studied by Chitta *et al.* which we are also analyzing in this dissertation.

Bullo *et al.* also utilized geometric mechanics to address two flavors of the motion

planning problem. The first approach address fully actuated mechanical systems, that is, systems that have as many input forces as the degrees of freedom of the robot. In fact, Bullo *et al.* used the geometric structure of the configuration space to devise better controllers for fully actuated systems [7, 9]. Their key idea was to define state errors in a coordinate free way to make their approach generalizable. Thus, using these controllers, they solved the motion planning problem by tracking a trajectory in the configuration space of a fully actuated mechanical system.

Additionally, Bullo and Lewis analyzed the motion planning problem for underactuated mechanical systems [8]. Their main contribution is in actually defining a kinematic reduction for simple mechanical systems, or in other words, reducing the dynamics of a system so that it can be represented as a kinematic system. Recall that kinematic systems are systems whose first derivative of the state vector is a linear combination of the control inputs. Then they study the controllability of these reduced systems and for certain examples, they were able to generate gaits for these systems. Bullo and Lynch *et al.* designed gaits by devising decoupling vector fields on the base space whose integral curves are candidate gaits. Along these curves, the system acts like a kinematic system, thus computing the position change is done by an integration step. Bullo *et al.* also concatenated these integral curves to plan motion between two points in the fiber space of underactuated systems like the Snakeboard©. For further reading about similar works, the reader is referred to [5, 24, 32, 35, 41, 42].

Finally, Mukherjee and Nakamura *et al.* in [34, 38, 39] solved the motion planning problem for the rolling disk problem. Utilizing Stokes' theorem, they related position change of the rolling disk to a volume integral. Then by limiting themselves to rectangular inputs, they were able to compute closed form solutions of these volume integrals and hence for changing the position of the rolling disk . We independently developed a similar but more general approach and generated gaits for two general types of mechanical systems: purely mechanical systems in [47] which is associated with the cat mid-air orientation change problem, and principally kinematic systems in [46] which is associated with the slithering of hyper-redundant robots. Note that, the rolling disk is a principally kinematic system. Finally, it is worth mentioning that there has been other prior work that directly relates to this approach by Yamada [58], where he was concerned with purely mechanical systems and generated gaits only for space robots.

In this thesis, we address the motion planning problem for several types of underactuated mechanical systems. We are particulary interested in under actuation since on one

hand it simplifies the mechanical design of robots by reducing the number of actuators and reducing the entire weight of the system. On the other hand, under actuation can be thought of as a backup plan where fully actuated robot is still able to locomote even though some of its actuators have failed. Thus, in this thesis, we approach the motion planning problem, by generating gaits for multi-bodied mechanical systems by specifying how the internal degrees of freedom should behave in such a way to produce a desired position change of the entire mechanical system. In other words, we prescribe changes in the actuated degrees of freedom of a mechanical system to control the rest of its unactuated degrees of freedom.

1.1 Technical Introduction

The types of mechanical systems we are considering in this dissertation belong to a spectrum. At one end of the spectrum are mechanical systems whose motion is governed solely by the conservation of momentum laws, while the other end represents systems whose motion is governed solely by the existence of the right number of non-holonomic velocity constraints. The two ends of the spectrum represent systems that are reminiscent of the cats orienting in mid-air and snakes slithering motivational problem we described earlier. Between these two extremes are mechanical systems whose motion is governed by both momentum conservation laws as well as non-holonomic constraints. We label these three types of systems we just described as *purely mechanical*, *principally kinematic*, and *mixed* systems, respectively.

Hence, the goal of this dissertation is to unify the gait generation technique for this entire spectrum of types of mechanical systems. More specifically, we utilize the configuration space's geometric structure, the Lagrangian of the mechanical system, and the non-holonomic set of velocity constraints acting on the mechanical system to formulate a generalized *reconstruction* equation for a generalized type of mechanical system that represents the entire above spectrum. Then, taking recourse to Lagrangian dynamics and geometric mechanics of locomotion, we utilize translational symmetries to rewrite the reconstruction equation and relate position change expressed in body coordinates to two decoupled quantities: the *geometric* and *dynamic* phase shift. We intuitively evaluate the geometric phase shift by relating it to the volume enclosed by a set of well-defined *height* functions. As for the dynamic phase shift, we introduce a new *scaled momentum* variable that simplifies the *momentum evolution* equation, which in turn simplifies the evaluation

of the dynamic phase shift by relating it to a definite integral of a product of another well-defined set of *gamma* functions and the scaled momentum variable.

Utilizing these intuitive evaluation tools we define a partition on the space of allowable gaits which allows us to propose gaits for which either or both of the phase shifts are non-zero, thus effectively proposing gaits that move the mechanical system along a desired direction. We apply our gait generation techniques to several well-known and some novel robotic systems that span the entire spectrum of types of mechanical systems we are considering in this thesis. For each of these example systems, we present a procedure for computing the reconstruction as well as the momentum evolution equations. Then we present our motion planning analysis to generate gaits that move these example systems along a specified direction. Moreover, we demonstrate our results on several robotic systems that were specifically constructed for this purpose.

1.2 Layout

This thesis builds upon prior work and in many cases we re-derived several results in what we think is a more direct and simpler way. This thesis is closely related to work done by Ostrowski in [40].

In Chapter 2 we introduce several mathematical structures like groups and manifolds. We also define Lie groups and their respective actions on configuration space and lifted action on tangent spaces. We define principal fiber bundles and the principal connection which we use to decompose the tangent space into a vertical and horizontal sub-spaces. Finally, we recall some results for calculus of variations and exterior algebra.

In Chapter 3 we utilize the fiber bundle structure to locally compute the principal connection. Then we introduce the locked inertia tensor and the momentum map to define a special principal connection, the *mechanical connection*, associated with mechanical systems. Computing the mechanical connection locally and expressing it in body coordinates allows us to compute the reconstruction equation which relates fiber velocities expressed in body coordinates to two decoupled quantities. The first of which is a function of the base variables and the second is a function of the base variables and momentum variables which in turn is described by a first order differential equation on the base space. Then, we take recourse to Lagrangian dynamics and compute the equations of motion of mechanical systems. Finally, we utilize symmetries in the system to reduce the equations of motion to a set of smaller order differential equations. We conclude this chapter by presenting

the reduced equations of motion for mechanical systems subject to a set of non-holonomic velocity constraints.

We start Chapter 4 by defining a generalized type of mechanical systems that represents all the mechanical systems we are considering in this dissertation. Then, by imposing certain conditions we introduce several sub-types of mechanical system, for which we will eventually generate gaits. We also compute the reconstruction equations for all the sub-types of mechanical systems.

In Chapter 5 we derive the momentum evolution equations and compute their special forms when evaluated at the fiber space identity element. Moreover, here we present one of the main assumptions of this thesis, that is, we limit ourselves to mechanical systems that have at most one generalized momentum variable. With this assumption we introduce a new scaled momentum variable which allows us to further simplify both the momentum evolution equation as well as the reconstruction equations which were presented in the previous chapter.

We present our gait generation techniques in Chapter 6. Here we substitute the scaled momentum into the reconstruction equations which we then integrate to solve for the position change represented in body coordinates. This allows us to relate this position change to two decoupled integrals which respectively compute the geometric and dynamic phase shifts. Then, we present evaluation tools to compute these two shifts. Specifically, we propose gaits that ensure that the values of these shifts are non-zero along a specified fiber direction. We equate the value of the geometric phase shift to a double integral which evaluates the volume under the graph of what we call *height functions* and is bounded by the proposed gait. We evaluate the dynamic phase shift by analyzing both another set of functions which we refer to as *gamma functions* as well as the evolution of the scaled momentum variable. Finally, using these evaluation tools, we synthesize gaits for all the sub-types of mechanical systems we are considering in this thesis.

In Chapter 7 we apply our gait generation techniques to six mechanical systems. We ensure that the examples span all the types of mechanical systems we are considering in this dissertation. Moreover, for all the examples, we present a procedure for, starting with the configuration space structure, the Lagrangian, and the non-holonomic constraints, computing the reconstruction and momentum evolution equations expressed in body coordinates in terms of the scaled momentum. Using these two equations, we extract the height and gamma functions for each system, which we then analyze and eventually utilize to generate gaits. Finally, we simulate the proposed gaits and verify that they are moving

the mechanical system along a specified direction. We also ensure that we include several robotic systems that were analyzed in the literature; additionally, we introduce a couple of novel mechanical systems. The most interesting of these novel systems is what we term the variable inertia snakeboard. This novel system is a generalization of the original snakeboard where we eliminate all the simplifications that were assumed in the prior work in order to verify the generality and applicability of our gait generation approach.

In Chapter 8, we apply our gait generation technique to an actual variable inertia snakeboard which was constructed specifically for this purpose. We implement several of our proposed gaits and compare the actual motion of the system to our simulated results. Moreover, in this chapter we present the "wave board" (or the "essboard") which is a special skate board where the rider propels himself forward by mimicking a wave surfing action. What is interesting about this toy is that its free-body diagram is almost identical to our variable inertia snakeboad.

1.3 Results and Contributions

In this dissertation we seek to generalize the motion planning problem for a large set of types of mechanical systems. Our goal is to verify that our generalized gait generation techniques apply to all the types of mechanical systems we are considering in this thesis document. We believe that our work presents the following technical results:

1. We define a general class of mechanical systems, *generalized mixed systems*, such that all other systems considered in related prior work and in this thesis are special cases of this type of mechanical systems. Moreover, we compute the reconstruction equation for this general type of mechanical systems from which we can deduce the reconstruction equations for all the other sub-systems.

2. We intuitively compute the geometric phase shift by relating it to a volume integral under the graphs of a set of well-defined height functions and bounded by the proposed gait. This intuitive evaluation allows us to devise simple rules to design curves in the base space that ensure that the geometric phase shift is non-zero along the desired fiber direction and zero along the rest of the fiber directions..

3. We introduce a new scaled momentum variable which simplifies the momentum evolution equations in such a way to allow us to easily study the sign-definiteness of this

new momentum variable. This in turn allows us to intuitively to evaluate the dynamic phase shift by analyzing another set of well-defined gamma functions. Again, using this intuitive evaluation tool, we can devise gaits that ensure that the dynamic phase shift is non-zero along the desired fiber direction and zero along the rest of the fiber directions.

4. We define a partition on the space of allowable gaits in such a way to ensure that the geometric phase shift, the dynamic phase shift, or both are non-zero. This partition does not restrict the gaits to be sinusoidal, as was the case of the prior related work.

5. We present a thorough procedure that, given the mechanical system's configuration manifold structure, its Lagrangian, and the non-holonomic constraints acting on it, allows one to compute the generalized reconstruction equation, the expression for the generalized non-holonomic momentum, and momentum evolution equation. We also recompute the generalized reconstruction and momentum evolution equations, however, expressed using the new scaled momentum variable.

6. We apply our gait generation techniques to six relatively complex examples for which the prior work approaches were inadequate. These example systems are complex in a sense that one can not make any educated guesses on how to generate gaits for them. Moreover, we introduce a novel mechanical system, the variable inertia snakeboard, which generalizes systems analyzed in the prior literature to verify the applicability and generality of our gait generation techniques.

To put the above results in perspective, next we present what we believe are the main contributions of this dissertation to the motion planning problem. We do not claim that we completely solved the motion planning problem for underactuated mechanical systems, however, we believe that our work presents a new approach for understanding and tackling the problem.

Researchers have been addressing the motion planning problem for underactuated mechanical system for more than a decade. There have been several enlightening results which our work builds upon as well as borrows from. Nonetheless, what is common to most of these results was the fact that all addresses specific parts of the motion planning problem. This was evident in the specific types of mechanical systems, or specific example systems in some cases, addressed and the restrictive types of allowable gaits. In this work we addressed both restrictions and devise analysis tools that apply to a large family of mechanical systems and eliminate the gait restrictions imposed by prior approaches.

We justify our claim that our approach is generalizable to a large family of mechanical systems by applying our techniques to numerous examples as shown in Chapter 7. Moreover, our gait generation techniques are not as restrictive as was the case in prior work approaches, that is, we do not limit our input to any particular family of gaits. In fact, for several examples we devised several gaits that were neglected by prior approaches nonetheless these gaits provided "better" solutions for the motion planning problem. Here better describes the relatively larger magnitudes of generated motion of the mechanical systems.

Another contribution of this work is that our gait generation techniques are not only intuitive but also unifying, both of which simplify approaching as well as understanding the motion planning problem. Using our approach we were able to tie and relate Ostrowski's locomotion techniques for dynamic systems with non-holonomic constraints to Bullo's techniques in locomoting kinematically reducible systems. What is interesting about our approach is the fact that not only it provides an intuitive explanation why gaits proposed in the prior work actually locomoted the mechanical system but also our approach unified why gaits from seemingly different approaches work. In fact, our analysis relates the prior works' proposed gaits by partitioning the space of allowable gaits into three distinct families. The motion due to a gait belonging to these families is exclusively related to either the geometric, dynamic, or both phase shifts associated with the proposed gait.

At a higher level, we believe that our approach will lead to a natural and efficient parametrization of the motion planning problem for a large class of mechanical systems. To be more specific, utilizing our work, we hope to develop evaluation tools whose analysis is geared towards the gait generation problem. One contribution of our work is developing simple intuitive gait evaluation tools. Not only do simpler gait evaluation tools make it easier to generate gaits, but also help form a better understanding of the locomotion problem. Better understanding, leads to better formulation of the problem and direct analysis of the gait parameters that matter. We also believe that better understanding of the locomotion problem compounded with a better parametrization will certainly simplify the problem of *optimal* gait generation, which is an even more challenging problem.

Chapter 2

Mathematical Preliminaries

In this chapter we introduce several terms and definitions that will be used throughout this thesis. This section is meant to refresh the readers about some terms and does not constitute either a reference or a tutorial. We will cite several references as we go along which should be useful but at the same time we give lots of examples to make the terms easier to grasp. The examples presented in this chapter will be tailored to provide intuition to make the reader more comfortable with the material presented in the rest of the thesis.

The goal of this chapter it to highlight the special structure of the *configuration space* of simple mechanical systems, that is, the space that represents the degrees of freedom of these systems. We introduce all the tools that eventually allow us to rigorously define this *principal fiber bundle* structure. Additionally, we define the *tangent spaces* associated with these configuration spaces which represent the velocities of the system. We also define several maps associated with the configuration space and its tangent space. Namely, we define the *action* and *lifted action* maps which utilize the *Lie group* structure of the *fiber space*, a sub-space of the configuration space, to map configurations and velocities, respectively. Finally, we introduce several other tools and results that we shall use later in this dissertation.

2.1 Groups and Matrix Groups

We start by recalling important kinds of groups and their properties. For a more involved reading, the reader is referred to [2,23,36]. We start with the definition of a group structure.

Definition 1 (Group) A group, $(G, *)$, is a set G together with a map $*$ taking $G \times G \rightarrow G$ that has following four properties:

1. **Closure:** Given g_1,$g_2 \in G$, then we have $g_1 * g_2 \in G$.

2. **Associativity**: Given g_1,g_2 and $g_3 \in G$, then we have $(g_1 * g_2) * g_3 = g_1 * (g_2 * g_3)$.

3. **Identity**: There should exist a unique element $e \in G$ such that $e * g = g * e = g$.

4. **Inverse**: For each $g \in G$ there exists unique element $g^{-1} \in G$ such that $g * g^{-1} = g^{-1} * g = e$.

An *Abelian* group is a group whose associated map is commutative, that is, for g_1,$g_2 \in G$ then we have $g_1 * g_2 = g_2 * g_1$. For example the real numbers with the addition operation, $(\mathbb{R}, +)$, form an Abelian group. Moreover, new groups can be formed by taking the Cartesian product of existing groups. The product of groups G and H forms a group which is usually denoted by $G \times H$.

An important example of groups are matrix groups where the elements of the set G are matrices. More specifically, for $n \in \mathbb{N}$, the set or natural numbers, let G be the set of $n \times n$ invertible matrices with real entries, that is, $G^i_j \in \mathbb{R}^1$. Then the set G together with the operation matrix multiplication form a group. Such a group is referred to as the *general linear group* which is usually denoted by $GL(n, \mathbb{R})$. Finally, note that, matrix groups are not Abelian since matrix multiplication in not commutative.

Next, we introduce several important matrix groups that are used to represent rigid body motions. We start with the groups of rigid rotation $SO(n)$, the *special orthogonal* groups. The set of elements for $SO(n)$ is given by

$$SO(n) = \{R \in \mathbb{R}^{n \times n} : RR^T = I^{n \times n}, \det R = +1\},$$

where $I^{n \times n}$ is the $n \times n$ identity matrix. For $n = 2$, the elements of $SO(2)$ have the following form:

$$SO(2) = \left\{ \begin{pmatrix} \cos\theta & -\sin\theta \\ \sin\theta & \cos\theta \end{pmatrix} : \theta \in \mathbb{R} \right\}.$$

Another important group is the group of rigid translations and rotations in an n-dimensional space. This group is referred to as the *special Euclidean* group and is usually denoted by $SE(n)$. The set on which this group is defined is given by

[1]Throughout this thesis document, G^i_j denotes the i^{th} row and j^{th} column of the matrix G.

$$SE(n) = \left\{ \left(\begin{array}{c|c} R^{n\times n} & p^{n\times 1} \\ \hline 0^{1\times n} & 1 \end{array} \right) : p \in \mathbb{R}^n, R^{n\times n} \in SO(n) \right\} = \mathbb{R}^n \times SO(n).$$

For $n = 2$, the group $SE(2)$ is used to represent the configuration of a rigid body in the plane.

2.2 Lie Groups and Group Actions

Having defined group structures, now we extend our definitions to include Lie groups. To define Lie groups we need introduce additional structures such as manifolds. Loosely speaking, a manifold is a topological space that locally looks like $\mathbb{R}^n$. Thus we need to define what is a topological space first.

Definition 2 (Topological space) A set X with a collection of open subsets T form a topological space if the following propoerties hold:

1. The empty set is in T
2. The entire set X is in T
3. The intersection of a finite number of sets in T is also in T
4. The union of an arbitrary number of sets in T is also in T.

Having defined topological spaces, we define manifolds next.

Definition 3 (Manifold) A manifold M is a topological space that has the following properties:

1. M is Hausdorff.
2. M is locally Euclidean.
3. M has a countable basis of open sets.

We will not elaborate on the first and third properties; however, we will elaborate on the locally Euclidean property since it is used in later definitions. The reader is referred to [6, 10, 19, 55] for a more involved reading.

Definition 4 (Locally Euclidean) A topological space, Q, is said to be locally Euclidean if for each point $q \in Q$ we have

- An open neighborhood $U \supset q$.
- An open set $\tilde{U} \subset \mathbb{R}^n$.
- A continuous bijection $\phi : U \to \tilde{U}$.

This map takes an open neighborhood of $q \in Q$ to an open subset of $\mathbb{R}^n$ along with the open neighborhood U is usually called a *coordinate chart* and denoted by (ϕ, U). Charts allow us to define functions on manifolds, compute their derivatives, and address the smoothness arguments of these maps. Usually, more than one chart is needed to map the entire manifold Q to $\mathbb{R}^n$. An *atlas* is a minimum collection of charts needed to map the entire manifold Q. If it happens that a point $q \in Q$ is mapped by more than two charts, we require these charts to be compatible.

Definition 5 (Compatible charts) Given a point $q \in Q$, and two charts (ψ_1, U_1) and (ψ_2, U_2) such that $q \in U_1 \cap U_2$. Then the two charts are said to be compatible if the two maps

$$\begin{aligned} \psi_1 \circ \psi_2^{-1} &: \psi_2(U_2) \to \psi_1(U_1) \text{ and} \\ \psi_2 \circ \psi_1^{-1} &: \psi_1(U_1) \to \psi_2(U_2) \end{aligned}$$

are differentiable.

Using compatible charts, we can define differentiable manifolds.

Definition 6 (Differentiable manifolds) A manifold Q is differentiable if there exists a family of charts $\mathcal{U} = (\psi_i, U_i)$ such that:

1. The open neighborhoods U_i cover Q.
2. (ψ_i, U_i) and (ψ_j, U_j) are compatible for all $U_i \cap U_j \neq \varnothing$.
3. If a chart (ψ, V) is compatible with a chart $(\psi_i, U_i) \in \mathcal{U}$, then $\mathcal{U} \ni (\psi, V)$.

Having defined differential manifold we can go ahead and define Lie groups.

Definition 7 (Lie Group) A Lie group is a manifold whose elements have an additional group structure such that the following maps are differentiable

- Product map: $G \times G \to G$
- Inverse map: $G \to G$.

Lie groups are also referred to as continuous groups, that is, the group elements act on each other in a continuous manner. The group examples described earlier, $SO(2)$ and $SE(2)$, are also Lie groups. Associated with Lie groups are maps which allow the manifold elements to act on each other, these maps are referred to as group actions.

Definition 8 (Group action) An action of a group G on a set Q is defined by the map $\Phi(g, q) : G \times Q \to Q$ for some $g \in G$ and $q \in Q$. The action Φ must satisfy the following properties for all $g, h \in G$, $q \in Q$ and e the identity element of G:

1. $\Phi(g, \Phi(h, q)) = \Phi(gh, q)$ and
2. $\Phi(e, q) = q$.

Fig. 2.2 depicts how the action Φ_g maps q to a new point $\Phi_g q$. Note that we did not specify the structure of the set Q at this moment; however, we will be more specific later when we define fiber bundles. Next, we present a detailed example to illustrate most of the terms introduced in the section thus far.

Example 1 (Rigid body transformation in a plane) We would like to study the motion of a rigid object as it moves in a plane. We need three numbers to identify both the body's location and orientation. We will study Elroy's Beanie which can be seen in Figure 2.1. This robot is composed of two rigid bodies that are allowed to rotate with respect to each other. Hence, the three numbers that identify the robot's location and orientation with respect to an inertial frame are (x, y, θ). Finally, ϕ specifies the relative angle between the rigid bodies.

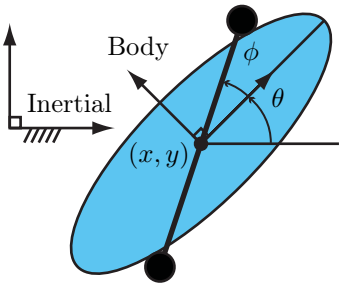

Figure 2.1: The Elroy beanie and its configuration variables.

The location and orientation of the beanie can be represented by the Lie group $SE(2)$. For an initial configuration $g = (x, y, \theta) \in SE(2)$ we can represent it as a matrix using homogeneous coordinates, where

$$g = \begin{pmatrix} \cos\theta & -\sin\theta & x \\ \sin\theta & \cos\theta & y \\ 0 & 0 & 1 \end{pmatrix}.$$

Then if we have another element $h = (u, v, \alpha) \in SE(2)$, we can compute the action of the group element h on the group element g

$$\begin{aligned} g.h &= \begin{pmatrix} \cos\alpha & -\sin\alpha & u \\ \sin\alpha & \cos\alpha & v \\ 0 & 0 & 1 \end{pmatrix} \cdot \begin{pmatrix} \cos\theta & -\sin\theta & x \\ \sin\theta & \cos\theta & y \\ 0 & 0 & 1 \end{pmatrix} \\ &= \begin{pmatrix} \cos(\theta+\alpha) & -\sin(\theta+\alpha) & u + x\cos\alpha - y\sin\alpha \\ \sin(\theta+\alpha) & \cos(\theta+\alpha) & v + x\sin\alpha + y\cos\alpha \\ 0 & 0 & 1 \end{pmatrix} \end{aligned}$$

Hence, $\Phi(h, g) = (u + x\cos\alpha - y\sin\alpha, v + x\sin\alpha + y\cos\alpha, \theta + \alpha)$ which physically represents the configuration of the robot after first being *translated* by a vector (u, v) and then *rotated* by an angle α. Note that the action of g on h yields a different answer since matrix multiplication is not commutative. $\Phi(g, h) = (x + u\cos\theta - v\sin\theta, y + u\sin\theta + v\cos\theta, \theta + \alpha)$.

The above actions acted on the Lie group elements. However, the same actions can act on the "bigger" spaces on which the Lie group is a sub-space. For example if we denote the configuration of the robot in Fig. 2.1 by the vector $q = (x, y, \theta, \phi)$ to include a representation of the relative angle between the two bodies, then the action of $SE(2)$ on Q is given by

$$\Phi(h, q) = \Phi((u, v, \alpha), (x, y, \theta, \phi)) = \begin{pmatrix} u + x\cos\alpha - y\sin\alpha \\ v + x\sin\alpha + y\cos\alpha \\ \theta + \alpha \\ \phi \end{pmatrix}.$$

Note that since the configuration Q is actually a product of two groups, $Q = SE(2) \times \mathbb{S}$,

then the action of $SE(2)$ on Q only affects the group part, $SE(2)$, of Q.

Moreover, note that the two actions $\Phi(h, g)$ and $\Phi(g, h)$ are not identical. This is because, in general, group operations are not necessarily commutative[2]. In particular, we verified that the group $SE(2)$ with the matrix multiplication operation is not commutative. Thus, we define two types of actions, *left* and *right* action.

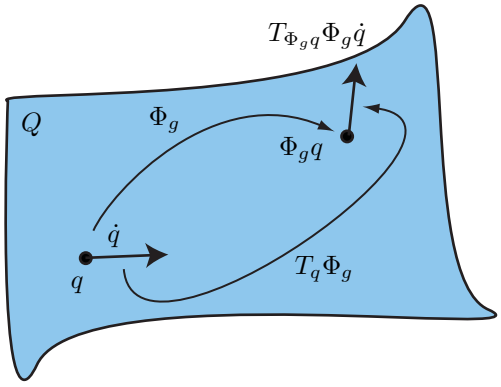

Figure 2.2: Actions and lifted actions on a manifold Q.

Definition 9 (Left and right actions) Left and right actions are defined on matrix groups such that $L(g, h) = gh$ and $R(g, h) = hg$.

For a deeper reading about actions the reader is referred to [5, 40]. We would like to conclude this section with couple of notational comments. Usually an action is denoted by $\Phi(g, q) = \Phi_g q$ or simply as $\Phi(g, q) = gq$. In this thesis will try to keep the notation as clear as possible and only use the shorthand notation whenever there is no risk of ambiguity.

2.3 Tangent Spaces, Lie Algebras and Lifted Actions

In the previous section we defined groups which were used to represent the configuration of a robot in space. In this section we introduce tangent spaces of manifolds which are used to represent velocities of the robot. For instance, in Example 1 we defined $q = (x, y, \theta, \phi) \in Q$ as the configuration of the robot, where Q is referred to as the *configuration manifold* of the mechanical system. We can define the tangent space of this manifold whose elements

[2]Commutative groups are also referred to as Abelian groups.

will represent the configuration velocity elements. We usually denote such elements as $\dot{q} = (\dot{x}, \dot{y}, \dot{\theta}, \dot{\phi})$.

Before we define tangent spaces for general manifolds we define it for the Euclidean space $\mathbb{R}^n$. This definition is much simpler and allows us to easily define cotangent spaces as well.

Definition 10 (Tangent spaces on $\mathbb{R}^n$) Given two points $p, q \in \mathbb{R}^n$, we define $X_p = (X, p)$, with $X = q - p$. X_p is referred to as the tangent vector to $\mathbb{R}^n$ at the point p. The collection of all vectors X_p as the point q moves in $\mathbb{R}^n$ is defined as the tangent space of $\mathbb{R}^n$ at the point p and is usually denoted by $T_p\mathbb{R}^n$. Note that $X_p \in T_p\mathbb{R}^n$. Then finally we define the tangent bundle, $T\mathbb{R}^n$, as the collection of all tangent spaces, $T_p\mathbb{R}^n$, as p moves in all of $\mathbb{R}^n$. Note that $T_p\mathbb{R}^n \in T\mathbb{R}^n$.

Before we go ahead and define tangent spaces on general manifolds, let us define cotangent spaces on $\mathbb{R}^n$.

Definition 11 (Cotangent spaces on $\mathbb{R}^n$) Given $p, q \in \mathbb{R}^n$ and $T_p\mathbb{R}^n$ the tangent space at p. Then we define the one-form at the point p as a linear map, $\phi : T_p\mathbb{R}^n \to \mathbb{R}$. Thus, a one-form is then a choice of smooth maps ϕ for all $p \in \mathbb{R}^n$. Hence we define the set of all one-forms at the point p as the cotangent space to $\mathbb{R}^n$ at the point p which is usually denoted by $T_p^*\mathbb{R}^n$. The set of all cotangent spaces on $\mathbb{R}^n$, $T_p^*\mathbb{R}^n$, is referred to as the cotangent bundle which is usually denoted by $T^*\mathbb{R}^n$.

Note that both the tangent space and the cotangent space are vector spaces that are dual to each other. There are standard bases associated with these spaces. Specifically, the basis for $T_p\mathbb{R}^n$ is $\{\frac{\partial}{\partial x^1}, \cdots, \frac{\partial}{\partial x^n}\}$ while the basis for $T_p^*\mathbb{R}^n$ is $\{dx^1, \cdots, dx^n\}$. Also note that, $dx^i \frac{\partial}{\partial x^j} = \{1 \text{ if } i = j, 0 \text{ otherwise}\}$.

Now we define tangent spaces on general differentiable manifolds. Previously, when we defined tangent spaces on $\mathbb{R}^n$, we took advantage of the flatness of $\mathbb{R}^n$ to define tangent vectors at a point. Such flatness does not hold in general. Hence, to define tangent vectors at a point we need to define curves passing through that point.

Consider a curve $\gamma(t)$ on a manifold Q that is parameterized by time and passes through a point $q \in Q$ at time $t = 0$. Then the velocity vector to the curve at $t = 0$ is given by $\gamma'(0)$. Now consider all possible curves passing though point q at $t = 0$, and there are infinitely many of them. The tangent vectors to these curves span a vector space, usually denote by T_qQ, which defines the *tangent space* of Q at point $q \in Q$. Moreover, the tangent bundle, usually denoted by TQ, is defined as

$$TQ = \bigcup_{q \in Q} T_q Q$$

Having defined tangent spaces on a manifold, we can define vector fields

Definition 12 (Vector field) A vector field is a smooth map, X, from a manifold Q to its tangent space T_qQ, such that

$$\begin{aligned} X \quad &: \quad Q \to T_qQ \\ &\qquad q \mapsto X(q) \end{aligned}$$

The set of all smooth vector fields on Q is denoted by $\chi(Q)$.

Moreover, if a manifold happens to have a group structure, that is, it is a Lie group, then the tangent space of the manifold at the identity group element constitutes a Lie algebra which is usually denoted by $\mathfrak{g} = T_eG$. We will remind the reader of the definition of an algebra before we rigorously define define Lie algebras.

Definition 13 (Real algebra) A real vector space V with an operation * is called an algebra if $x * y \in V$ for all $x, y \in V$ and

- $(x + y) * z = x * z + y * z$ for all $x, y, z \in V$.
- $z * (x + y) = z * x + z * y$ for all $x, y, z \in V$.
- $(ax) * y = x * (ay) = a(x * y)$ for all $x, y \in V$ and $a \in \mathbb{R}$.

The vector space $\mathbb{R}^3$ with the operation cross product forms a real algebra. Now we define a Lie algebra.

Definition 14 (Lie algebra) A Lie algebra is a vector space $\mathfrak{g}$ together with a binary operator $[\cdot, \cdot] : \mathfrak{g} \times \mathfrak{g} \to \mathfrak{g}$, usually called the Lie bracket, where the bracket must satisfy the following properties

1. $[\xi, \xi] = 0$ for all $\xi \in \mathfrak{g}$.
2. Bilinearity , that is, $[a\xi, b\eta] = a[\xi, \eta] + b[\xi, \eta]$ and $[\xi, a\eta + b\lambda] = a[\xi, \eta] + b[\xi, \lambda]$, for all $a, b \in R$ and $\xi, \eta, \lambda \in \mathfrak{g}$.
3. Jacobi identity, that is, $[[\xi, \eta], \lambda] + [[\lambda, \xi], \eta] + [[\eta, \lambda], \xi] = 0$, for all $\xi, \eta, \lambda \in \mathfrak{g}$.

Lie algebras are important since they have linear vector space structure and they are easier to analyze than Lie groups. Moreover, Lie algebra elements act like generators where they can be used to recover the entire Lie group. This is done with the *exponential map* which we define next after we give an example of a Lie algebra.

Example 2 (Lie algebra of $SO(3)$) The Lie algebra of the special orthogonal group $SO(3)$ is usually denoted by $so(3)$ and defined by

$$so(3) = \{\hat{\omega} \in \mathbb{R}^{3\times 3} : \hat{\omega}^T = -\hat{\omega}\}.$$

Here we used the fact that for $\omega = (\omega_1, \omega_2, \omega_3) \in \mathbb{R}^3$, we define matrix representation of ω using the "hat" operator where

$$\hat{\omega} = \begin{pmatrix} 0 & -\omega_3 & \omega_2 \\ \omega_3 & 0 & -\omega_1 \\ -\omega_2 & \omega_1 & 0 \end{pmatrix}.$$

Note that $\hat{\omega}$ is a skew symmetric matrix.

Definition 15 (Exponential map) Given a Lie group G with its associated Lie algebra $\mathfrak{g}$ then for $\xi \in \mathfrak{g}$ and $t \in \mathbb{R}$ we define the exponential map by

$$\begin{aligned} \exp \quad : \quad & \mathfrak{g} \to G \\ & \xi \mapsto g = \exp(t\xi) \end{aligned}$$

Thus, the exponential map yields a configuration fiber variable that is reached by flowing along the fiber for time t, and whose initial velocity was ξ. If G is a matrix Lie group then $\exp t\xi$ is defined as the matrix exponential acting on the matrix $t\xi$.

$$\exp t\xi = \sum_{n=0}^{\infty} \frac{(t\xi)^n}{n!}$$

Example 3 (Exponential of $so(3)$) Consider rotations around the x-axis, then $\omega = (1, 0, 0)$. Now we use Rodrigues' formula to compute the exponential of $\hat{\omega}$

$$\begin{aligned}
\exp\theta\hat{\omega} &= I + \hat{\omega}\sin\theta + \hat{\omega}^2(1-\cos\theta) \\
&= \begin{pmatrix} 1 & 0 & 0 \\ 0 & 1 & 0 \\ 0 & 0 & 1 \end{pmatrix} + \begin{pmatrix} 0 & 0 & 0 \\ 0 & 0 & -1 \\ 0 & 1 & 0 \end{pmatrix}\sin\theta + \begin{pmatrix} 0 & 0 & 0 \\ 0 & -1 & 0 \\ 0 & 0 & -1 \end{pmatrix}(1-\cos\theta) \\
&= \begin{pmatrix} 1 & 0 & 0 \\ 0 & \cos\theta & -\sin\theta \\ 0 & \sin\theta & \cos\theta \end{pmatrix} \in SO(3).
\end{aligned}$$

Note that the last matrix is exactly the rotation matrix for rotations about the x-axis by an angle θ.

In the previous section we defined group actions that acted on group and configuration elements, now we will define what is termed as *lifted actions* that act on tangent vectors of manifolds.

Definition 16 (Lifted action) Consider a manifold Q. Then the lifted action is a linear map defined by

$$\begin{aligned}
T_q\Phi_g &: T_qQ \to T_{\Phi_g q}Q \\
&\quad \dot{q} \mapsto T_{\Phi_g q}\Phi_g \dot{q}
\end{aligned}$$

Fig. 2.2 depicts how the action and the lifted action map q and $\dot{q}$ to a new configuration $\Phi_g q$ and velocity $T_{\Phi_g q}\Phi_g \dot{q}$, respectively.

Similar to group actions we have to make the distinction between left and right lifted actions, however, in this case the distinction has a deep physical intuition. For a given group velocity, $\dot{g}$, the left lifted action maps $\dot{g}$ to the Lie algebra is the *body velocity* representation of $\dot{g}$. Similarly, using the right lifted action yields the *spatial velocity* representation.

Definition 17 (Body and spatial velocity representations) Given a Lie group G, a point $g \in G$, and $v_g \in T_gG$, we define the body and spatial body representations respectively by

$$\xi^b = T_g L_{g^{-1}} v_g \tag{2.1}$$

$$\xi^s = T_g R_{g^{-1}} v_g \tag{2.2}$$

According to [36], body velocity represents the velocity of body as seen in the inertial coordinate frame but represented in the body-attached coordinate frame. Spatial velocity is the velocity of an imaginary point rigidly attached to the body as it passes through the origin of the inertial coordinate frame and again represented in body frame. The following example helps the reader understand the difference between the two velocity representations.

Example 4 (Lifted actions and different velocity representations) In Example 1, we worked out the group actions on the groups $SE(2)$. Now we will work out the lifted action for the beanie example. For $q = (x, y, \theta, \phi)$ and $h = (u, v, \alpha)$, we have $L_h q = (u + x\cos\alpha - y\sin\alpha, v + x\sin\alpha + y\cos\alpha, \theta + \alpha, \phi)$ and $R_h q = (x + u\cos\theta - v\sin\theta, y + u\sin\theta + v\cos\theta, \theta + \alpha)$. Hence we can compute the lifted maps $T_g L_h \dot{q}$ and $R_g L_h \dot{q}$

$$
\begin{aligned}
T_g L_h \dot{q} &= \begin{pmatrix} \frac{\partial L_h q}{\partial x} & \frac{\partial L_h q}{\partial y} & \frac{\partial L_h q}{\partial \theta} & \frac{\partial L_h q}{\partial \phi} \end{pmatrix} \\
&= \begin{pmatrix} \cos\alpha & -\sin\alpha & 0 & 0 \\ \sin\alpha & \cos\alpha & 0 & 0 \\ 0 & 0 & 1 & 0 \\ 0 & 0 & 0 & 1 \end{pmatrix} \begin{pmatrix} \dot{x} \\ \dot{y} \\ \dot{\theta} \\ \dot{\phi} \end{pmatrix} \\
T_g R_h \dot{q} &= \begin{pmatrix} 1 & 0 & -u\sin\theta - v\cos\theta & 0 \\ 0 & 1 & u\cos\theta - v\sin\theta & 0 \\ 0 & 0 & 1 & 0 \\ 0 & 0 & 0 & 1 \end{pmatrix} \begin{pmatrix} \dot{x} \\ \dot{y} \\ \dot{\theta} \\ \dot{\phi} \end{pmatrix}
\end{aligned}
$$

To illustrate the difference between body and spatial velocities, we select an action that maps the current configuration to the group identity element, e. Hence, if the beanie in Example 1 is located at configuration $q = (g, \phi) = (x, y, \theta, \phi)$ and has a velocity $\dot{q} = (\dot{x}, \dot{y}, \dot{\theta}, \dot{\phi})$, (Figure 2.3), then we define $h \in G$ such that $h = g^{-1}$. Now we have $L_{g^{-1}} q = R_{g^{-1}} q = (e, \phi) = (0, 0, 0, \phi)$. Then we compute the lifted maps $T_g L_{g^{-1}} \dot{q}$ and $T_g R_{g^{-1}} \dot{q}$. In general $T_g L_{g^{-1}} \dot{q} \neq T_g R_{g^{-1}} \dot{q}$ as seen in Figure 2.3. This difference is due to the non-commutativity of the $SE(2)$. To measure this non-commutativity we use the *adjoint* map.

Definition 18 (Adjoint map) The adjoint map is a map from a Lie algebra to itself

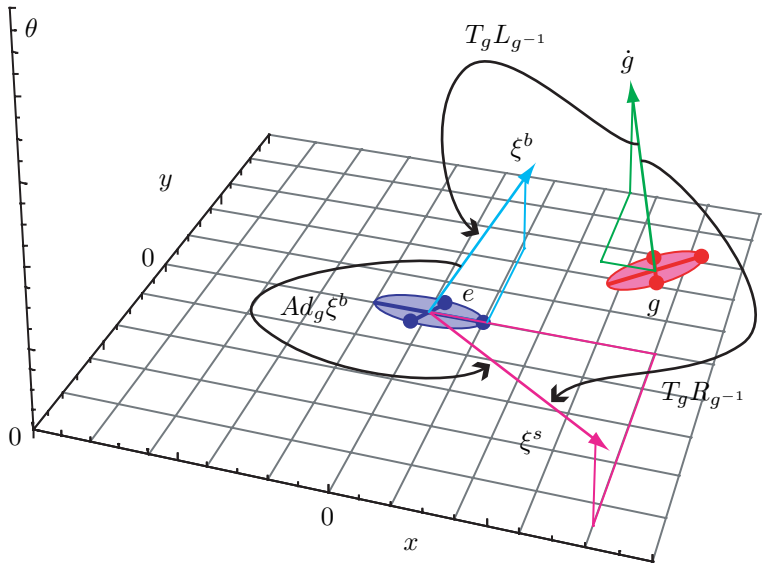

Figure 2.3: Actions and lifted actions for the beanie example.

and is defined as follows

$$\begin{aligned} Ad_g \quad &: \quad \mathfrak{g} \to \mathfrak{g} \\ &\qquad \xi \mapsto T_g R_{g^{-1}}(T_e L_g \xi) \end{aligned}$$

Computing the adjoint for $SE(2)$ we get:

$$Ad_g = \begin{pmatrix} \cos\theta & -\sin\theta & y \\ \sin\theta & \cos\theta & -x \\ 0 & 0 & 1 \end{pmatrix}, \text{ and}$$

$$Ad_{g^{-1}} = (Ad_g)^{-1} \begin{pmatrix} \cos\theta & \sin\theta & -x\sin\theta - y\cos\theta \\ -\sin\theta & \cos\theta & x\cos\theta - y\sin\theta \\ 0 & 0 & 1 \end{pmatrix}.$$

Note that the Adjoint map allows us to map velocities from spatial to body representations and viceversa. Thus, using (2.1) and (2.2) we get

$$
\begin{aligned}
\xi^s &= T_g R_{g^{-1}} v_g \\
&= T_g R_{g^{-1}} (T_g L_{g^{-1}})^{-1} \xi^b \\
&= T_g R_{g^{-1}} T_g L_{g^{-1}} \xi^b \\
&= Ad_g \xi^b, \text{ and} \qquad (2.3) \\
\xi^b &= T_g L_{g^{-1}} v_g \\
&= T_g L_{g^{-1}} (T_g R_{g^{-1}})^{-1} \xi^s \\
&= (T_e L_g T_g R_{g^{-1}})^{-1} \xi^s \\
&= Ad_{g^{-1}} \xi^s. \qquad (2.4)
\end{aligned}
$$

2.4 Fiber Bundles

Earlier in this document, we referred to configuration manifolds of mechanical systems. Now we will define such manifolds more rigorously. According to [5], a configuration is the minimum number of variables needed to uniquely specify the location in two or three dimensions of each physical point of the mechanism or robot. So for rigid bodies that have a fixed shape, the location and orientation of a body-attached reference coordinate frame is enough. However, if the robot or mechanism is made up of many rigid bodies then additional variables are needed to specify the robot's shape. Hence, for multi-bodied robots, the configuration space is composed of a position and shape variables.

We will assume that the position variables are elements of a set that has a group structure such as $\mathbb{R}^n$, $SO(n)$, or $SE(n)$. Additionally, the position variables belong to the configuration manifold, hence the position variables are governed by a Lie group structure. For mechanical system, we assume that a general configuration manifold is usually denoted by $Q = G \times M$, where G is the *fiber space* specifying the position of the robot and M is the *base space* specifying the internal shape of the robot. In this document we deal with configuration manifolds that have a *principal fiber bundle* structure.

Definition 19 (Fiber bundle) For a manifold Q with a base subspace M and a projection map $\pi : Q \to M$, define a fiber, $G(r)$, as the pre-image of $r \in M$ in Q with respect to the map π, that is, $G = \pi^{-1}(r)$. Then, Q is said to be a fiber bundle if for every neighborhood $U \subset M$ of r we have

$\pi^{-1}(U)$ is homeomorphic to $G \times U$, that is,

locally we have $Q \cong M \times G$. We usually denote fiber bundle by $Q = (G, M)$.

Note that if the fiber G has a group structure then Q is a *principal* fiber bundle, and if $Q = G \times M$ globally, then Q is a *trivial* fiber bundle. The configuration space of all mechanical systems are trivial principal fiber bundles. Referring to Example 1, the configuration space is $Q = SE(2) \times \mathbb{S}^1$ which is a trivial principal bundle.

The projection map associated with the fiber bundle manifold does induce a lifted map that acts on the manifold's tangent space,

$$\pi : Q \to M \Rightarrow T\pi : TQ \to TM.$$

This lifted map allows us to decompose the manifold's tangent space into two subspaces:

Definition 20 (Vertical and horizontal spaces) Given a fiber bundle Q with an associated projection map $\pi : Q \to M$, then a vertical space V_q is defined at a point $q \in Q$ as

$$V_q = \ker(T\pi).$$

Then the horizontal space H_q is defined as the complement of the vertical space such that

$$T_qQ = V_q \oplus H_q.$$

Moreover, for a configuration manifold with a principal fiber bundle structure, we can define a *principal connection*, but first we need to define a *Lie group generator*. We have mentioned earlier that Lie algebras represent the entire group using the exponential map. Now we will extend this notion to principal fiber bundles.

Definition 21 (Lie group generator) Given a trivial principal fiber bundle $Q = G \times M$ and an action $\Phi(g, q) : Q \to Q$ then define a generator on Q by

$$\begin{aligned} \xi_Q \quad : \quad & \mathfrak{g} \to TQ \\ & \xi \mapsto \frac{d}{dt} \left(\Phi(\exp t\xi, q) \right)_{t=0} \end{aligned}$$

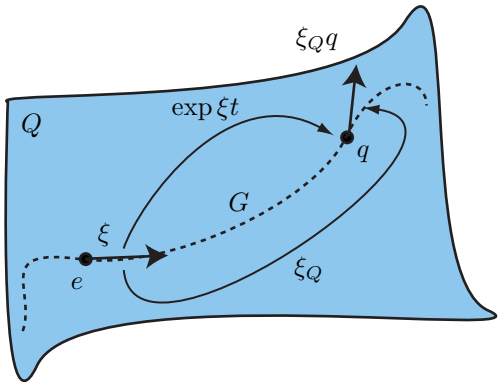

Figure 2.4: The exponential map and the vector field generation on Q along the fiber G.

Figure 2.4 illustrates how the exponential map and generator are related. When the generator is applied to the principal bundle, it has a very specific form which is presented in the following Lemma.

Lemma 1 (Generator on principal bundles) *For a given principal fiber bundle, $Q = G \times M$, the Lie group generator can be written as*

$$\xi_Q(g, r) = (T_e R_g \xi, \dot{r}). \tag{2.5}$$

PROOF Computing the generator using its definition

$$\begin{aligned}
\xi_Q(g,r) &= \frac{d}{dt}\left(\Phi(\exp(t\xi),(g,r))\right)_{t=0} \\
&= \frac{d}{dt}\left(\exp(t\xi)g, r\right)_{t=0} \\
&= \frac{d}{dt}\left(R_g(\exp(t\xi)), r\right)_{t=0} \\
&= \left(T_e R_g \xi(\exp(t\xi)), \dot{r}\right)_{t=0} \\
&= (T_e R_g \xi, 0)
\end{aligned}$$

■

The above result was mentioned in [5, 40]; however, here we presented a more explicit proof.

Example 5 (Generator on $SE(2)$) Given $g = (x, y, \theta) \in SE(2)$ and $\xi = (\xi_1, \xi_2, \xi_3) \in se(2)$. Using the computed lifted maps in Example 4 and Lemma 1, we can compute the

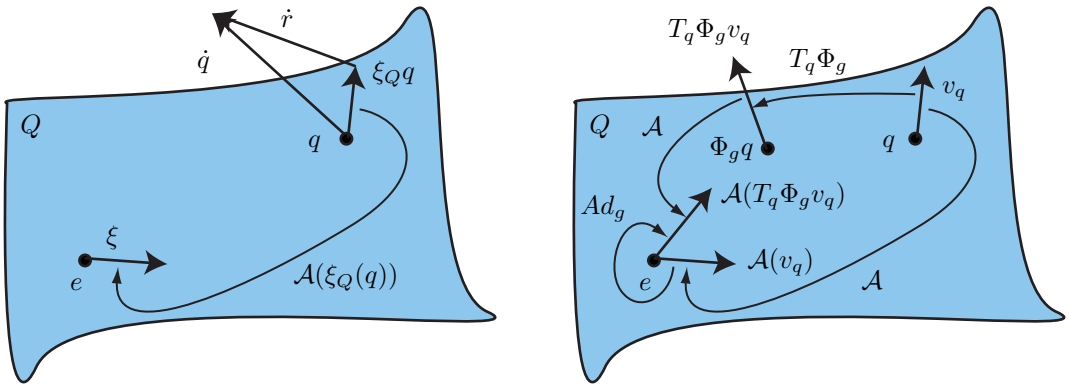

Figure 2.5: Configuration of the two-mass example.

generator on $SE(2)$

$$T_e R_g = T_h R_g|_{h=e} = \begin{pmatrix} 1 & 0 & -x\sin\alpha - y\cos\alpha \\ 0 & 1 & x\cos\alpha - y\sin\alpha \\ 0 & 0 & 1 \end{pmatrix}_{(u=0,v=0,\alpha=0)} = \begin{pmatrix} 1 & 0 & -y \\ 0 & 1 & x \\ 0 & 0 & 1 \end{pmatrix}.$$

Then we have

$$\xi_{SE(2)}(g) = T_e R_g \xi = \begin{pmatrix} 1 & 0 & -y \\ 0 & 1 & x \\ 0 & 0 & 1 \end{pmatrix} \begin{pmatrix} \xi_1 \\ \xi_2 \\ \xi_3 \end{pmatrix} = \begin{pmatrix} \xi_1 - y\xi_3 \\ \xi_2 + x\xi_3 \\ \xi_3 \end{pmatrix}$$

Having defined the generator we can go ahead and define a principal connection map.

Definition 22 (Principal connection) Given a trivial principal fiber bundle manifold $Q = G \times M$ with and associated projection map $\pi : Q \to M$, then a principal connection is a Lie algebra valued map $\mathcal{A} : TQ \to \mathfrak{g}$, such that

- $\mathcal{A}(\xi_Q(q)) = \xi$, for all $\xi \in \mathfrak{g}$ and $q \in Q$.
- $\mathcal{A}(T_q\Phi_g v_q) = Ad_g \mathcal{A}(v_q)$, for all $q \in Q$, $v_q \in T_q Q$, and $g \in G$.

The first property implies that if a vector in the tangent space of Q was generated by Lie group generator, then the principal connection maps the generated vector back to the Lie algebra element which generated it as shown in the first plot of Fig. 2.5. The second property implies that if two elements in the tangent space of Q are related by a lifted

map $T_q\Phi_g$, then Lie algebra elements corresponding to these vectors are related by the Adjoint map as shown in the second plot of Fig. 2.5. Moreover, we can utilize the principal connection to redefine the horizontal space more rigorously.

Lemma 2 (Kernel of the principal connection) *Given a principal bundle manifold, $Q = G \times M$, and an associated projection map $\pi : Q \to M$, let V_q denote the vertical space at $q \in Q$, then the horizontal space is defined by $H_q = \ker \mathcal{A}(v_q)$ such that $T_qQ = V_q \oplus H_q$.*

PROOF Given $v_q \in T_qQ$, let $\xi = \mathcal{A}(v_q)$. Then we have $\mathcal{A}(v_q - \xi_Q(q)) = \mathcal{A}(v_q) - \mathcal{A}(\xi_Q(q)) = \xi - \xi = 0$. This implies that $(v_q - \xi_Q(q)) \in H_q$. Moreover, we know that since $T_q\pi(\xi_Q(q)) = 0$, we have $\xi_Q(q) \in V_qQ$. Thus, defining, $hor(v_q) = (v_q - \xi_Q(q))$ and $ver(v_q) = \xi_Q q$, we have

$$hor(v_q) = v_q - ver(v_q) \Rightarrow v_q = hor(v_q) + ver(v_q).$$

This implies that $T_qQ = V_qQ + H_qQ$.

■

This result is stated in [5,40] but we have never seen an intuitive proof for it. Hence, for a given principal fiber bundle, we use the kernels of the projection map and the principal connection to respectively define the vertical and horizontal subspaces of the bundle's tangent space.

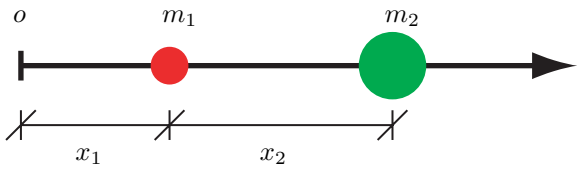

Figure 2.6: Configuration variables of the two-mass example.

Example 6 (Fiber bundles and connections) Now we will present a simple but very useful example. Consider a two mass system that moves along a line. The position of first mass is measured from the origin of an inertial frame, x_1, and the position of the second mass is measured relative to the first mass, x_2 as shown in Fig. 2.6. The configuration manifold is $Q = \mathbb{R} \times \mathbb{R}$. Since $\mathbb{R}$ is a Lie group, then Q is a principal bundle. Now we

can compute the projection map and the lifted projection map. Given a configuration $q = (x_1, x_2) \in Q$ and a velocity $v_q = (\dot{x}_1, \dot{x}_2) \in T_qQ$, then we have

$$\begin{aligned} \pi: \quad & Q \to \mathbb{R} & \qquad T\pi: \quad & TQ \to T\mathbb{R} \\ & (x_1, x_2) \mapsto x_2 & & (\dot{x}_1, \dot{x}_2) \mapsto \dot{x}_2 \end{aligned}$$

Alternative, in matrix representation we have $\pi = \begin{pmatrix} 0 & 1 \end{pmatrix}$ and $T\pi = \begin{pmatrix} 0 & 1 \end{pmatrix}$. Now let us choose a principal connection such that: $\mathcal{A}((\dot{x}_1, \dot{x}_2)) = \dot{x}_1 + A(x_1, x_2)\dot{x}_2$. We can easily verify this connection satisfies both properties in Definition 22. In matrix representation we have $\mathcal{A} = \begin{pmatrix} 1 & A(x_1, x_2) \end{pmatrix}$. Having computed both the lifted projection and the principal connection we can go ahead and compute the vertical and horizontal spaces.

$$\begin{aligned} V_q = \ker \begin{pmatrix} 0 & 1 \end{pmatrix} = span \begin{pmatrix} 1 & 0 \end{pmatrix} \text{ and} \\ H_q = \ker \begin{pmatrix} 1 & A(x_2, x_2) \end{pmatrix} = span \begin{pmatrix} -A(x_1, x_2) & 1 \end{pmatrix}. \end{aligned}$$

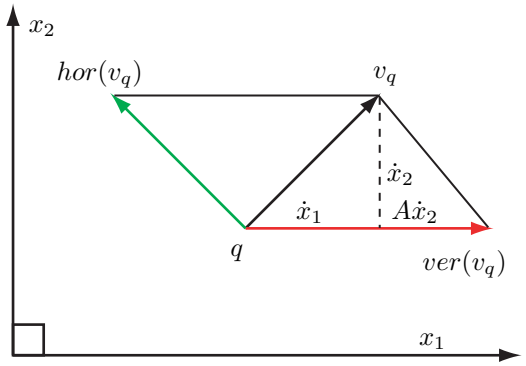

Figure 2.7: The vertical and horizontal components of v_q.

The exponential map for the group $\mathbb{R}$ is given by $\exp(t\xi) = t\xi$ and the generator is given by $\xi_Q(q) : \xi \mapsto \begin{pmatrix} \xi & 0 \end{pmatrix}$. Now we can compute the vertical and horizontal components of a vector $v_q \in T_qQ$.

$$\begin{aligned} ver(v_q) = \mathcal{A}(v_q)_Q = (\dot{x}_1 + A(x_1, x_2)\dot{x}_2)_Q = \begin{pmatrix} \dot{x}_1 + A(x_1, x_2)\dot{x}_2 & 0 \end{pmatrix}, \text{ and} \\ hor(v_q) = v_q - ver(v_q) = \begin{pmatrix} -A(x_1, x_2)\dot{x}_2 & \dot{x}_2 \end{pmatrix}. \end{aligned}$$

A graphical representation of the vertical and horizontal components of v_q can be seen

in Figure 2.7. Note that a motion in the base, that is, a pure horizontal velocity only occurs if m_2 moves with velocity $\dot{x}_2$ and m_1 will move with velocity $-A(x_1, x_2)\dot{x}_2$. In other words if the connection $A(x_1, x_2) \neq 0$ then a horizontal base motion will induce a vertical fiber motion.

As we shall see later in the document, for unconstrained mechanical systems, the principal connection has a specific definition which has conservation of momentum embedded within. In other words, if the shape of the robot changes, its position will change in such a way that momentum is conserved.

2.5 Calculus of Variations

The calculus of variations allows us to solve numerous physical problems. Moreover, we can use calculus of variation to produce the dynamic equations of motion for mechanical systems with and without non-holonomic constraints. The reader is referred to [15, 16].

Definition 23 (Basic problem in the Calculus of variations [15]) Given $a, b, A, B \in \mathbb{R}$ with $a < b$ and $f : [a, b] \times \mathbb{R} \times \mathbb{R} \to \mathbb{R}$. Let

$$\mathcal{Y} := \{y \in \mathcal{C}^1[a, b] | y(a) = A \text{ and } y(b) = B\},$$

where $\mathcal{C}^n[a, b]$ is the set of continuous functions on the closed interval $[a, b]$ that are n-differentiable. Then define $J(y) : \mathcal{Y} \to \mathbb{R}$ as

$$J(y) = \int_a^b f(x, y(x), y'(x))dx \quad \forall y \in \mathcal{Y}.$$

The basic problem in the calculus of variation is to minimize or maximize J over $\mathcal{Y}$. The function $f(x, y(x), y'(x))$ is called *functional*.

Definition 24 (Admissible variations [15]) For $v \in \mathcal{X}$, a linear vector space, and $y \in \mathcal{Y}$, we say that v is a $\mathcal{Y}$-admissible variation at y if there exists an open interval $I \subset \mathbb{R}$ with $0 \in I$ such that $[y + \epsilon v] \in \mathcal{Y}$ for every $\epsilon \in I$. The set of $\mathcal{Y}$-admissible variations at y is denoted by $\mathcal{V}_y$.

Definition 25 (Gâteaux variations [15]) Let $y \in \mathcal{Y}$ and $v \in \mathcal{V}_y$ be given and put

$$\delta J(y; v) = \lim_{\epsilon \to 0} \frac{J(y + \epsilon v) - J(y)}{\epsilon},$$

provided the limit exists. When the limit exists, $\delta J(y;v)$ is called the Gâteaux variation of J at y in the v direction.

Definition 26 (First Euler-Lagrange equation [15]) Given $a, b, A, B \in \mathbb{R}$ with $a < b$ and $f : [a,b]\times\mathbb{R}\times\mathbb{R} \to \mathbb{R}$. Assume that f has continuous second order partial derivatives. Let $\mathcal{X} = \mathcal{C}^2[a,b]$ and define $\mathcal{Y} \subset \mathcal{X}$

$$\mathcal{Y} := \{y \in \mathcal{C}^1[a,b] | y(a) = A \text{ and } y(b) = B\}.$$

Then define $J(y) : \mathcal{Y} \to \mathbb{R}$ by

$$J(y) = \int_a^b f(x, y(x), y'(x))dx \quad \forall y \in \mathcal{Y}.$$

Let $y_* \in \mathcal{Y}$ be a minimizer of J, then f is governed by the First Euler-Lagrange equation

$$\frac{\partial}{\partial y_*(x)}\left(f(x, y_*(x), y'_*(x))\right) - \frac{d}{dx}\left[\frac{\partial}{\partial y'_*(x)}\left(f(x, y_*(x), y'_*(x))\right)\right] = 0, \forall x \in [a,b]. \tag{2.6}$$

Definition 27 (Second Euler-Lagrange equation [15]) Given $a, b, A, B \in \mathbb{R}$ with $a < b$ and $f : [a,b] \times \mathbb{R} \times \mathbb{R} \to \mathbb{R}$. Assume that f has continuous second order partial derivatives. Let $y = \mathcal{C}^2[a,b]$ be given and y satisfies

$$\frac{\partial}{\partial y(x)}\left(f(x, y(x), y'(x))\right) - \frac{d}{dx}\left[\frac{\partial}{\partial y'(x)}\left(f(x, y(x), y'(x))\right)\right] = 0, \forall x \in [a,b].$$

Then there exists a constant $c \in \mathbb{R}$ such that

$$f(x, y(x), y'(x)) - y'(x)\frac{\partial}{\partial y'(x)}\left(f(x, y(x), y'(x))\right) = c + \int_a^x \frac{\partial}{\partial x}\left(f(t, y(t), y'(t))\right) dt, \forall x \in [a,b].$$

This equation is referred to ar the Second Euler-Lagrange equations.

We will not include the Lagrangian multipliers definition, since it is very mathematical and omitting it will not disturb the readers intuition. Finally we will introduce two very important lemmas that will be useful in relating body and spatial velocity represnetations. For the proof of the lemmas, the reader is referred to [15].

Lemma 3 (Lagrange Lemma) *Let $g(x) \in \mathcal{C}^1[a,b]$ be given, and assume that $\int_a^b g(x)v(x)dx = 0$ for all $v \in \mathcal{C}^2[a,b]$ such that $v(a) = v(b) = 0$. Then $g(x) = 0$ for all $x \in [a,b]$.*

Lemma 4 (du Bois-Reymond Lemma) *Let $g(x) \in \mathcal{C}^1[a,b]$ be given, and assume that $\int_a^b g(x)v'(x)dx = 0$ for all $v \in \mathcal{C}^1[a,b]$ such that $v(a) = v(b) = 0$. Then there exist a constant $c \in \mathbb{R}$ such that $g(x) = c$ for all $x \in [a,b]$.*

The definitions in the section will come useful when we are optimizing gaits and even when presenting the equations of motion due to Lagrangian dynamics.

2.6 Exterior Algebra

Finally, we present couple of results from exterior algebra theory. First, we shall review Stokes' theorem in its most general form.

Theorem 1 (Stokes' Theorem) *Given a one-form ω and its exterior derivative $d\omega$, we have*

$$\oint_{\partial N} \omega = \int_N d\omega, \tag{2.7}$$

where ∂N is the boundary of the manifold N.

The exterior derivative of an m dimensional one-form,

$$\omega = \sum_{i=1}^{m} f_i(\sigma_1, \sigma_2, \cdots, \sigma_m) d\sigma_i, \tag{2.8}$$

yields a two-form and is given by

$$d\omega = \sum_{i,j=1, i<j}^{m} \left(\frac{\partial f_j}{\partial \sigma_i} - \frac{\partial f_i}{\partial \sigma_j} \right) (d\sigma_i \wedge d\sigma_j), \tag{2.9}$$

where $\wedge$ represents the wedge product [14, 31].

Chapter 3

Mechanics of Locomotion

In this chapter, we present several results from the geometric mechanics and the Lagrangian dynamics fields. Even though some of these results are not novel, we still present them and actually provide our own intuitive proofs to help the reader understand these results.

The main idea in this chapter is how to utilize the special structure of the configuration space of mechanical systems to simplify the dynamic equations of motion. In this dissertation we use the Lagrangian formulation to compute the equation of motion for a mechanical system. These equations are a set second order differential equations whose solution describes the evolution of the degrees of freedom of a mechanical system due to a set of input forces. In general, these equations are highly nonlinear thus rendering the motion planning problem quite challenging, that is, proposing input forces that will cause the degrees of freedom to evolve in a desired way. Thus, it is clear that a simplification of the dynamic equations of motion is necessary for approaching the motion planning problem.

It is the special geometric structure of the configuration space which allows us to simplify the dynamic equations of motion. In fact, we utilize the principal fiber bundle structure of the configuration space to define a principal connection which we then utilize to relate internal shape to position velocities. This relation which is referred to as the *reconstruction equation* which, in its most general form, is dictated by both the conservation of momentum along the allowable directions and the non-holonomic constraints acting on the systems.

The other tool we utilize to simplify the equations of motion is the symmetry of the laws of physics. Here symmetry is defined as the invariance of the Lagrangian and the non-holonomic constraints with respect to the Lie group actions. This invariance allows us to rewrite the equations of motion in a body attached coordinate frame, thus, eliminating

the significance of the placement of the inertial coordinate frame. Utilizing this invariance we actually rewrite the original equations of motion in a simpler *reduced* form. The original equations describing the evolution of the position variables are rewritten as a set of first order differential *momentum evolution equations* while the original equations of motion describing the internal changes will be decoupled from the position of the robot and expressed are the *reduced base dynamic equations*. Thus, in this chapter we work towards computing and obtaining these sets of reduced equations of motion.

3.1 Geometric Mechanics

In this section we summarize most of the results from [40], where we include intuitive proofs for some results. This makes the material presented easier to grasp and expose the reader to some useful concepts used in mechanics. For more involved reading, the reader is referred to [1, 5, 40].

3.1.1 Connections on Principal Bundles

Earlier in the Chapter 2 we have presented principal connections on principal bundles. If the configuration space under investigation is trivial, which is the case with all mechanical systems, then a very useful result can be attained. We present this result in the following proposition.

Proposition 1 (Local trivialization of the principal connection) *Given a principal connection $\mathcal{A}$ on a* ***trivial*** *principal bundle $Q = G \times M$, the connection is locally written as*

$$\mathcal{A}(\dot{g}, \dot{r}) = Ad_g(T_g L_{g^{-1}} \dot{g} + A(r)\dot{r}). \tag{3.1}$$

where Ad_g is the adjoint map, $T_g L_{g^{-1}}$ is the lifted map acting on $\dot{g}$, and $A(r)$ is the local form of the principal connection multiplying the base velocity, $\dot{r}$.

Proof The principal connection is linear, that is,

$$\mathcal{A}_{(g,r)}(\dot{g}, \dot{r}) = \mathcal{A}_(g, r)(\dot{g}, 0) + \mathcal{A}_(g, r)(0, \dot{r})$$

Next we compute each of the two terms in the right hand side of the above equation. There should exist a Lie algebra element $\xi \in \mathfrak{g}$ such that the generated left-invariant vector

field evaluated at the point (g, r) yields the tangent element $(\dot{g}, 0)$, that is, $\xi_Q(g, r) = (\dot{g}, 0)$. Moreover, we know from Equation 2.5 that $\xi = T_g R_{g^{-1}} \dot{g}$, then we have

$$\begin{aligned}
\mathcal{A}_{(g,r)}(\dot{g}, 0) &= \mathcal{A}_{(g,r)} \xi_Q(g, r), \\
&= \xi, \\
&= T_g R_{g^{-1}} \dot{g}, \\
&= T_g R_{g^{-1}} (T_e L_g)(T_g L_{g^{-1}}) \dot{g}, \\
&= Ad_g (T_g L_{g^{-1}} \dot{g}).
\end{aligned}$$

Here we used the first property of the principal connection map given in Definition 22. Moreover, we used the fact that the map $(T_g L_{g^{-1}})$ is the inverse map of $(T_e L_g)$. As for computing the second term, without loss of generality we will assume that $\Phi_q(h, s) = (L_g h, s)$, and $T_{(h,s)} \Phi_g(\dot{h}, \dot{s}) = (T_h L_g \dot{h}, \dot{s})$. Then we have

$$\begin{aligned}
\mathcal{A}_{(g,r)}(0, \dot{r}) &= \mathcal{A}_{\Phi_g(e,r)}(0, \dot{r}), \\
&= \mathcal{A}_{\Phi_g(e,r)}(T_e L_g 0, \dot{r}), \\
&= \mathcal{A}_{\Phi_g(e,r)} T_{(e,r)} \Phi_g(0, \dot{r}), \\
&= Ad_g \mathcal{A}_{(e,r)}(0, \dot{r}), \\
&= Ad_g (A(r) \dot{r}),
\end{aligned}$$

where $A(r)$ is called the local form[1] of the connection. Here we used the second property of the principal connection map given in Definition 22. Finally, we finish the proof to arrive at

$$\begin{aligned}
\mathcal{A}_{(g,r)}(\dot{g}, \dot{r}) &= \mathcal{A}_(g, r)(\dot{g}, 0) + \mathcal{A}_(g, r)(0, \dot{r}), \\
&= Ad_g (T_g L_{g^{-1}} \dot{g}) + Ad_g (A(r) \dot{r}), \\
&= Ad_g (T_g L_{g^{-1}} \dot{g} + A(r) \dot{r}).
\end{aligned}$$

■

[1] Throughout this thesis document, "local" means that the terms are computed at the Lie group identity.

This is an important proposition since it allows us to decouple our configuration velocities, $\dot{q} = (\dot{g}, \dot{r})$, at the identity of the group into the two terms $T_g L_{g^{-1}} \dot{g}$ and $A(r)\dot{r}$. This idea will be illustrated further in a later example.

Up until now, we have been considering an arbitrary connection map, $\mathcal{A}_q(\dot{q})$, on the principal fiber bundle configuration space, Q. Nonetheless, for mechanical systems, this connection takes a special form. Before we present this special form, we need to introduce two additional terms, specifically, the locked inertia tensor and the momentum map.

Definition 28 (Locked inertia tensor) The locked inertia tensor represents the inertia of the mechanical system when all its base variables are locked, that is, fixing the robot's shape. The locked inertial tensor denoted by $\mathbb{I}$ is represented by the map, $\mathbb{I} : \mathfrak{g} \to \mathfrak{g}^*$ which is defined as

$$\langle \mathbb{I}\eta, \xi \rangle = \langle\langle \eta_Q(q), \xi_Q(q) \rangle\rangle, \tag{3.2}$$

where $\eta, \xi \in \mathfrak{g}$ and $\eta_Q(q), \xi_Q(q) \in T_qQ$. Note that $\mathfrak{g}^*$ is the dual Lie algebra of $\mathfrak{g}$.

We distinguish between the kinetic energy metric and the dot product. The operation $\langle \cdot, \cdot \rangle$ is the natural pairing between a vector, $v_q \in T_qQ$, and co-vector, $\omega_q \in T_q^*Q$, which is computed using the simple dot product operation $\langle v_q, \omega_p \rangle = v_q^T \omega_q$, and the operation $\langle\langle \cdot, \cdot \rangle\rangle$ is computed using the kinetic energy metric, that is, $\langle\langle v_q, v_p \rangle\rangle = \frac{1}{2} v_q^T M v_p$, where M is the mass matrix and $v_p, v_q \in T_qQ$. The reader is referred to [5, 9, 32] for an involved reading about kinetic energy metrics.

Definition 29 (Momentum map) The momentum map computes the momentum of the system for a given velocity v_q. To be more specific, the momentum map, denoted by J, maps $J : T_qQ \to \mathfrak{g}^*$. Mathematically, we define the momentum map as

$$\langle J(v_q), \xi \rangle = \langle\langle v_q, \xi_Q(q) \rangle\rangle, \tag{3.3}$$

where $\xi \in \mathfrak{g}$ and $v_q, \xi_Q(q) \in T_qQ$.

Now illustrate the above two maps using the following example.

Example 7 (Locked inertia and momentum maps) Referring to Figure 2.1 in Example 1, the kinetic energy is given by $KE = 1/2 \left(m(\dot{x}^2 + \dot{y}^2) + J\dot{\theta}^2 + J_r(\dot{\theta} + \dot{\phi})^2 \right)$. Let

us rewrite it in matrix form to extract the mass matrix,

$$KE = \frac{1}{2}\begin{pmatrix} \dot{x} & \dot{y} & \dot{\theta} & \dot{\phi} \end{pmatrix} \begin{pmatrix} m & 0 & 0 & 0 \\ 0 & m & 0 & 0 \\ 0 & 0 & J+J_r & J_r \\ 0 & 0 & J_r & J_r \end{pmatrix} \begin{pmatrix} \dot{x} \\ \dot{y} \\ \dot{\theta} \\ \dot{\phi} \end{pmatrix} = \frac{1}{2}\dot{q}^T M \dot{q}.$$

Now using the result from Example 5, we can compute the locked inertia and momentum maps. Let $\xi = (\xi_1, \xi_2, \xi_3)$, $\eta = (\eta_1, \eta_2, \eta_3)$ and $v_q = (v_x, v_y, v_\theta, v_\phi)$, then we have

$$\begin{aligned}
\eta_Q(q)^T M \xi_Q(q) &= \begin{pmatrix} \eta_1 - y\eta_3 \\ \eta_2 + x\eta_3 \\ \eta_3 \\ 0 \end{pmatrix}^T \begin{pmatrix} m & 0 & 0 & 0 \\ 0 & m & 0 & 0 \\ 0 & 0 & J+J_r & J_r \\ 0 & 0 & J_r & J_r \end{pmatrix} \begin{pmatrix} \xi_1 - y\xi_3 \\ \xi_2 + x\xi_3 \\ \xi_3 \\ 0 \end{pmatrix} \\
&= \begin{pmatrix} \eta_1 \\ \eta_2 \\ \eta_3 \end{pmatrix}^T \underbrace{\begin{pmatrix} m & 0 & -my \\ 0 & m & mx \\ -my & mx & J+J_r+m(x^2+y^2) \end{pmatrix}}_{\mathbb{I}} \begin{pmatrix} \xi_1 \\ \xi_2 \\ \xi_3 \end{pmatrix}, \text{ and} \\
v_q^T M \xi_Q(q) &= \begin{pmatrix} v_x \\ v_y \\ v_\theta \\ v_\phi \end{pmatrix}^T \begin{pmatrix} m & 0 & 0 & 0 \\ 0 & m & 0 & 0 \\ 0 & 0 & J+J_r & J_r \\ 0 & 0 & J_r & J_r \end{pmatrix} \begin{pmatrix} \xi_1 - y\xi_3 \\ \xi_2 + x\xi_3 \\ \xi_3 \\ 0 \end{pmatrix} \\
&= \underbrace{\begin{pmatrix} v_x \\ v_y \\ v_\theta \\ v_\phi \end{pmatrix}^T \begin{pmatrix} m & 0 & -my \\ 0 & m & my \\ 0 & 0 & J+J_r \\ 0 & 0 & J_r \end{pmatrix}}_{J(v_q)} \begin{pmatrix} \xi_1 \\ \xi_2 \\ \xi_3 \end{pmatrix}.
\end{aligned}$$

3.1.2 Mechanical Connection

For mechanical systems that have a configuration space with a principal fiber bundle structure, the principal connection has a very specific form [5, 40].

Definition 30 (Mechanical Connection) Given a configuration manifold Q for a me-

chanical systems that has a fiber bundle structure, $Q = G \times M$, we define the mechanical connection as

$$\begin{array}{rcl} \mathcal{A}(\dot{q}) : T_qQ & \rightarrow & \mathfrak{g} \\ (q, \dot{q}) & \mapsto & \mathbb{I}^{-1}(q)J(\dot{q}) \end{array} \tag{3.4}$$

where $\mathbb{I}$ is the locked inertia tensor and J is the momentum map.

Example 8 (Mechanical connection) In Example 7 we computed the locked inertia tensor and the momentum map. Hence, we can compute the mechanical connection for Elroy's beanie seen in Figure 2.1.

$$\mathcal{A}(v_q) = \begin{pmatrix} v_x + y\left(v_\theta + \frac{J_r}{J+J_r}v_\phi\right) & v_y + x\left(v_\theta + \frac{J_r}{J+J_r}v_\phi\right) & v_\theta + \frac{J_r}{J+J_r}v_\phi \end{pmatrix}$$

Multiplying the above quantity by $Ad_{g^{-1}}$ from Definition 18, and grouping terms we arrive at

$$\begin{array}{rcl} Ad_{g^{-1}}\mathcal{A}(v_q) & = & \begin{pmatrix} \cos\alpha & \sin\alpha & 0 \\ -\sin\alpha & \cos\alpha & 0 \\ 0 & 0 & 1 \end{pmatrix} \begin{pmatrix} v_x \\ v_y \\ v_\theta \end{pmatrix} + \begin{pmatrix} 0 \\ 0 \\ \frac{J_r}{J+J_r} \end{pmatrix} v_\phi \\ & = & T_gL_{g^{-1}}v_g + A(r)v_r. \end{array}$$

This result agrees with Proposition 1. Note that $Ad_{g^{-1}}\mathcal{A}(v_q)$ is nothing but the mechanical connection written in body coordinates as seen in Equations 2.3 and 2.4.

Proposition 2 (Mechanical connection in body coordinates) *For a simple mechanical system whose configuration space is a trivial principal fiber bundle and whose Lagrangian defines a kinetic energy metric, then the mechanical connection represented in body coordinated has the following form*

$$\mathcal{A}_q^b(\dot{q}) = I^{-1}(r)J^b(\dot{q}) = \xi^b + A(r)\dot{r} \tag{3.5}$$

where $I(r) = \mathbb{I}(e, r)$ is the local form of the locked inertia tensor computed at the Lie group identity, e, $J^b(\dot{q})$ is the momentum map represented in body coordinates, and $A(r)$ is the local form of the mechanical connection.

PROOF We start by expressing the momentum map and the locked inertia tensor in the body coordinates as was shown in [5] to arrive at

$$\begin{aligned} J^b(\dot{q}) &= Ad_g^* J(\dot{q}), \text{ and} \\ \mathbb{I}(q) &= Ad_h^* \mathbb{I}(\Phi_h q) Ad_h \\ &= Ad_{g^{-1}}^* \mathbb{I}(\Phi_{g^{-1}} q) Ad_{g^{-1}} \\ &= Ad_{g^{-1}}^* \mathbb{I}(e, r) Ad_{g^{-1}} \end{aligned}$$

where Ad_g^* is the dual map of Ad_g. In the second set of equations we utilized the fact that the locked inertia tensor is Ad_g-invariant. Here we mapped the locked inertia tensor to the Lie group identity by using the map $\Phi_h q = \Phi_{g^{-1}} q = (e, r)$. Next, we substitute the above two expressions into the definition of the mechanical connection to arrive at

$$\begin{aligned} \mathcal{A}_q(\dot{q}) &= \mathbb{I}^{-1}(q) J(\dot{q}) \\ &= \left(Ad_{g^{-1}}^* \mathbb{I}(e, r) Ad_{g^{-1}} \right)^{-1} \left(Ad_g^* \right)^{-1} J^b(\dot{q}) \\ &= Ad_g \mathbb{I}^{-1}(e, r) Ad_g^* \left(Ad_g^* \right)^{-1} J^b(\dot{q}) \\ &= Ad_g I^{-1}(r) J^b(\dot{q}) \\ &= Ad_g \mathcal{A}_q^b(\dot{q}) \end{aligned}$$

Here, we label the term $\mathbb{I}(e, r)$ by $I(r)$ which is the local form of the locked inertia tensor. Moreover, in the last line we have defined the mechanical connection in body coordinates such that $\mathcal{A}_q^b(\dot{q})$ to be equal to $I^{-1}(r) J^b(\dot{q})$. Next, we shall see how the principal connection computed at the Lie group identity allows us to decouple a configuration velocity. Thus, expressing the mechanical connection, which is a principal connection, in body coordinates and substituting for it using the result from Proposition 1 we arrive at

$$\begin{aligned} \mathcal{A}_q^b(\dot{q}) &= Ad_{g^{-1}} \mathcal{A}_q(\dot{q}) \\ I^{-1}(r) J^b(\dot{q}) &= Ad_{g^{-1}} \left(Ad_g (T_g L_{g^{-1}} \dot{g} + A(r) \dot{r}) \right) \\ I^{-1}(r) J^b(\dot{q}) &= T_g L_{g^{-1}} \dot{g} + A(r) \dot{r} \end{aligned}$$

Finally recall that $\xi^b = T_g L_{g^{-1}} \dot{g}$ which is the body representation of the fiber velocity $\dot{g}$. Hence, solving for ξ^b we arrive at

$$\xi^b = -A(r)\dot{r} + I^{-1}(r)J^b(\dot{q}) \tag{3.6}$$

■

Later in the thesis, we will further simplify this expression. Specifically, we will present how to compute the momentum map in body coordinates, $J^b(\dot{q})$, using the reduced Lagrangian. The reconstruction equation given in (3.6) is important, since we not only utilize it to define a partition on the types of mechanical systems we are considering in this thesis, but we also use it to generate gaits for these types of mechanical systems.

3.2 Lagrangian Dynamics

In this section we present the Lagrangian approach to model the dynamics of mechanical systems and compute the governing equations of motion. Then we define the Lagrangian invariance with respect to Lie group action which physically means that the placement of the inertial coordinate frame can be arbitrary. We utilize this invariance, or symmetry, to reduce the order of differential equations of motion of the mechanical system. For a thorough reference for Lagrangian dynamics, the reader is referred to [1, 5, 18].

3.2.1 Fundamentals

Given a system with an n-dimensional configuration space Q, then the Lagrangian is a map $L(t, q, \dot{q}) : [a, b] \times \mathbb{R}^n \times \mathbb{R}^n \to \mathbb{R}$. For mechanical systems composed of multiple rigid bodies, the Lagrangian takes a very specific form. Before we define the Lagrangian for mechanical systems let us define the kinetic energy and the mass matrix for a multi-bodied mechanical system.

Definition 31 (Kinetic energy of multi-bodied mechanical systems) For a mechanical system composed of n rigid bodies and whose configuration space is Q, the kinetic energy is given by

$$KE = \sum_{i=1}^{n} \frac{1}{2} \left(\dot{q}_i^T m_i \dot{q}_i + \dot{\mu}_i^T j_i \dot{\mu}_i \right), \tag{3.7}$$

where $\dot{q}_i$ is the linear velocity of the center of mass of each rigid body, μ_i is the angular velocity of each of the bodies, m_i and j_i are the mass and inertia of each of the bodies.

Associated with the kinetic energy of mechanical systems, we can define a kinetic energy metric utilizing the mass matrix.

Definition 32 (Mass matrix) For a mechanical system whose configuration space is Q and whose kinetic energy is KE, we can define the kinetic energy metric on the tangent space of the configuration manifold such that

$$KE = \langle\langle v_1, v_2 \rangle\rangle = \frac{1}{2} v_1^T M(q) v_2 \tag{3.8}$$

where $v_1, v_2 \in T_q Q$ and $M(q)$ is the mass matrix.

Now we can define the Lagrangian for mechanical systems.

Definition 33 (Lagrangian for mechanical systems) For a mechanical systems with configuration space Q, the Lagrangian is defined by

$$L(q, \dot{q}) = \frac{1}{2} \dot{q}^T M \dot{q} - V(q), \tag{3.9}$$

where M is the mass matrix of the mechanical system, $\frac{1}{2}\dot{q}^T M \dot{q}$ is its kinetic energy, and $V(q)$ is its potential energy.

For the rest of the thesis, we will assume that the potential energy is zero unless specified otherwise. Next, we present how to compute the equations of motion for a mechanical system.

Definition 34 (Action integral) For a mechanical system whose configuration space Q, and whose Lagrangian is given by $L(q, \dot{q})$, the action integral is defined by

$$\int_{t_0}^{t_1} L(q, \dot{q}) dt. \tag{3.10}$$

Taking recourse to Lagrangian dynamics, we know that mechanical systems evolve with time according to the principal of *least action*. In other words, mechanical systems evolve in time such that the action integral given in (3.10) is minimized. Thus, computing the dynamic equations of motion for mechanical systems is simply equivalent to computing the first Euler-Lagrange equations, (2.6), associated with the variational problem that minimizes the functional $f(t, q(t), q'(t)) = L(q(t), \dot{q}(t))$.

3.2.2 The Euler-Lagrange Equations

Given a mechanical system with configuration space Q and Lagrangian $L(q, \dot{q})$, the configuration of the system will evolve along the curve $q(t)$ which is a minimizer of the action integral (3.10). Hence, $q(t)$ must satisfy the first Euler-Lagrange equations given in (2.6) which are the dynamic equations of motion,

$$\frac{d}{dt}\left(\frac{\partial}{\partial \dot{q}_i}L(q,\dot{q})\right) - \frac{\partial}{\partial q_i}L(q,\dot{q}) = 0, \quad (i = 1, \ldots, n). \tag{3.11}$$

Equation 3.11 is the governing equation of motion for isolated mechanical systems, that is, no external forces and no non-holonomic constraints acting on the system. Next we present the more general equations of motion for mechanical systems with external forces but with zero potential energy, that is,

$$\frac{d}{dt}\left(\frac{\partial}{\partial \dot{q}_i}L(q,\dot{q})\right) - \frac{\partial}{\partial q_i}L(q,\dot{q}) = \tau_i, \quad (i = 1, \ldots, n), \tag{3.12}$$

where τ_i are the generalized external forces. Moreover, for mechanical systems that are subject to k non-holonomic constraints given in the Pfaffian form, $\omega(q)\dot{q} = 0$, the dynamic equations of motion are given by

$$\frac{d}{dt}\left(\frac{\partial}{\partial \dot{q}_i}L(q,\dot{q})\right) - \frac{\partial}{\partial q_i}L(q,\dot{q}) = \lambda_j \omega_i^j + \tau_i, \quad (i = 1, \ldots, n, \quad j = 1, \ldots, k) \tag{3.13}$$

where λ_j's are the Lagrange multipliers. The next Example will illustrate how to write the equations of motion for a general mechanical system with external forces and non-holonomic constraints.

Example 9 (Unicycle) Given a unicycle as shown in Figure 3.1. The robot's configuration is represented by the vector $q = (x, y, \theta, \phi)$ where x and y denote the position of the contact point of the wheel, θ denotes the wheel's orientation, and ϕ measures the rotation of the wheel. Hence, the configuration manifold is four-dimensional, $Q = \mathbb{R} \times \mathbb{R} \times \mathbb{S} \times \mathbb{S}$. Let $Q = G \times M$ where $G = \mathbb{R} \times \mathbb{R}$ is the fiber Lie group and $M = \mathbb{S} \times \mathbb{S}$ is the base space. The Lagrangian of the unicycle which is equal to its kinetic energy and is given by

$$L(q,\dot{q}) = \frac{1}{2}\left(m(\dot{x}^2 + \dot{y}^2) + J\dot{\theta}^2 + J_w\dot{\phi}^2\right)$$

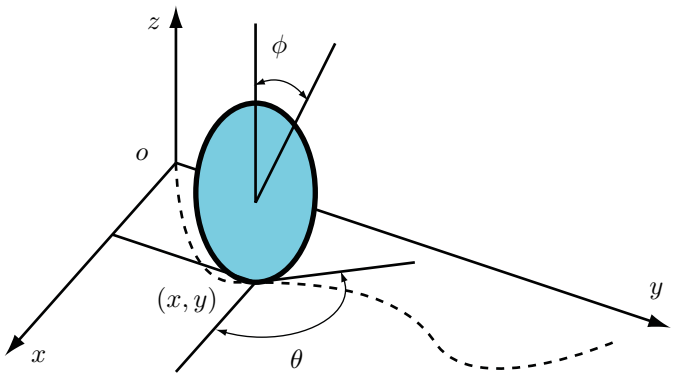

Figure 3.1: An illustration for the unicycle example.

where m is the robot's total mass, J is its inertia about the z axis, and J_w is the wheel's rolling inertia. The two non-holonomic constraints are given by

$$\begin{aligned} \dot{x}\cos\theta + \dot{y}\sin\theta - r\dot{\phi} &= 0 \text{ [Rolling without slipping]}, \\ \dot{x}\sin\theta - \dot{y}\cos\theta &= 0 \text{ [No sideways slipping]}. \end{aligned}$$

Assuming that the generalized forces in the steering and rolling directions are τ_θ and τ_ϕ respectively, Then using Equation 3.13 we can write the equations of motion to arrive at

$$\begin{aligned} m\ddot{x} &= \lambda_1\cos\theta + \lambda_2\sin\theta, \\ m\ddot{y} &= \lambda_1\sin\theta - \lambda_2\cos\theta, \\ J\ddot{\theta} &= \tau_\theta, \text{ and} \\ J_w\ddot{\phi} &= \lambda_1 r + \tau_\phi. \end{aligned}$$

3.2.3 Symmetries and Momentum Maps

In 1915, Emmy Noether introduced a theorem which exploits symmetry in the laws of physics to extract conserved quantities [5, 40]. For example, the invariance (or symmetry) of the kinetic energy with respect to translations in space leads to conservation of momentum. In the context of thesis, symmetry will be encountered as invariance of a quantity with respect to some action.

Definition 35 (Lagrangian invariance) The Lagrangian, $L(q, \dot{q})$, of a mechanical system with a trivial principal bundle configuration manifold, $Q = G \times M$, is said to be invariant if

$$L(q, \dot{q}) = L(\Phi_g q, T_q \Phi_g \dot{q}). \tag{3.14}$$

where Φ_g is the Lie group action on Q and $T_q\Phi_g$ is the lifted action on TQ.

Similarly, we can define the invariance of vector fields, $X(q) : Q \to T_qQ$, and one-forms, $f(v_q) : T_qQ \to \mathbb{R}$. Specifically, we can verify the invariance of the non-holonomic constraints which are a set of one-forms using the following equations

$$\omega(q)\dot{q} = \omega(\Phi_g q) T_q \Phi_g \dot{q}. \tag{3.15}$$

Example 10 (Elroy's beanie: Invariance) Referring to Figure 2.1 we can compute the Lagrangian of the robot

$$L((x, y, \theta, \phi), (\dot{x}, \dot{y}, \dot{\theta}, \dot{\phi})) = \frac{1}{2}\left(m(\dot{x}^2 + \dot{y}^2) + J\dot{\theta}^2 + J_r(\dot{\theta} + \dot{\phi})^2\right).$$

where m is the entire mass of the robot, J is its inertia, and J_r is the rotor's inertia. In Example 1 we computed the action for $SE(2)$ and its lifted action.

$$\begin{aligned} \Phi_h q &= (u + x\cos\alpha - y\sin\alpha, v + x\sin\alpha + y\cos\alpha, \theta + \alpha, \phi), \text{ and} \\ T_q\Phi_h \dot{q} &= (\cos\alpha\dot{x} - \sin\alpha\dot{y}, \sin\alpha\dot{x} + \cos\alpha\dot{y}, \dot{\theta}, \dot{\phi}). \end{aligned}$$

Then we can verify that

$$\begin{aligned} L(\Phi_g q, T_q\Phi_g\dot{q}) &= \frac{1}{2}\left(m((\cos\alpha\dot{x} - \sin\alpha\dot{y})^2 + (\sin\alpha\dot{x} + \cos\alpha\dot{y})^2) + J\dot{\theta}^2 + J_r(\dot{\theta} + \dot{\phi})^2\right) \\ &= \frac{1}{2}\left(m((\cos^2\alpha + \sin^2\alpha)\dot{x}^2 + m((\cos^2\alpha + \sin^2\alpha)\dot{y}^2) + J\dot{\theta}^2 + J_r(\dot{\theta} + \dot{\phi})^2\right) \\ &= \frac{1}{2}\left(m(\dot{x}^2 + \dot{y}^2) + J\dot{\theta}^2 + J_r(\dot{\theta} + \dot{\phi})^2\right) \\ &= L(q, \dot{q}). \end{aligned}$$

In the next section we will see how to exploit this invariance to reduce the dynamic equations of motion.

3.2.4 Reduction

We will present how symmetry can simplify the differential equations of motion by reducing them from a set of second to first order differential equations. For the sake of clarity, we will do an example for the one-dimensional case to help give some intuition.

Example 11 (Reduction in one dimension) Given an invariant Lagrangian[2] $L(x(t), \dot{x}(t))$, we can compute the dynamic equation of motion using (2.6) to arrive at

$$\frac{d}{dt}\left(\frac{\partial L(x(t), \dot{x}(t))}{\partial \dot{x}(t)}\right) - \frac{\partial L(x(t), \dot{x}(t))}{\partial x(t)} = 0. \tag{3.16}$$

Now we define the momentum in the x direction by

$$p = \frac{\partial L(x(t), \dot{x}(t))}{\partial \dot{x}(t)}.$$

Then using (2.6) we can write out the first Euler-Lagrange equation in terms of p to get

$$p' = \frac{\partial L(x(t), \dot{x}(t))}{\partial x(t)}.$$

If we assume that the Lagrangian is invariant with respect to the variable s, then we have

$$\begin{aligned}
0 &= \frac{\partial L(x(s), \dot{x}(s))}{\partial s} \text{ [Invariance]} \\
&= \frac{\partial L(x(s), \dot{x}(s))}{\partial x(s)}\frac{dx(s)}{ds} + \frac{\partial L(x(s), \dot{x}(s))}{\partial \dot{x}(s)}\frac{d\dot{x}(s)}{ds} \text{ [Product rule]} \\
&= p'(s)\frac{dx(s)}{ds} + p(s)\frac{d\dot{x}(s)}{ds} \text{ [Substitutions]} \\
&= \left(p(s)\frac{dx(s)}{ds}\right)' \text{ [Regrouping]} \\
\Leftrightarrow c &= p(s)\frac{dx(s)}{ds}
\end{aligned}$$

Thus, the quantity $p(s)\frac{dx(s)}{ds}$ is conserved. Note that order of the last differential equation is one. This is a one-fold reduction from the original Euler-Lagrange equations (3.16).

[2]For this example, we assume that the Lagrangian is solely the kinetic energy of the system.

Similar proofs can be done for a general n-dimensional Lagrangian. Next we will present the result due to reduction without proof. For further details the reader is referred to [1,5,40]. It is convenient to define different reference frames for representing the equations of motion of the robot. In this document the *body* representation will play an important role.

Definition 36 (Body Coordinates) Let $\dot{q} = (\dot{g}, \dot{r}) \in T_qQ$ be a configuration velocity at the point $q = (g, r)$ and let the body frame be rigidly attached to the robot. The body representation of $\dot{q}$ is given by

$$T_q\Phi_{g^{-1}}(\dot{q}) = (T_gL_{g^{-1}}\dot{g}, \dot{r})$$

In fact, we already defined body representation on a Lie group, G, as shown in (2.1), however, here we are defining the action on the entire manifold, Q. In the rest of this thesis, we will use body representation and hence ξ will always refer to ξ^b. Remember that the body velocity is the velocity of the body computed in the inertial frame but represented in the body frame [36].

The invariance of the Lagrangian means that we can compute the Lagrangian anywhere on the configuration manifold and get the same value provided that we map the velocities using the lifted actions. One special configuration to compute the Lagrangian is at the Lie group identity element, e. This yields an expression of the Lagrangian that is independent of the fiber variables g. This special Lagrangian is referred to as the *reduced Lagrangian*. According to [40], the reduced Lagrangian is given by

$$\begin{aligned} l(\xi, r, \dot{r}) &= L(\Phi_{g^{-1}}q, T_q\Phi_{g^{-1}}\dot{q}) \\ &= L(g^{-1}g, r, T_gL_{g^{-1}}\dot{g}, \dot{r}) \\ &= L(e, r, \xi, \dot{r}). \end{aligned} \tag{3.17}$$

Moreover, according to [40] the reduced Lagrangian will have the following form

$$l(\xi, r, \dot{r}) = \frac{1}{2}\begin{pmatrix} \xi \\ \dot{r} \end{pmatrix}^T \tilde{M}(r) \begin{pmatrix} \xi \\ \dot{r} \end{pmatrix} \tag{3.18}$$

Here, $\tilde{M}(r)$ is the reduced mass matrix associated with the reduced Lagrangian can be written in the following form

$$\tilde{M}(r) = \begin{pmatrix} I(r) & I(r)A(r) \\ (I(r)A(r))^T & m(r) \end{pmatrix}, \tag{3.19}$$

where $A(r)$ is the local form of the mechanical connection, $I(r)$ is the local form of the locked inertia tensor, $I = \mathbb{I}(e, r)$, and $m(r)$ is a matrix depending only on base variables. Next, we utilize the reduced Lagrangian to compute the momentum map at the group identity. We will utilize the above structure of the reduced Lagrangian to simplify the computation of the reconstruction and momentum evolution equations.

Proposition 3 (Body representation of the momentum map) *For a simple mechanical system whose Lagrangian is invariant with respect to the Lie group action, the momentum map can be computed using the reduced Lagrangian map as follows*

$$\boxed{J^b(\dot{q}) = \frac{\partial l(\xi, r, \dot{r})}{\partial \xi}} \tag{3.20}$$

where $l(\xi, r, \dot{r})$ is the reduced Lagrangian and ξ is the body representation of the fiber velocity $\dot{g}$.

PROOF Recall the the momentum map is computed using the equation $\langle J(v_q), \xi \rangle = \langle\langle v_q, \xi_Q(q) \rangle\rangle$. Using this expression, we compute the momentum map at the Lie group identity by setting $q = (e, r)$ and $\dot{q} = (\xi, \dot{r})$. Hence, we get

$$\begin{aligned} \langle J^b(\dot{q}), \xi \rangle &= \langle J(\xi, \dot{r}), \xi \rangle \\ &= \langle\langle (\xi, \dot{r}), \xi_Q(e, r) \rangle\rangle \\ &= \langle\langle (\xi, \dot{r}), (\xi, 0) \rangle\rangle \\ &= \begin{pmatrix} \xi \\ \dot{r} \end{pmatrix}^T M(e, r) \begin{pmatrix} \xi \\ 0 \end{pmatrix} \\ &= \xi^T \tilde{M}(r) \xi \\ &= \langle \xi^T \tilde{M}(r), \xi \rangle \end{aligned}$$

Thus, it is obvious that $J^b(\dot{q}) = \xi^T \tilde{M}(r)$. Moreover, we know that the reduced Lagrangian is given by $l(\xi, r, \dot{r}) = \frac{1}{2}(\xi, \dot{r})^T \tilde{M}(r)(\xi, \dot{r})$. Hence, we can conclude that

$$J^b(\dot{q}) = \xi^T \tilde{M}(r) = \frac{\partial l(\xi, r, \dot{r})}{\partial \xi}.$$

■

Finally, we conclude this section by computing the reduced non-holonomic constraints. On other words, we utilized the invariance of the non-holonomic constraints to represent their Pfaffian form in the body-attached coordinate frame. The result is presented in the following Lemma.

Lemma 5 (Local form of the non-holonomic constraints) *For a mechanical system whose configuration space is a trivial principal fiber bundle, $Q = G \times M$, and which is subject to k linearly independent non-holonomic constraints, $\omega(q)\dot{q} = 0$, that are invariant with respect to left group actions, then the reduced non-holonomic constraints are given by*

$$\bar{\omega}_\xi(r)\xi + \bar{\omega}_r(r)\dot{r} = 0.$$

PROOF Given the triviality of the configuration space and the invariance of the constraints with respect to left group actions, then we have

$$\begin{aligned} \omega(q) \cdot \dot{q} &= \omega(\Phi_h q) \cdot T_q \Phi_h \dot{q} = 0, \text{ or} \\ \Leftrightarrow \omega(g, r) \cdot (\dot{g}, \dot{r})^T &= \omega(L_h g, r) \cdot (T_g L_h \dot{g}, \dot{r})^T = 0, \end{aligned}$$

where $\Phi_h q$ and $T_q \Phi_h \dot{q}$ are the left and lifted left actions on the manifold Q, [5, 41]. Note that these actions act only on the fiber part of q. Let $h = g^{-1}$ we arrive at

$$\begin{aligned} 0 = \omega(g, r) \cdot (\dot{g}, \dot{r})^T &= \omega(L_{g^{-1}} g, r) \cdot (T_g L_{g^{-1}} \dot{g}, \dot{r})^T \\ &= \omega(g^{-1} g, r) \cdot (T_g L_{g^{-1}} \dot{g}, \dot{r})^T \\ &= \omega(e, r) \cdot (T_g L_{g^{-1}} \dot{g}, \dot{r})^T. \end{aligned}$$

Now, define the local form of $\omega(q)$ to be $\bar{\omega}(r) = \omega(e, r)$. Moreover, we know that $\xi = \xi^b = T_g L_{g^{-1}} \dot{g}$. Thus, the non-holonomic constraints, expressed in the body-attached frame are given by

$$\begin{aligned} 0 &= \bar{\omega}(r) \begin{pmatrix} \xi \\ \dot{r} \end{pmatrix}, \\ 0 &= \bar{\omega}_\xi(r)\xi + \bar{\omega}_r(r)\dot{r}, \end{aligned} \tag{3.21}$$

where $\bar{\omega}_\xi(r)$ and $\bar{\omega}_r(r)$ are the $k \times l$ and $k \times m$ sub-matrices of $\bar{\omega}(r)$. Note that, the reduced non-holonomic constraints are independent on the fiber variable, g.

■

3.3 Reduced Equations of Motion

In this final section, we present the reduced equations of motion for unconstrained systems. For more details, the reader is referred to [5, 9, 24, 40].

For unconstrained mechanical systems that have a trivial principal fiber bundle configuration space, $Q = G \times M$, and whose Lagrangian is invariant with respect to the Lie group action, we use the reduced Lagrangian to define the *generalized momentum variable*, p such that

$$p = \frac{\partial l(\xi, r, \dot{r})}{\partial \xi}.$$

Note that p is actually the momentum map represented in body coordinates as shown in Proposition 3. Hence, for unconstrained mechanical systems, we can rewrite the reconstruction equation, (3.6) in terms of the generalized momentum variable to arrive at

$$\xi = T_g L_{g^{-1}} \dot{g} = -A(r)\dot{r} + I^{-1}(r)p^T \tag{3.22}$$

where $\xi = \xi^b$, $A(r)$ is the local form of the mechanical connection, and $I(r)$ is the local form of the locked inertia tensor. Later in the thesis, we will re-derive this equation and compute it for mechanical systems with non-holonomic constraints.

The reconstruction equation presented above can be used to solve for the fiber velocities, $\dot{g} = T_e L_g \xi$, given the base configuration and velocity variables, $(r, \dot{r})$, and the momentum variable, p. Thus, we need additional sets of equations that prescribe the evolution of the base and momentum variables. Such equations were presented by Ostrowski

in [40]. Hence, we can rewrite the dynamic equations of motion as follows

$$\dot{g} = T_e L_g \left(-A(r)\dot{r} + I^{-1}(r)p^T\right), \tag{3.23}$$

$$\dot{p} = ad^*_\xi p + \tau^e_g, \text{ and} \tag{3.24}$$

$$\ddot{r} = -\bar{M}^{-1}(r)\left(\dot{r}^T\tilde{C}(r)\dot{r} + \tilde{N}(r) + B(r)\tau^e_r\right). \tag{3.25}$$

The last two equations, (3.23) and (3.25), describe the evolution of the momentum and base variables for a given generalized fiber and base forces, τ^e_g and τ^e_r, pulled to the group identity, e. Thus, giving these input generalized forces, one can solve for the base and momentum variables and plug them into the reconstruction equation and solve for the fiber velocity, $\dot{g}$.

Moreover, note that both the reconstruction equation, (3.24), and the momentum evolution equation, (3.24), are a set of l first order differential equations, where l is the dimension of the fiber space G. The reduced[3] base dynamics equations, (3.25) are a set of m second order differential equations, where m is the dimension of the base space, M. Hence, we reduced the original set of $n(= l + m)$ second order dynamic equations of motion, (3.12), to a set of $2l$ first order and m second order differential equations.

Finally, we conclude this chapter with the following assumption. Throughout this thesis, we assume that we have full control solely over the base space configuration and velocity variables, $(r, \dot{r})$. Hence, for the rest of the thesis, we will neglect the reduced dynamic equations of motion on the base space (3.25), thus, we will use only the reconstruction and momentum evolution equations to represent the systems dynamics for all types of mechanical system we are considering in this thesis. In the following two chapters, we will derive both the reconstruction and momentum evolution equations for several types of mechanical systems which we will utilize later to eventually generate gaits for these systems.

[3]Here the word "reduced" describes the fact that the system dynamics is projected on the base space.

Chapter 4

Mechanical Systems Classification

In this chapter we build upon the background material presented in Chapter 3 and tailor the results into new forms that serve our gait generation techniques. Specifically, we define a partition over the family of simple mechanical systems. We start by defining a general type of systems, *generalized mixed systems*, which represents a superset of all the mechanical systems considered in this thesis. Then we introduce the other types of mechanical systems which are merely special cases of the generalized mixed systems type. The partition is defined in terms of additional conditions that we impose on the generalized type of mixed systems. Finally, we present the respective reconstruction equations for these mechanical systems.

Definition 37 (Generalized mixed systems) A simple mechanical system[1] that has an n-dimensional configuration space that has a trivial principal fiber bundle structure, $Q = G \times M$, where G is an l-dimensional Lie group fiber space and M is an m-dimensional base space, and that is subject to a k-dimensional set of non-holonomic constraints is said to be of the *generalized mixed* type if

1. Its Lagrangian is equal solely to the system's kinetic energy,

$$L(q, \dot{q}) = \frac{1}{2}\dot{q}^T M(q)\dot{q},$$

   where $M(q)$ is the $n \times n$ mass matrix defining the kinetic energy metric.

2. The non-holonomic constraints acting on the system can be written in a Pfaffian from

$$\omega(q)\dot{q} = 0,$$

[1] We are using Smale's definition of simple mechanical systems as presented in [51, 52],

where $\omega(q)$ is a $k \times n$ matrix describing the constraints.

3. Both the Lagrangian and the set of non-holonomic constraints are invariant with respect to the fiber group Lie actions, that is,

$$\begin{aligned} L(q,\dot{q}) &= L(\Phi_g q, T_q\Phi_g \dot{q}), \text{ and} \\ \omega(q)\dot{q} &= \omega(\Phi_g q) T_q\Phi_g \dot{q}, \end{aligned}$$

where Φ_g is the Lie group action on Q and $T_q\Phi_g$ is the lifted action on TQ.

4. Away from singular configurations of the system, the non-holonomic constraints are linearly independent, that is,

$$\det\left(\omega(q)\right) \neq 0.$$

The last requirement ensures that none of the constraints is a linear combination of the other velocity constraints.

In the rest of the thesis, we will assume that the mechanical systems we are considering are of the generalized mixed type. Before we define other sub-types of mechanical systems, we will compute the reconstruction equation. In the next chapter we will compute the momentum evolution equation for generalized mixed systems.

Note that, computing these two equations for the most general type of systems, generalized mixed systems, will simplify their respective computation for the other types of system as they are special cases of generalized mixed systems and will help us compare these sub-types of mechanical systems.

4.1 Reconstruction Equation for Generalized Mixed Systems

In this section, we compute the reconstruction equation for the generalized mixed type of mechanical systems. The results of this section can be found in the prior work, [5] and [40], however, we re-derive the same result in what we believe is a more compact way and we shall use this derivation later in the paper.

Given a generalized mixed mechanical system whose Lagrangian and non-holonomic constraints are, by definition, invariant with respect to its fiber space group action and

lifted action, then the reduced Lagrangian and reduced non-holonomic constraints are respectively given by

$$l(\xi, r, \dot{r}) = \frac{1}{2}\begin{pmatrix} \xi & \dot{r} \end{pmatrix}^T \begin{pmatrix} I & IA \\ (IA)^T & m \end{pmatrix} \begin{pmatrix} \xi \\ \dot{r} \end{pmatrix}, \tag{4.1}$$

$$0 = \bar{\omega}\begin{pmatrix} \xi \\ \dot{r} \end{pmatrix} = \begin{pmatrix} \bar{\omega}_\xi & \bar{\omega}_r \end{pmatrix}\begin{pmatrix} \xi \\ \dot{r} \end{pmatrix}, \tag{4.2}$$

where I is the local form of the locked inertia tensor, A is the local form of the mechanical connection, $\bar{\omega}_\xi$ and $\bar{\omega}_r$ are sub-matrices of the constraint matrix $\bar{\omega} = (\bar{\omega}_\xi, \bar{\omega}_r)$. All of the above matrices are independent of the fiber variable, g, and depend only on the shape variables, r. We define the *generalized non-holonomic momentum* along the allowable directions by $p = \frac{\partial l}{\partial \xi}\bar{\Omega}^T$ where $\bar{\Omega}^T$ is a basis of $\mathcal{N}(\bar{\omega}_\xi)$, the null space of $\bar{\omega}_\xi$. Then using (4.1) we have

$$p = \frac{\partial l}{\partial \xi}\bar{\Omega}^T = \left(\xi^T I^T + \dot{r}^T (IA)^T\right)\bar{\Omega}^T. \tag{4.3}$$

Note that the transpose of the generalized non-holonomic momentum has the following form

$$p^T = \begin{pmatrix} \bar{\Omega}I & \bar{\Omega}IA \end{pmatrix}\begin{pmatrix} \xi \\ \dot{r} \end{pmatrix} = \begin{pmatrix} \eta_\xi & \eta_r \end{pmatrix}\begin{pmatrix} \xi \\ \dot{r} \end{pmatrix}, \tag{4.4}$$

where the η's are functions of the base variables. Note the resemblance in structure of the reduced non-holonomic constraints in (4.2) to the generalized momentum in (4.4). Rewriting (4.2) and (4.4) we get

$$\bar{\omega}_\xi \xi = 0 - \bar{\omega}_r \dot{r} \tag{4.5}$$

$$\bar{\Omega} I \xi = p^T - \bar{\Omega} I A \dot{r} \tag{4.6}$$

The above two equations allow us to solve for a unique ξ provided that the matrix composed by stacking $\bar{\omega}_\xi$ and $\bar{\Omega}I$ is invertible as we shall show in the following Lemma.

Lemma 6 (Invertibility of the $\begin{pmatrix} \bar{\omega} & \bar{\Omega}I \end{pmatrix}^T$ matrix) *Let $\bar{\Omega}^T$ be a basis of $\mathcal{N}(\bar{\omega})$, the null space of $\bar{\omega}$, where $\bar{\omega}$ is a full row rank matrix. Moreover, let I be a symmetric positive*

definite matrix. Then the matrix composed by stacking $\bar{\omega}$ and $\bar{\Omega}I$ is invertible.

PROOF Since $\bar{\Omega}$ is full row rank and I is a symmetric positive definite matrix we conclude that $\bar{\Omega}I$ is full row rank. Moreover, since I is positive definite we know that there exists a symmetric positive definite matrix J such that $I = JJ$.

Now, suppose that the matrix $\begin{pmatrix} \bar{\omega} & \bar{\Omega}I \end{pmatrix}^T$ is singular, then we have $\mathcal{R}(\bar{\omega}) \cap \mathcal{R}(\bar{\Omega}I) \neq \varnothing$ where $\mathcal{R}(\bar{\omega})$ is the range space of $\bar{\omega}$. Let $z = (x, y) \in R(\bar{\omega}) \cap \mathcal{R}(\bar{\Omega}I)$ where x and y are nonzero, then we have

$$\begin{aligned} x^T\bar{\omega} &= y^T\bar{\Omega}I, \\ x^T\bar{\omega}J^{-1} &= y^T\bar{\Omega}(JJ)J^{-1} = y^T\bar{\Omega}J. \end{aligned}$$

Now consider the product of the following matrices

$$\begin{aligned} (x^T\bar{\omega}J^{-1})(y^T\bar{\Omega}J)^T &= x^T\bar{\omega}J^{-1}J^T\bar{\Omega}^T y, \\ &= x^T\bar{\omega}J^{-1}J\bar{\Omega}^T y, \\ &= x^T\bar{\omega}\bar{\Omega}^T y = 0, \end{aligned}$$

since the columns of $\bar{\Omega}^T \in \mathcal{N}(\bar{\omega})$. Therefore, the matrices $(x^T\bar{\omega}J^{-1})$ and $(y^T\bar{\Omega}J)$ are orthogonal. Moreover, we proved that the two matrices are identical, hence, $(x^T\bar{\omega}J^{-1}) = (y^T\bar{\Omega}J) = 0$. Since, both $(\bar{\omega}J^{-1})$ and $(\bar{\Omega}J)$ are full row rank (J is nonsingular) then $x = 0$ and $y = 0$, which contradicts our assumption. Thus, we conclude that $\begin{pmatrix} \bar{\omega} & \bar{\Omega}I \end{pmatrix}^T$ must be nonsingular.

■

Having proved that the matrix composed by stacking $\bar{\omega}_\xi$ and $\bar{\Omega}I$ is invertible, we use (4.5) and (4.6) to solve for ξ to arrive at

$$\xi = -\begin{pmatrix} (\bar{\omega}_\xi)^{k\times l} \\ (\bar{\Omega}I)^{(l-k)\times l} \end{pmatrix}^{-1} \begin{pmatrix} (\bar{\omega}_r)^{k\times m} \\ (\bar{\Omega}IA)^{(l-k)\times m} \end{pmatrix} \dot{r} + \begin{pmatrix} \bar{\omega}_\xi \\ \bar{\Omega}I \end{pmatrix}^{-1} \begin{pmatrix} \mathbf{0}^{k\times 1} \\ (p^T)^{(l-k)\times 1} \end{pmatrix} \quad (4.7)$$

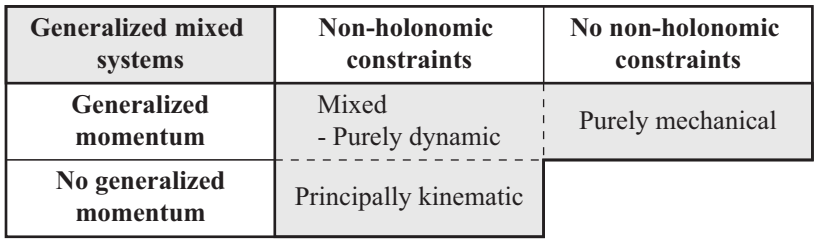

Figure 4.1: A diagram depicting the various types of mechanical systems.

This is the reconstruction equation for generalized mixed systems. Note that, the matrices multiplying both the base velocity, $\dot{r}$, and the generalized momentum variable, p, are independent on the group variable, g, and depend solely on the base variable, r. Next, we define other specific types of mechanical systems and compute their reconstruction equations.

4.2 Sub-types of Mixed Systems

Here, we define sub-types of mechanical systems (Fig. 4.1) by imposing additional conditions on the dimensions of fiber and base spaces and the number of non-holonomic constraints. We start with mixed systems which were mentioned in the [5, 40].

Definition 38 (Mixed systems) Mixed systems are systems that belong to the generalized mixed system family and additionally have at least one non-holonomic constraint and at most one less non-holonomic constraints than the dimension of the fiber space, that is,

$$0 < k < l$$

where l is the dimension of the fiber space and k is the number of non-holonomic velocity constraints acting on the system.

Mixed systems are mechanical systems that do not have enough non-holonomic constraints to fully span the fiber space. Thus, there should exist directions of motion that are "orthogonal" to all the non-holonomic constraints acting on the system. Along these allowable directions, we can define generalized momentum variables that are instantaneously

conserved and are governed by a first order differential equation as we shall show in the next chapter.

As for the reconstruction equation for mixed systems, we regroup terms we can rewrite (4.7) as follows

$$\xi = -\mathbf{A}(r)\dot{r} + \Gamma(r)p^T, \tag{4.8}$$

where $\mathbf{A}(r)$ is an $l \times m$ matrix that represents the local form of the *mixed connection* and $\Gamma(r)$ is an $l \times (l-k)$ matrix multiplying the transpose of the generalized non-holonomic momentum. Thus, only using the non-holonomic constraints, $\bar{\omega}_\xi$ and $\bar{\omega}_r$, as well as the components of reduced mass matrix, I and IA, we compute the local form of the mixed connection $\mathbf{A}(r)$ as shown in (4.7).

The next sub-type of mechanical systems we define is for the case when we have enough non-holonomic constraints to completely specify the systems velocity.

Definition 39 (Principally kinematic systems) Principally kinematic systems[2] are systems that have just enough non-holonomic constraints to fully span the fiber space, that is,

$$k = l$$

where l is the dimension of the fiber space and k is the number of non-holonomic velocity constraints acting on the system.

In other words, for principally kinematic systems the non-holonomic constraints are sufficient to fully specify the systems' fiber velocity for a given base velocity. We can clearly see this by computing the reconstruction equation for principally kinematic systems. Setting $l = k$ in (4.7) we can see that there will be no generalized momentum variables. Thus, (4.7) reduces to

$$\xi = -\bar{\omega_\xi}^{-1}\bar{\omega}_r\dot{r} = -\mathbb{A}(r)\dot{r}, \tag{4.9}$$

where $\mathbb{A}(r)$ is an $l \times m$ matrix that represents local form of the *principal connection*. Next, we define a third sub-type of mechanical systems which belong to the opposite end of the spectrum across from principally kinematic systems, that is, these systems are not subject to any non-holonomic constraints.

[2]Sometimes, these systems are referred to as *Chaplygin*.

Definition 40 (Purely mechanical systems) Purely mechanical systems are systems that have no non-holonomic constraints acting on the system, that is,

$$k = 0$$

where k is the number of non-holonomic velocity constraints action on the system.

Thus, for purely mechanical systems, setting $k = 0$ in (4.7), the reconstruction equation reduced to

$$\xi = -A(r)\dot{r} + I^{-1}(r)p^T, \tag{4.10}$$

where $A(r)$ is an $l \times m$ matrix that represents local form of the *mechanical connection* and $I(r)$ is an $l \times l$ matrix that represents local form of *locked inertia tensor*.

Later in the thesis, we will impose an additional condition on purely mechanical system to simplify their reconstruction equation. More specifically, we ensure that there are no external forces acting on the system and that the system starts from rest. This will force all the momentum variables to start and stay at zero for all time. Thus, for such purely mechanical systems, the reconstruction equation simplifies to

$$\xi = -A(r)\dot{r}, \tag{4.11}$$

where $A(r)$ is an $l \times m$ matrix that represents local form of the *mechanical connection*. Note the similar structure of the reconstruction equations for both principally kinematic and purely mechanical systems in (4.9) and (4.11), respectively. Finally, we will introduce one last sub-type of mechanical systems.

Definition 41 (Purely dynamic systems) Purely dynamic are a special family of the mixed type of systems whose base space is one-dimensional, that is,

$$m = 1,$$

where m is the dimension of the base space M.

What is unique about purely dynamic systems is the fact that for cyclic gaits, their motion is attributed solely to the dynamic part of the reconstruction equation of the mixed type systems, $\Gamma(r)p^T$. Recall, that ξ is a base space velocity at the group identity. Later in this dissertation, we shall be integrating the reconstruction equations to generate gaits.

System type	Condition	Reconstruction equation
Mixed	$0 < l < k$	$\xi = -\mathbf{A}(r)\dot{r} + \Gamma(r)p^T$
Principally kinematic	$l = k$	$\xi = -\mathbb{A}(r)\dot{r}$
Purely mechanical	$k = 0$ and $p(t) = 0$	$\xi = -A(r)\dot{r}$
Purely dynamic	$m = 1$	$\xi = \Gamma(r)p^T$

Table 4.1: A list of the types of mechanical systems and their respective reconstruction equations.

Hence, if we integrate the reconstruction equation of purely dynamic systems over a *closed* curve, we can clearly see that the first term in (4.12) is equal to zero since

$$\int_0^\tau \mathbf{A}^i(r)\dot{r}dt = \oint_{r(0)}^{r(\tau)} \mathbf{A}^i(r)dr = 0,$$

where $r(0) = r(\tau)$. Hence, if we are considering cyclic gaits, which is the case for this entire thesis, the reconstruction equation for purely dynamic systems reduces to

$$\xi = \Gamma(r)p^T, \tag{4.12}$$

where $\Gamma(r)$ is an $l \times (l - k)$ matrix multiplying the transpose of the generalized non-holonomic momentum variable, p.

We have summarized the various types of mechanical systems we have presented in this chapter in Table 4.1. Moreover, Fig. 4.1 depicts the various types of mechanical systems and their relations to each others.

Chapter 5

Generalized and Scaled Momentum

In Chapter 4, we presented a classification of several types of mechanical systems and presented their respective reconstruction equations. In this chapter, we present the respective generalized momentum evolution equations for these various types of mechanical systems.

In earlier chapters, we utilized the structure of the configuration space to devise a relationship between of base and fiber velocities. This relation is represented by the reconstruction equation. Here we invoke another tool to further simplify the dynamic equations of motion. We utilize symmetry of the laws of physics to actually reduce the order of the equations of motion along the fiber directions. The reduction is done by representing the dynamics in terms of a generalized momentum variable, thus, reducing the order of the governing differential equations of motion. Finally, for a certain general family of mechanical systems, we present and even simpler representation of the fiber space dynamics. This is done by introducing a scaled momentum variable and expressing the dynamics in terms of it. In later chapters, we shall see how representing the dynamics in terms of the scaled momentum variable simplifies our approach to the gait generation problem.

5.1 Reduced Dynamics of Mechanical Systems

In this section, we take recourse to mechanics of locomotion and recall several useful results. Mainly, we present the reduced dynamic equations of motion for simple mechanical systems that are subject to a set of non-holonomic velocity constraints. The results presented in this section are similar to those presented in Section 3.3 in Chapter 3 where unconstrained systems were analyzed.

The main idea of reducing the equations of motion is to utilize the Lagrangian in-

variance as well as the non-holonomic constraints invariance to rewrite the equations of motion at the Lie group identity. This eliminates any fiber configuration variables from the equations of motions and allows the base dynamics to be expressed solely in terms of the base variables. Note that, since the new set of dynamic equations, the reduced base dynamics and the momentum evolution equations, are independent of the fiber variables, we use the reconstruction equations presented in the previous chapter to reconstruct the fiber variables from the base and momentum variable.

Recall the equations of motion for mechanical systems that are subject to non-holonomic constraints are shown in (3.13). Rewriting these equations at the group identity is given in the following Proposition.

Proposition 4 (Reduced momentum evolution equation) *For a generalized mixed system, that is, the configuration space has a trivial principal fiber bundle, $Q = G \times M$, and the Lagrangian, as well as the set of non-holonomic constraints acting on the system, are invariant with respect to the Lie group actions, the dynamic equations of motion evaluated at the Lie group identity have the following form*

$$\frac{d}{dt}\left(\frac{\partial l}{\partial \xi^a}\right) - ad^*_\xi \frac{\partial l}{\partial \xi^a} = \left(\lambda_c \omega^c_b + \tau_b\right)\left(T_e L_g\right)^b_a , \tag{5.1}$$

$$\frac{d}{dt}\left(\frac{\partial l}{\partial \dot{r}^a}\right) - \frac{\partial l}{\partial r^a} = \lambda_c \omega^c_i + \tau_i, \tag{5.2}$$

where l is the reduced Lagrangian, ξ is a Lie algebra element or a fiber velocity at the group identity such that $\xi = T_g L_{g^{-1}} \dot{g}$, ω is the matrix representing the non-holonomic constraints, and λ is the a vector representing the constraint forces. The term ad^*_ξ is the "derivative" of the lifted adjoint map, Ad_g[1].

We will not provide a rigorous proof for this above proposition as it was presented in Proposition 3.12 in [40]. However, we will present a sketch of the proof, but before that we shall present the following Lemma.

Lemma 7 (Pfaffian constraints at the group identity) *For a mechanical system whose configuration space has a* trivial *principal fiber bundle, $Q = G \times M$, and whose Lagrangian as well as the set of non-holonomic constraints acting on the system are invariant with*

[1]For $\xi, \eta \in \mathfrak{g}$, $ad_\xi \eta = [\xi, \eta]$ which can be computed using the structure constants of the Lie algebra. Then $ad^*_\xi p$ is the dual map to $ad_\xi \eta$ [40].

respect to the Lie group actions, the Pfaffian non-holonomic constraints are expressed in the following form

$$\omega(q)^c_b \left(T_e L_g\right)^b_a \xi^a + \omega(q)^c_d \dot{r}^d = 0 \tag{5.3}$$

PROOF The Pfaffian non-holonomic constraints are expressed as $\omega(q)\dot{q} = 0$. Using the triviality of the configuration space we can write the non-holonomic constraints in coordinate as follows

$$\begin{aligned} 0 &= \omega(q)^c_b \dot{q}^b \\ &= \omega(q)^c_b \dot{g}^b + \omega(q)^c_d \dot{r}^d \\ &= \omega(q)^c_b \left(T_e L_g\right)^b_a \xi^a + \omega(q)^c_d \dot{r}^d \\ &= \omega(e,r)^c_b \left(T_e L_g\right)^b_a \xi^a + \omega(e,r)^c_d \dot{r}^d \end{aligned}$$

■

Moreover, we proved in (3.21) that the invariance of the constraints with respect to the Lie group action allows us to express the constraints in body coordinates where we have

$$0 = \left(\bar{\omega}_\xi\right)^c_a \xi^a + \left(\bar{\omega}_r\right)^c_d \dot{r}^d$$

Thus, we conclude that $\left(\bar{\omega}_\xi\right)^c_a = \omega(q)^c_b \left(T_e L_g\right)^b_a$ and $\left(\bar{\omega}_r\right)^c_d = \omega(q)^c_d$ which we shall use later.

PROOF (SKETCH OF THE PROOF OF PROPOSITION 4) The main idea for this proof is to rewrite the dynamic equations of motion at the Lie group identity using a change of variables, $g \to \xi$. Next, we provide the first steps of writing the fiber space equations of motion at the group identity. We start by rewriting the first two terms of the Euler-Lagrange equations of motion, $\frac{d}{dt}\left(\frac{\partial L}{\partial \dot{g}}\right)$ and $\frac{\partial L}{\partial g}$.

$$\begin{aligned}\frac{d}{dt}\left(\frac{\partial L}{\partial \dot{g}}\right) &= \frac{d}{dt}\left(\frac{\partial l}{\partial \xi}\frac{\partial \xi}{\partial \dot{g}}\right) \\ &= \frac{d}{dt}\frac{\partial l}{\partial \xi}\left(T_g L_{g^{-1}}\right) + \frac{\partial l}{\partial \xi}\frac{d}{dt}\left(T_g L_{g^{-1}}\right) \\ &= \frac{d}{dt}\frac{\partial l}{\partial \xi}\left(T_g L_{g^{-1}}\right) + \frac{\partial l}{\partial \xi}\frac{\partial}{\partial g}\left(T_g L_{g^{-1}}\right)\dot{g}\end{aligned}$$

Here, we used the fact that $\xi = T_g L_{g^{-1}}\dot{g}$. Similarly, the second term of the equations of motion is rewritten as

$$\begin{aligned}\frac{\partial L}{\partial g} &= \frac{\partial l}{\partial \xi}\frac{\partial \xi}{\partial g} \\ &= \frac{\partial l}{\partial \xi}\frac{\partial\left(T_g L_{g^{-1}}\right)}{\partial g}\dot{g} \\ &= \frac{\partial l}{\partial \xi}\frac{\partial\left(T_g L_{g^{-1}}\right)}{\partial g}\left(T_e L_g\right)\xi\end{aligned}$$

Then, we substitute the above two terms into the original equations of motion, (3.13), and solve for the term $\frac{d}{dt}\frac{\partial l}{\partial \xi}$. Thus, it is clear that we have to post multiply by the matrix $(T_e L_g)$. This explains the fact what the constraints matrix and the generalized forces are post multiplied by $(T_e L_g)$ in the right hand side of (5.1). Finally, we can see that the term $ad^*_\xi \frac{\partial l}{\partial \xi}$ represents all the other leftover terms as was shown in [40].

■

5.2 Momentum Evolution Equation

Thus far, we were able to write the equation of motion on the fiber space in terms of the generalized momentum variable $p = \frac{\partial l}{\partial \xi}$. Next, we express the same equations of motion, nonetheless, using the generalized non-holonomic momentum variable, $p = \frac{\partial l}{\partial \xi}\bar{\Omega}^T$. Moreover, we verify that the first derivative of p is equal to a quadratic expression in the generalized non-holonomic momentum and base velocity variables.

Proposition 5 (Momentum evolution equation) *For a mechanical system whose configuration space has a trivial principal fiber bundle, $Q = G \times M$, and whose Lagrangian as well as the set of non-holonomic constraints acting on the system are invariant with respect to the Lie group actions, the dynamic equations of motion evaluated at the Lie group*

identity expressed using the non-holonomic generalized momentum will have the following form

$$\dot{p}_c = \dot{r}^T \left(\sigma_{\dot{r}\dot{r}}\right)_c \dot{r} + \dot{r}^T \left(\sigma_{\dot{r}p}\right)_c p + p^T \left(\sigma_{pp}\right)_c p \tag{5.4}$$

where p_c is the c^{th} column of p and the σ's are matrices of appropriate dimensions whose components are functions solely of the base variables, r.

PROOF Recall that the non-holonomic generalized momentum is given by $p = \frac{\partial l}{\partial \xi}\bar{\Omega}^T$, where $\bar{\Omega}^T$ is a basis element of the null space of $(\bar{\omega}_\xi)$, that is,

$$\begin{aligned} 0 &= \left(\bar{\omega}_\xi\right)_a^c \left(\bar{\Omega}^T\right)_c^a \\ &= \omega_b^c \left(T_e L_g\right)_a^b \left(\bar{\Omega}^T\right)_c^a \end{aligned}$$

Computing the derivative the c^{th} element of the non-holonomic generalized momentum, p, we get

$$\dot{p}_c = \frac{\partial l}{\partial \xi^a}\frac{d}{dt}\left(\bar{\Omega}^T\right)_c^a + \frac{d}{dt}\left(\frac{\partial l}{\partial \xi^a}\right)\left(\bar{\Omega}^T\right)_c^a. \tag{5.5}$$

Now, we Substitute (5.1) into (5.5) and solving for $\dot{p}_c$ to arrive at

$$\begin{aligned} \dot{p}_c &= \frac{\partial l}{\partial \xi^a}\frac{d}{dt}\left(\bar{\Omega}^T\right)_c^a - \left(ad_\xi^* \frac{\partial l}{\partial \xi^a} - \lambda_c \omega_b^c \left(T_e L_g\right)_a^b\right)\left(\bar{\Omega}^T\right)_c^a, \\ &= \frac{\partial l}{\partial \xi^a}\frac{d}{dt}\left(\bar{\Omega}^T\right)_c^a - ad_\xi^* \frac{\partial l}{\partial \xi^a}\left(\bar{\Omega}^T\right)_c^a + \lambda_c \omega_b^c \left(T_e L_g\right)_a^b \left(\bar{\Omega}^T\right)_c^a, \\ &= \frac{\partial l}{\partial \xi^a}\frac{d}{dt}\left(\bar{\Omega}^T\right)_c^a - ad_\xi^* \frac{\partial l}{\partial \xi}\left(\bar{\Omega}^T\right)_c, \\ &= \frac{\partial l}{\partial \xi^a}\frac{d}{dt}\left(\bar{\Omega}^T\right)_c^a - \frac{\partial l}{\partial \xi}[\xi, \left(\bar{\Omega}^T\right)_c], \\ &= \frac{\partial l}{\partial \xi^a}\frac{d}{dt}\left(\bar{\Omega}^T\right)_c^a - \frac{\partial l}{\partial \xi^a}[\xi, \left(\bar{\Omega}^T\right)_c]^a, \\ &= \frac{\partial l}{\partial \xi^a}\frac{d}{dt}\left(\bar{\Omega}^T\right)_c^a - \frac{\partial l}{\partial \xi^a} C_{de}^a \xi^d \left(\bar{\Omega}^T\right)_c^e, \\ &= \frac{\partial l}{\partial \xi^a}\left(\frac{d}{dt}\left(\bar{\Omega}^T\right)_c^a - C_{de}^a \left(\bar{\Omega}^T\right)_c^e \xi^d\right). \end{aligned}$$

Here, we used the fact that $\omega_b^c \left(T_e L_g\right)_a^b \left(\bar{\Omega}^T\right)_c^a = 0$ by definition and we used the prop-

erty of the adjoint map $ad^*_\xi \frac{\partial l}{\partial \xi} = \frac{\partial l}{\partial \xi}[\xi, .]$ Moreover, we used the structure constants of the Lie algebra to compute the Lie bracket, that is, $[\xi, \eta]^a = C^a_{bc}\xi^b\eta^c$. Next, we compute the term $\frac{d}{dt}\left(\bar{\Omega}^T\right)^a_c$ to arrive at

$$\frac{d}{dt}\left(\bar{\Omega}^T\right)^a_c = \frac{\partial\left(\bar{\Omega}^T\right)^a_c}{\partial r^e}\dot{r}^e.$$

Recall that, using the reconstruction equation for generalized mixed systems, (4.12), we can computed the fiber velocity expressed in body coordinates which we rewrite as

$$\begin{aligned}
\xi^d &= -\mathbf{A}^d_e\dot{r}^e + \Gamma^d_e\left(p^T\right)^e \text{ and} \\
\left(\xi^T\right)_e &= \left(\xi^e\right)^T = -\left(\dot{r}^T\right)_f\left(\mathbf{A}^T\right)^f_e + p_f\left(\Gamma^T\right)^f_e.
\end{aligned}$$

Now, we utilize both the expression of the reduced Lagrangian, (4.1), to compute the term $\frac{\partial l}{\partial \xi^a}$ to get

$$\begin{aligned}
\frac{\partial l}{\partial \xi^a} &= \left(\xi^T\right)_e\left(I^T\right)^e_a + \left(\dot{r}^T\right)_f\left(A^T I^T\right)^f_a, \\
&= \left(-\left(\dot{r}^T\right)_f\left(\mathbf{A}^T\right)^f_e + p_f\left(\Gamma^T\right)^f_e\right)\left(I^T\right)^e_a + \left(\dot{r}^T\right)_f\left(A^T I^T\right)^f_a, \\
&= \left(\dot{r}^T\right)_f\left(\left(A^T I^T\right)^f_a - \left(\mathbf{A}^T\right)^f_e\left(I^T\right)^e_a\right) + p_f\left(\Gamma^T\right)^f_e\left(I^T\right)^e_a, \\
&= \left(\dot{r}^T\right)_f\left(\left(A^T - \mathbf{A}^T\right)I^T\right)^f_a + p_f\left(\Gamma^T I^T\right)^f_a.
\end{aligned}$$

Substituting back into the equation of p_c we arrive at

$$\begin{aligned}
\dot{p}_c &= \left(\left(\dot{r}^T\right)_f\left(\left(A^T - \mathbf{A}^T\right)I^T\right)^f_a + p_f\left(\Gamma^T I^T\right)^f_a\right) \\
&\qquad \left(\frac{\partial\left(\bar{\Omega}^T\right)^a_c}{\partial r^e}\dot{r}^e - C^a_{de}\left(\bar{\Omega}^T\right)^e_c\left(-\mathbf{A}^d_e\dot{r}^e + \Gamma^d_e\left(p^T\right)^e\right)\right) \\
&= \dot{r}^T\left(\sigma_{\dot{r}\dot{r}}\right)_c\dot{r} + \dot{r}^T\left(\sigma_{\dot{r}p}\right)_c p + p^T\left(\sigma_{pp}\right)_c p
\end{aligned}$$

where the σ's have the following expressions

$$
\begin{aligned}
(\sigma_{\dot{r}\dot{r}})_c &= \left(\left(A^T - \mathbf{A}^T\right) I^T\right)_a \left(\frac{\partial \left(\bar{\Omega}^T\right)_c^a}{\partial r} + C_{de}^a \left(\bar{\Omega}^T\right)_c^e \mathbf{A}^d\right) \\
(\sigma_{\dot{r}p})_c &= -\left(\left(A^T - \mathbf{A}^T\right) I^T\right)_a C_{de}^a \left(\bar{\Omega}^T\right)_c^e \Gamma^d + \left(\Gamma^T I^T\right)_a \left(\frac{\partial \left(\bar{\Omega}^T\right)_c^a}{\partial r} + C_{de}^a \left(\bar{\Omega}^T\right)_c^e \mathbf{A}^d\right) \\
(\sigma_{pp})_c &= -\left(\Gamma^T I^T\right)_a C_{de}^a \left(\bar{\Omega}^T\right)_c^e \Gamma^d
\end{aligned}
$$

■

Recall that for certain types of mechanical systems, the reconstruction equation is a function of the generalized momentum as shown in Table 4.1. Even though, we proved that the evolution momentum equation is a first order differential equation and the first derivative of the generalized momentum is equal to the quadratic term we presented above, this equation does not furnish a closed form solution. Thus, the above equation is not as helpful as we wished for utilizing to solve for the generalized momentum. Next we define a new momentum variable that will allow us to rewrite the reconstruction and momentum evolution equations in "useful" forms to apply our gait generation technique.

5.3 Scaled Momentum

In this section, we introduce a novel scaled momentum variable. For a certain family of mechanical systems, expressing the momentum evolution equation in terms of this novel momentum variable simplifies it even more. This simplification allows us to easily verify the sign definiteness of the scaled momentum variable which we utilize to eventually generate gaits for mechanical systems as we shall see in the next chapter.

Before we define this novel momentum variable, we will make the following assumption which will be assumed true for the rest of the thesis unless otherwise specified.

Assumption 1 (One-dimensional generalized momentum) *We assume that for all the mechanical systems considered in this thesis the dimension of fiber space is one more than the number of non-holonomic constraints action on the system, that is,*

$$l - k = 1,$$

where l is the dimension of the fiber space and k is the number of non-holonomic constraints acting on the system.

For such systems, only one generalized non-holonomic momentum variable exists. This is clear from the definition of the generalized non-holonomic momentum where $p = \frac{\partial l}{\partial \xi}\bar{\Omega}^T$ since $\bar{\Omega}$ is an $(l-k) \times l = 1 \times l$ matrix. Moreover, Ostrowski in [40] proved that for such systems, the term σ_{pp} in (5.4) is equal to zero . Hence, for such system, the momentum evolution equation (5.4) reduces to

$$\dot{p} = \dot{r}^T \sigma_{\dot{r}\dot{r}} \dot{r} + \dot{r}^T \sigma_{\dot{r}p} p \tag{5.6}$$

Note that we removed the c subscript since we only have one momentum variable. Next, we define the new scaled momentum variable.

Definition 42 (Scaled momentum variable) For mechanical system whose momentum evolution equation has the from given in (5.6), define the scaled momentum variable,

$$\rho = f(r)p \tag{5.7}$$

such that $f(r)$ is an integrating factor[2] of the first order differential equation (5.6).

Using this novel scaled momentum variable, we can rewrite the momentum evolution equation in an even more simplified from presented in the following Lemma.

Lemma 8 (Scaled momentum evolution equation) *For generalized mixed mechanical systems that have one less non-holonomic velocity constraints than the dimension of the systems fiber space, the momentum evolution equation has the following form*

$$\boxed{\dot{\rho} = \dot{r}^T \Sigma(r) \dot{r}} \tag{5.8}$$

where ρ is the scaled momentum variable, and Σ is an $m \times m$ matrix whose components are a function of the base variables where m is the dimension of the base space.

PROOF Taking the derivative of the scaled momentum variable given in (5.7) we arrive at

[2]Integrating factors allow us to rewrite first order differential equations of the form $dp/dt = f(r, p, \dot{r})$ as $d(h(r)p)/dt = \bar{f}(r, \dot{r})$, [54].

$$\begin{aligned}\dot{\rho} &= \frac{d}{dt}\left(f(r)p\right) \\ &= f(r)\dot{p} + \frac{\partial f}{\partial r}\dot{r}p \\ &= f(r)\left(\dot{p} + \frac{\partial f/\partial r}{f}\dot{r}p\right)\end{aligned}$$

Moreover, since f is an integrating factor of (5.6), we know that $\frac{\frac{\partial f}{\partial r}}{f(r)} = -\sigma_{\dot{r}p}$. Substituting into the above equation we get

$$\begin{aligned}\dot{\rho} &= f(r)\left(\dot{r}^T\sigma_{\dot{r}\dot{r}}\dot{r}\right) \\ &= \dot{r}^T\Sigma(r)\dot{r}\end{aligned}$$

where $\Sigma(r) = f(r)\sigma_{\dot{r}\dot{r}}$.

■

Finally, we can rewrite the reconstruction equations for mixed systems in terms of the scaled momentum variable to get

$$\xi = -\mathbf{A}(r)\dot{r} + \bar{\Gamma}(r)\rho, \tag{5.9}$$

where $\bar{\Gamma}(r) = \Gamma(r)/f(r)$. Now that we have written the reconstruction and momentum evolution equations in terms of the scaled momentum variable, we are ready to generate gaits by studying and analyzing the three terms, $\mathbf{A}(r)$, $\bar{\Gamma}(r)$, and $\Sigma(r)$.

Chapter 6

Gait Generation

In this chapter, we utilize both the momentum evolution equation, (5.8) as well as the reconstruction equation, (5.9) to evaluate the motion due to any closed curve in the base space. We start with by integrating the reconstruction equation of generalized mixed mechanical systems, the most general type of mechanical systems, and then relating position change expressed in body coordinated to two decoupled quantities, the geometric and dynamic phase shift. Thus, the main idea in this chapter is how to intuitively evaluate the values of these shifts, so that we can use these evaluation tools to actually generate gaits.

Our approach is to relate the value of geometric phase shift to the volume under a well-defined *height function* which is bounded by a proposed closed base space curve. As for the dynamic phase shift, we utilize the new scaled momentum variable as well as another set of well-defined *gamma functions* to intuitively evaluate the dynamic shift value to a closed base space curve. Finally, we utilize both evaluation tools for computing the geometric and dynamic phase shift to actually synthesize and generate gaits for mixed non-holonomic system. We start this chapter by defining a base space gait as follows:

Definition 43 (Gait) We define a gait to be a continuous closed curve, ϕ, in the base space, M, that is,

$$\begin{aligned} \phi \quad : \quad & \mathbb{R} \to M, \\ & t \mapsto r, \end{aligned}$$

such that $\phi(t) = \phi(t + \tau)$, where $\tau \in \mathbb{R}$ is the period of the gait.

Thus, since all gaits are periodic, after each period of time, the mechanical system

returns to the same point in the base space, that is, it retains the same shape at the end of each cycle. Since our gait generation analysis requires that the mechanical system can perform any gait or curve in the base space, we will assume that the actuation of the underactuated mechanical system occurs on the base space, that is, we assume that the base space is fully actuated as presented in the following assumption.

Assumption 2 (Fully actuated base space) *We assume that all the base variables are fully actuated, that is, we assume that we can independently control each of the base configuration variables.*

6.1 Geometric and Dynamic Phase Shift

In Chapter 4, for generalized mixed systems, we related the fiber velocity, expressed in body coordinates, ξ, to two decoupled quantities as shown in (4.7). Then in Chapter 5 we defined a new scaled momentum variable which changed the expression of the reconstruction equation, nonetheless, the right hand side was still composed of two terms as shown in (5.9).

Define the variable ζ as the integral of ξ, that is, $\dot{\zeta} = \xi$. Thus, integrating the i^{th} row of the reconstruction equation (5.9) with respect to time we get

$$\begin{aligned}
\Delta\zeta^i &= \int_{t_0}^{t_1} \dot{\zeta}^i dt = \int_{t_0}^{t_1} \xi^i dt \\
&= \int_{t_0}^{t_1} \left(-\sum_{j=1}^{m} \mathbf{A}_j^i(r)\dot{r}^j + \sum_{j=1}^{l-k} \bar{\Gamma}_j^i(r)\rho^j \right) dt \\
&= \oint_{r(t_0)}^{r(t_1)} \left(-\sum_{j=1}^{m} \mathbf{A}_j^i(r) \right) dr^j + \int_{t_0}^{t_1} \left(\sum_{j=1}^{l-k} \bar{\Gamma}_j^i(r)\rho^j \right) dt
\end{aligned} \tag{6.1}$$

where we transformed the first integral from a time definite integral to a line integral of an m-dimensional one-form. Next, along the i^{th} fiber direction, we define the geometric phase shift, I^i_{GEO}, and dynamic phase shift, I^i_{DYN}, respectively as the values of the first and second integrals in (6.1), that is,

$$I^i_{GEO} = \oint_{r(t_0)}^{r(t_1)} \left(-\sum_{j=1}^{m} \mathbf{A}^i_j(r) \right) dr^j, \tag{6.2}$$

$$I^i_{DYN} = \int_{t_0}^{t_1} \left(\sum_{j=1}^{l-k} \bar{\Gamma}^i_j(r) \int \left(\dot{r}^T \Sigma(r) \dot{r} \right)^j dt \right) dt, \tag{6.3}$$

where we substituted for the value of the scaled momentum, ρ, using (5.8). Hence, the position change expressed in body coordinates is equal to the sum of the two phase shifts, that is,

$$\Delta\zeta^i = I^i_{GEO} + I^i_{DYN} \tag{6.4}$$

6.2 Evaluation of the Geometric and Dynamic Phase Shifts

Thus far, we equated the position change due to any base-space curve to *two* decoupled terms I_{GEO} and I_{DYN}. In this section, we present how to design curves in such a way to ensure that the any of these terms is non-zero along a specified fiber direction, that is, we effectively present two evaluation techniques that allow us to propose base space curves that ensure either the geometric phase shift, the dynamic phase shift, or both are non-zero.

Later in this chapter, we define a partition on the space of allowable gaits such that the motion of the system is exclusively due to either of the phase shifts, I_{GEO} or I_{DYN}, or both. Thus, we can simply use the evaluation tools presented in this section to generate such families of gaits.

6.2.1 Geometric Phase Shift Evaluation

In this section, we synthesize gaits that yield a non-zero geometric phase shift, (6.2), along the specified fiber direction, that is, $I^i_{GEO} \neq 0$. Actually, there are two approaches for synthesizing geometric gaits. The first of which is by defining a variational problem whose solution constitutes an optimal gait. Rather than numerically solving this constrained variational problem, which we present as part of our future work in Section 9.5, we chose a second more intuitive approach. In fact, this second approach uses Stokes' theorem to

transform the line integral in (6.2) to a volume integral. This will provide us with a simple gait evaluation technique that measures the geometric or kinematic motion contribution due to *any* closed curve in the base space. This evaluation tool is simple enough that we can utilize it to actually synthesize gaits.

Note that the integrand in (6.2), $\sum_j \mathbf{A}^i_j(r)dr^j$, is a one-form, hence, we can use Stokes' theorem to transform the integral to an integral of a two-form which is the exterior derivative of the original one-form. Thus, we rewrite the change in position due to the geometric phase and expressed in body coordinated as

$$\begin{aligned} I^i_{GEO} &= \int\int_\Phi \sum_{o,j=1,o<j}^{m} \left(\bar{\mathbf{A}}^{\,i}_{oj}(r)\right) dr^o dr^j \\ &= \sum_{o,j=1,o<j}^{m} \int\int_\Phi \bar{\mathbf{A}}^{\,i}_{oj}(r) dr^o dr^j, \end{aligned} \tag{6.5}$$

where Φ is the region enclosed by the gait ϕ and $\bar{\mathbf{A}}^{\,i}_{oj}(r)$ are the components of the two-form given in (2.9). Thus, the integrand of (6.5) is a two-from and I^i_{GEO} computes the volume integral of the two-from over Φ which is the interior of a region on an arbitrary two-surface bounded by ϕ.

Note that, I^i_{GEO} is equated to the volume under what we term as *height functions*, which are the components of the two-form. We label these height functions by $F^i_{oj} = \bar{\mathbf{A}}^{\,i}_{oj}$. Hence, we have equated the position change for any closed curve in the base space, ϕ, to the volume that this curve envelopes under several well-defined functions. These height functions are simply composed of partial derivatives of the components of the mixed connection matrix, $\mathbf{A}(r)$, with respect to the base variables. By studying the properties of these height functions we are actually able to design curves that produce a desired non-zero I^i_{GEO}.

Thus, we synthesize gaits by only analyzing the components of the two-form $\bar{\mathbf{A}}^{\,i}_{oj}(r)$. We refer to these gaits as *geometric* since the motion to the system is solely due to the geometric phase shift of the designed gait. At this point, for simplicity we make the second main assumption in this thesis.

Assumption 3 (Two-dimensional base space) *we assume that the base space, M, is two-dimensional, that is,*

$$m = 2,$$

where m is the dimension of the base space.

This assumption allows us to easily think about the volume integrals, I_{GEO}, as simply computing the volume under the graph of the *height functions* in the two dimensional base space. Thus, using Green's theorem, the two-dimensional version of Stokes' theorem, we define the height functions for each fiber direction as

$$F_i(r^1, r^2) = \frac{\partial \mathbf{A}_2^i}{\partial r_1} - \frac{\partial \mathbf{A}_1^i}{\partial r_2}, \tag{6.6}$$

where $\mathbf{A}_j^i$'s are the components of the mixed non-holonomic connection. Then the position change due to the geometric phase shift, I_{GEO}, is given by

$$I_{GEO}^i = \int\int_{\Phi} F_i(r^1, r^2) dr^1 dr^2, \tag{6.7}$$

By studying the integrands in (6.7) and by designing and placing curves in the base space, we are able to generate geometric gaits that yield a non-zero geometric phase shift along a desired direction.

We remind the reader that I_{GEO}^i is an integral of a body representation of a fiber velocity, ξ^i. Hence, it does not necessarily relate trivially to inertial position change, Δg^i. This is the case only when the fiber space has a commutative group structure, that is, the lifted action map is the identity map.

Properties of Height Functions

By studying certain properties of the integrand functions of (6.7) we are able to evaluate the motion of the system due to closed curves in the base space. We study the following properties of the height functions which we shall utilize later to actually synthesize geometric gaits.

Symmetry: We study the height functions periodicity which allows us to investigate smaller portions of the base space. Moreover, we find the set of points or lines about which the height function is even or odd. Note that, a gait that is symmetric about an odd point of the height function yields zero volume, and thus yields zero geometric phase shift. However, a gait that changes orientation as it passes through an odd point is guaranteed to have a non-zero geometric phase shift.

Signed regions: Since we are integrating a height function over a closed region, it is important to know where the height functions are positive, negative, or zero. Not

only does this allow us to control the direction of motion along the fiber but also to optimize gaits by restricting them to lie in a strictly positive or negative regions.

Unboundedness: While designing gaits, one should stay away from regions where the height functions tend to infinity. A gait that passes through such regions might yield infinite volume, that is, infinite position change for a finite shape change. Usually this is an indication that a non-holonomic constraint is being violated, or that the system has passed through a problematic singularity.

By inspecting the above properties of the height functions we are able to evaluate the position change of the robot due to following any closed curve in the base space. Note that for purely mechanical systems, the height functions are never unbounded as we prove in the following Lemma.

Lemma 9 (Height functions for purely mechanical system) *For a purely mechanical system as defined in Chapter 4, the height functions for each of the fiber variables are bounded over the entire base space.*

PROOF Recall that for purely mechanical systems, the reconstruction equation is given by $\xi = -A(r)\dot{r}$ as shown in (4.11), where $A(r)$ is local form of the mechanical connection. Moreover, we can compute $A(r)$ using the components, I and (IA), of the reduced mass matrix given in (3.19), where we know that $A = I^{-1}(IA)$. Thus, we know that the matrices I and (IA), being sub-matrices of the mass matrix, are composed of bounded analytic function of the base variables. Moreover, we know that

$$I^{-1} = \frac{\text{adj}(I)}{\det(I)},$$

where $\text{adj}(I)$ and $\det(I)$ are the adjugate[1] and determinant of I, respectively. Since, the components of $\text{adj}(I)$ are also bounded analytic functions of the base variables, the components $\text{adj}(I)(IA)$ are also bounded analytic functions of the base variables. Moreover, since I is symmetric positive definite, we know that $\det(I) \neq 0$. Thus, we conclude that the components of $\frac{1}{\det(I)}\text{adj}(I)(IA) = I^{-1}(IA) = A$ are bounded analytic functions of the base variables.

Finally, since the height function along each of the fiber directions is evaluated by taking partial derivative of each row of the local connection matrix with respect to the

[1]The transpose of the *adjugate* of a matrix A is given by $(-1)^{i+j}B^i_j$, where B^i_j is a matrix whose components are the determinants of the sub-matrices of A composed by deleting its i^{th} row and j^{th} column.

base variables, we conclude that the height functions for purely mechanical systems are bounded.

■

Synthesizing Gaits Using Height Functions

Now, we utilize the above properties of height functions to actually synthesize geometric gaits. We devise the following set of rules to generate geometric gaits

1. **Closed non-self-intersecting curves:** Any closed non-self-intersecting curve that lies entirely in a positive or negative region is guaranteed to produce a non-zero I_{GEO}.

2. **Closed self-intersecting curves:** Any closed self-intersecting curve is guaranteed to produce a non-zero I_{GEO} provided that the curve spans two regions of opposite signs, the self-intersection occurs at the zero line separating the two regions, and the curve changes orientation as it passes from one region to the other.

3. **Symmetric non-intersecting curves around "odd" points:** Let K_{odd} be the set of all points about which the height function is odd, that is, $F(k+r) = -F(k-r)$ where $k \in K_{odd}$. Then any curve symmetric with respect to points in K_{odd} will enclose equal areas in two or more adjacent regions that have opposite signs. Integrating the volume under such curves will yield zero, that is, the fiber motion for such gaits is identically zero.

4. **Symmetric intersecting curves around "even" points:** Let K_{even} be the set of all points about which the height function is even along a fixed direction, that is, $F(k+r) = F(k-r)$ where $k \in K_{even}$. For any self intersecting curve symmetric with respect to points in K_{even} along the specified direction, the intersection will occur in the set K_{even}. For curves that change orientation at the intersection point, they will enclose equal areas but of opposite signs, hence, such curves will yield zero, that is, the fiber motion for such gaits is identically zero.

Note that the first two rules are active rules which help in designing gaits that produce motion, while the last two rules are passive rule that ensure null motion of the system. All rules are equally important as we use the first two rules to produce motion along a specified height function while the last two rules are used to ensure zero motion along the rest of the height functions.

We should point our that, these rules do not impose any additional constraints on the shape of the input curves. For instance, as long as the curve stays entirely in one region and does not intersect itself, it is guaranteed to generate a non-zero fiber motion. The bigger the area enclosed by the curve within a positive or negative region, the bigger the generated geometric phase shift. This eliminates the restriction of sinusoidal inputs which was required in prior work.

6.2.2 Dynamic Phase Shift Evaluation

Now, we will analyze the second term in (6.4), to propose gaits that ensure that I_{DYN} is non-zero along a desired fiber direction. Earlier, we verified that for each fiber direction the integrand of I_{DYN} in (6.3) is composed of the product of two terms: the scaled momentum variable, ρ, and the *gamma function*, $\bar{\Gamma}^i(r)$.

In this thesis, we propose base space curves that ensure that the scaled momentum is sign definite, that is, $\rho \geq 0$ or $\rho \leq 0$. Given the sign-definiteness of the scaled momentum, we can design dynamic gaits by simply analyzing the gamma function.

As for the gamma functions, we analyze the same properties we did for the height functions as we presented in Section 6.2.1, that is, we study the gamma functions symmetry, signed regions, and unboundedness. Thus, by picking gaits that are located in a same signed region of one of the gamma functions and ensuring that the gaits are odd about the odd points of the rest of the gamma functions, we can verify that the integrand of I_{DYN} is non-zero along a desired fiber direction. Moreover, we use the same rules presented in Section 6.2.1 to propose curves that will yield a non-zero dynamic phase shift along the desired fiber direction.

Note that, for gamma functions, we analyze their signs as the systems traverses a gait in the base space, we do not analyze the volume under the gamma functions as we did for the height functions. Volume under the gamma functions is insignificant since the dynamic phase shift is a equated to a time definite integral and not a volume integral as was the case for the geometric phase shift.

6.3 Gait Generation for Mixed System

In this section, we utilize our geometric and dynamic phase shift evaluation tools presented in Section 6.2 to generate gaits for mixed systems, the most general type of mechanical systems we are considering in this thesis. Next, we define a partition on the allowable gait

space which allows us to independently analyze I_{GEO} and I_{DYN} and generate gaits using our synthesis tools. We respectively label the two families of gaits as *purely kinematic* and *purely dynamic* gaits. Moreover, we propose a third type of gait that simultaneously utilizes both shifts, I_{GEO} and I_{DYN}, to produce motions with relatively larger magnitudes. We label this family of gaits as *kino-dynamic* gaits.

6.3.1 Purely Kinematic Gaits

Purely kinematic gaits are gaits whose motions are solely due to I_{GEO}, that is, $I_{DYN} = 0$ for all time. A solution for such a family of gaits is to set $\rho = 0$ in (6.1) which sets the integrand of I_{DYN} to zero. Thus, we define purely kinematic gaits as gaits for which $\rho = 0$ for all time. Hence, for *mixed systems*, we generate purely kinematic gaits by the following two step process:

- Solve the scaled momentum evolution equation, (5.8), for which $\rho = \dot{\rho} = 0$. This step defines vector fields over the base space whose integral curves are either candidate purely kinematic gaits or candidate curves that can be used to construct purely kinematic gaits.
- Use our geometric gait synthesis analysis to either pick the integral curves or construct gaits by concatenating parts of integral curves that enclose a non-zero volume only under the desired height functions.

Sometimes, purely kinematic gaits are referred to as *geometric* gaits, since the produced motion is solely due to the generated geometric phase. Moreover, purely kinematic gaits are structurally similar to gaits proposed by Bullo in his kinematic reduction of mechanical systems in [9]. The vector fields defined above essentially serve the same purpose of the de-coupling vector fields presented in Bullo's work. Even though, Bullo defined and evaluated their de-coupling vector fields in a different way, they essentially define directions along which the system's generalized momentum is conserved. This is exactly the purpose of our vector fields that we utilize to design purely kinematic gaits.

Recall that for purely mechanical systems $p = \rho = 0$ by definition and for principally kinematic systems $I_{DYN} = 0$ since $p = \varnothing$. Thus, for both types of systems, the right hand side of the reconstruction equation is equal to the kinematic part. Thus, all gaits for purely mechanical and principally kinematic systems are necessarily purely kinematic. As for purely dynamic systems, their gaits are never of the purely kinematic type since the geometric phase shift for such systems is identically zero for all gaits.

6.3.2 Purely Dynamic Gaits

As the name suggests, purely dynamic gaits are gaits that produce motion solely due to the dynamic phase shift, that is, $I_{GEO} = 0$ while $I_{DYN} \neq 0$. These gaits are relatively easy to design since these are gaits that enclose no "volume" in the base space. Thus, purely dynamic gaits should not enclose any area in the base space. A simple solution would be to ensure that a gait retraces the same curve in the second half cycle of the gait but in the opposite direction. Thus, we propose the following purely dynamic families of gaits.

Proposition 6 (Purely dynamic families of gaits) *For a mechanical system whose configuration manifold has a trivial principle bundle structure, $Q = G \times M$, and whose base space is two-dimensional, $m = 2$, the following families of curves enclose zero area in the base base.*

$$\begin{aligned} r_1(t) &= \sum_{i=0}^{n} a_i \left(f(t)\right)^i, \\ r_2(t) &= f(t), \end{aligned}$$

where $f(t) = f(t+\tau)$ is a periodic real function and a_i's are real numbers.

PROOF Given a parametric curve $(r_1(t), r_1(t))$ in the two dimensional base space, we can compute the area enclosed in the curve using the following expression

$$\begin{aligned} Area &= \int_{t=0}^{\tau} \left(r_1 \frac{\partial r_2}{\partial t} \right) dt, \\ &= \int_{t=0}^{\tau} \left(\sum_{i=0}^{n} a_i \left(f(t)\right)^i f'(t) \right) dt, \\ &= \oint_{f(0)}^{f(\tau)} \left(\sum_{i=0}^{n} a_i \left(f(t)\right)^i \right) df, \\ &= 0, \end{aligned}$$

since $f(0) = f(\tau)$.

■

Moreover, if we can verify that for the above family of gaits, the scaled momentum variable is sign-definite, that is, $\rho \leq 0$ or $\rho \geq 0$ for all time, then generating purely dynamic gaits reduces to the following simple procedure:

- Select gaits from the above described family and check the sign of the scaled momentum variable ρ.
- Analyze the gamma functions depicted in (6.3) to pick the gaits that ensure that the integrand of I_{DYN} is non-zero for the desired fiber direction.

Note that, for systems that have only *one* base variable, all their gaits are necessarily purely dynamic, since $I_{GEO} = 0$ using (6.2) where $m = 1$. Thus, we using the purely dynamic gait synthesis to generate gaits for the purely dynamic class of mechanical system defined in Chapter 4. Finally, not that there does not exist any purely dynamic gaits for purely mechanical and principally kinematic systems since the dynamic phase shift for both system type is identically zero for all gait.

6.3.3 Kino-dynamic Gaits

Finally, we have the third type of gaits which we term as kino-dynamic gaits. These gaits have both I_{GEO} and I_{DYN} not equal to zero, that is, the motion of the system is due to both the geometric phase shift as well as the dynamic phase shift which are associated with I_{GEO} and I_{DYN}, respectively. We design kino-dynamic gaits in a two step process.

- First we do the volume integration analysis on I_{GEO} to find a set of candidate gaits that move the robot in the desired direction.
- The second step is to compute I_{DYN} for the candidate gaits and verify that the effect of I_{DYN} actually enhances the desired motion.

Kino-dynamic gaits are variations of purely kinematic gaits. We start by generating a purely kinematic gait but by neglecting the constraints that the gait has to be an integral curve of the vector field that prescribes the purely kinematic gaits. Thus, we know that scaled momentum is not necessarily zero for all time, that is, $I_{DYN} \neq 0$. Moreover, it is easy to verify the sign of the gamma function for a particular proposed gaits. However, to ensure that the dynamic phase shift additively contributes to the geometric phase shift, we have to analyze the evolution of the scaled momentum. Nonetheless, since we already have a proposed gait, solving for the evolution of the momentum is done straight forward by solving the momentum evolution equation.

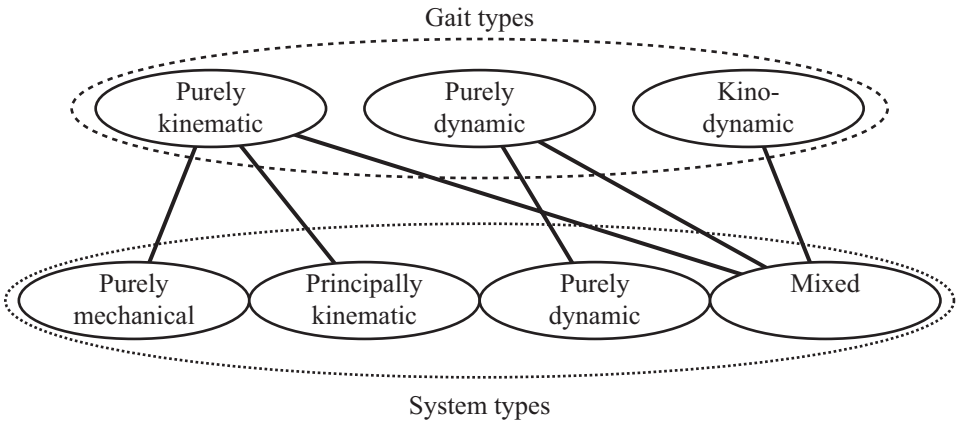

Figure 6.1: The gaits synthesis techniques used for various types of mechanical systems.

Thus far, for the examples we have analyzed, our initial guesses at kino-dynamic gaits produced geometric and dynamic shifts with similar signs, hence, effectively producing fiber motions with bigger magnitudes. However, we do not expect this to be the case in general and an additional iteration step might be required to find kino-dynamic gaits. We plan to address this particular issue in our future work.

In this Section, we proposed three types of gait synthesis that we will utilize to generate gaits for mixed mechanical systems and their sub-type families of systems. Figure 6.1 depicts which gait synthesis technique will be used to generate gaits for each of the types of mechanical systems we are considering in the thesis.

Chapter 7

Applications

In this chapter, we apply our gait generation analysis to several robotic systems. We ensure that we pick at least one example for each of the families of mechanical system we presented in Chapter 4. More specifically, in Section 7.1, we generate purely kinematic gaits for two purely mechanical systems, the floating three link snake robot and the pivoting dynamic model shown in Fig. 7.1 and Fig. 7.6, respectively. In Section 7.2, we generate purely kinematic gaits for the three link kinematic snake robot (Fig. 7.13) which is a principally kinematic system. In Section 7.3, we generate purely dynamic gaits for the simplified Trikke shown in Fig. 7.17. Finally, in Section 7.4, we generate three types of gait, purely kinematic, purely dynamic, and kino-dynamic gaits for two mixed type mechanical systems, the original and the variable inertia snakeboards shown respectively in Fig 7.22 and Fig. 7.30.

All of the example sections will have a similar structure, that is, we start by defining the systems configuration space and attaching a body coordinate frame to the system. After we compute the kinetic energy and non-holonomic constraints acting on the system, we utilize the fiber space Lie group structure to define the group actions and lifted action to rewrite the kinetic energy and non-holonomic constraints in their reduced from. Moreover, where applicable, we compute the generalized momentum which allows us to compute the reconstruction equation for each example. We also present the systems momentum evolution equation and find an integrating factor which allows us to define the scaled momentum variable. Using the scaled momentum variable, we rewrite both the momentum evolution equation, (5.8) and the reconstruction equation, (5.9). We utilize the first of which to compute the height and gamma functions, while we use the latter of which to compute the sigma functions which allow us to study the sign-definiteness of the scaled

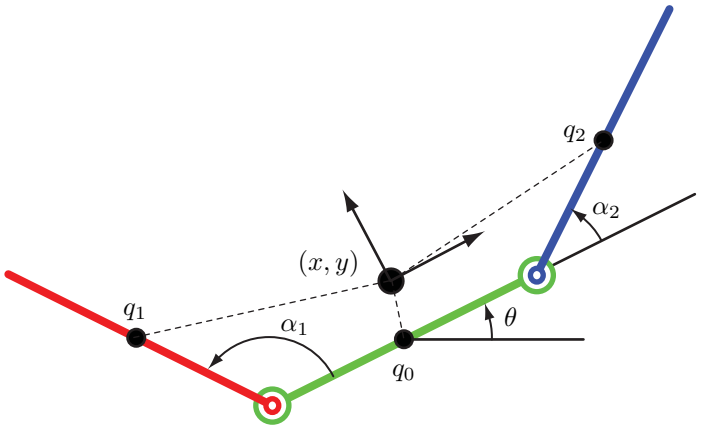

Figure 7.1: A depiction of the floating three link snake with its configuration variables.

momentum. Finally, by analyzing the height functions, gamma functions, and sigma functions, we generate the appropriate type of gaits for each example.

7.1 Purely Mechanical Systems

In this section we generate gaits for two purely mechanical system, the floating three link snake robot, and the pivoting dynamic model of the Rocking and Rolling Robot which was introduced by Balasubramanian in [3]. Recall that we will use the purely kinematic gait generation tools to generate gaits for purely mechanical systems as was shown in Fig. 6.1.

7.1.1 Floating Three Link Snake Robot

The floating three link snake robot shown in Fig. 7.1 is composed if three rigid links that are connected to each other by revolute joints. The axes of the revolute joints are parallel, thus, the links are always co-planer for any value of the inter-link angles, α_1 and α_2. We assume that each of the three links has a mass m centered at the middle of the link, q_i, and each link as an inertia j about the link's center of mass. Moreover, we assume that each link has a length $2l$ and the inertia of each link $j = ml^2$.

To locate the snake in the plane, we attach a body frame at the center of mass of the entire snake as shown in Fig. 7.1, where x and y depict the position of the center of mass. We also align the first axis of the body frame along the middle link of the snake which makes an angle θ with the horizontal. Hence, we need five variables, $(x, y, \theta, \alpha_1, \alpha_2)$, to completely identify the configuration of the three link snake robot. Moreover, we can clearly see that

θ_0	$=$	θ
θ_1	$=$	$\theta + \alpha_1$
θ_2	$=$	$\theta + \alpha_2$
x_1	$=$	$x - L\cos(\theta) - \frac{2}{3}L\cos(\theta + \alpha_1) - \frac{1}{3}L\cos(\theta + \alpha_2)$
y_1	$=$	$y - L\sin(\theta) - \frac{2}{3}L\sin(\theta + \alpha_1) - \frac{1}{3}L\sin(\theta + \alpha_2)$
x_2	$=$	$x + \frac{1}{3}L(\cos(\theta + \alpha_1) - \cos(\theta + \alpha_2))$
y_2	$=$	$y + \frac{1}{3}L(\sin(\theta + \alpha_1) - \sin(\theta + \alpha_2))$
x_3	$=$	$x + L\cos(\theta) + \frac{1}{3}L\cos(\theta + \alpha_1) + \frac{2}{3}L\cos(\theta + \alpha_2)$
y_3	$=$	$y + L\sin(\theta) + \frac{1}{3}L\sin(\theta + \alpha_1) + \frac{2}{3}L\sin(\theta + \alpha_2)$

Table 7.1: Computing the links' center of mass locations and global orientations in terms of the configurations variables.

the configuration space of the three link snake robot is a five-dimensional principal fiber bundle $Q = G \times M$ where $G = SE(2)$, the special Euclidean group representing the fiber space and $M = (\mathbb{S} \times \mathbb{S})$ representing the base space.

Now, we compute the kinetic energy of the floating three link snake which is computed using the following equation

$$KE = \frac{1}{2}\sum_{i=0}^{2}\left(\dot{q}_i^T m \dot{q}_i + j\dot{\theta}_i^2\right),$$

where $q_i = (x_i, y_i)$ and θ_i are the global position of the center of mass and orientation of each link. Note that the kinetic energy is a function of the configuration variable, q, and velocities, $\dot{q}$ since we can substitute for q_i and θ_i in terms of the configuration variables as shown in Table 7.1. For this example, we assume that the three link snake is floating in a horizontal plane, thus, the potential energy is constant. Thus, we can equate the Lagrangian to the kinetic energy, that is, $L(q, \dot{q}) = KE$.

Using the structure of the Lie group, $SE(3)$, we can compute the matrix form of the lifted action which we presented in Example 4 to arrive at

$$T_g L_{g^{-1}} = \begin{pmatrix} \cos(\theta) & -\sin(\theta) & 0 \\ \sin(\theta) & \cos(\theta) & 0 \\ 0 & 0 & 1 \end{pmatrix}. \tag{7.1}$$

Using the lifted action, we can verify the Lagrangian invariance and compute the reduced Lagrangian at the Lie group identity. This is simply done by making the substitution

in $\dot{g} = T_e L_g \xi = \left(T_g L_{g^{-1}}\right)^{-1} \xi$ into the Lagrangian $L(q, \dot{q})$. The reduced Lagrangian has the form given in (3.18), where the components of the reduced mass matrix for the floating three link snake are given by

$$
\begin{aligned}
I &= \begin{pmatrix} 3\,m & 0 & 0 \\ 0 & 3\,m & 0 \\ 0 & 0 & \frac{l^2\,m\,(19+6\,\cos(\alpha_1)+2\,\cos(\alpha_1-\alpha_2)+6\,\cos(\alpha_2))}{3} \end{pmatrix}, \\
IA &= \begin{pmatrix} 0 & 0 \\ 0 & 0 \\ \frac{l^2\,m\,(5+3\,\cos(\alpha_1)+\cos(\alpha_1-\alpha_2))}{3} & \frac{l^2\,m\,(5+\cos(\alpha_1-\alpha_2)+3\,\cos(\alpha_2))}{3} \end{pmatrix}, \text{ and} \\
m &= \begin{pmatrix} \frac{5\,l^2\,m}{3} & \frac{l^2\,m\,\cos(\alpha_1-\alpha_2)}{3} \\ \frac{l^2\,m\,\cos(\alpha_1-\alpha_2)}{3} & \frac{5\,l^2\,m}{3} \end{pmatrix}.
\end{aligned}
$$

Note that the components of the reduced mass matrix are a functions of the base variables, (α_1, α_2). Thus, using the components of the reduced mass matrix, we compute the local from of the mechanical connection, $A = I^{-1}(IA)$, to arrive at

$$
A = \begin{pmatrix} 0 & 0 \\ 0 & 0 \\ \frac{5+3\,\cos(\alpha_1)+\cos(\alpha_1-\alpha_2)}{19+6\,\cos(\alpha_1)+2\,\cos(\alpha_1-\alpha_2)+6\,\cos(\alpha_2)} & \frac{5+\cos(\alpha_1-\alpha_2)+3\,\cos(\alpha_2)}{19+6\,\cos(\alpha_1)+2\,\cos(\alpha_1-\alpha_2)+6\,\cos(\alpha_2)} \end{pmatrix}.
$$

Note that for our choice of body frame and system parameters, $(m, l, j = ml^2)$, the local from of the mechanical connection is independent of any of these parameters.

Assuming that the floating three link snake has no external forces acting on it, and that it starts from rest, we can easily verify that it belongs to the family of *purely mechanical systems*. Thus, the reconstruction equation, (4.11), for the three link floating snake is given by $\xi = -A(r)\dot{r}$, where A was computed in the above equation.

Using the local form of the mechanical connections, we can compute the height functions corresponding to the group variables. The first two height functions corresponding to the ξ_1 and ξ_2 are zero, since the first two rows of the mechanical connection are zeroes. The implication is that for whatever base space motion, that is, inter link motion, the center of mass of the entire robot will never move. This agrees with our intuition and abides by Newtonian mechanics, that is, since there are no external forces and since the

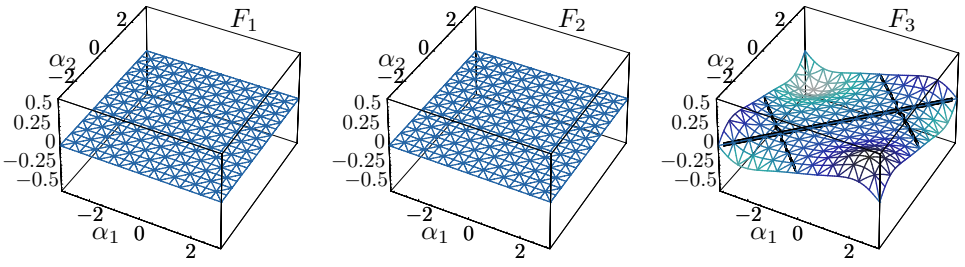

Figure 7.2: The three height functions for the floating three link snake. The darker shades indicate the positive regions which are separated from the light colored negative regions by the solid lines.

system is starting from rest, the center of mass of the entire mechanical system remains fixed. As for the height function along the third fiber variable, F_3, we compute it as follows

$$\begin{aligned} F_3(\alpha_1, \alpha_2) &= \frac{\partial A_1^3}{\partial \alpha_2} - \frac{\partial A_2^3}{\partial \alpha_1}, \\ &= \frac{24\ (\sin(\alpha_1) - \sin(\alpha_2))}{(19 + 6\ \cos(\alpha_1) + 2\ \cos(\alpha_1 - \alpha_2) + 6\ \cos(\alpha_2))^2}. \end{aligned}$$

Before, we generate any gaits, we will analyze the height functions and study their properties as was discussed in Section 6.2.1. The first two height functions, F_1 and F_2 are zero everywhere on the base space as shown in Fig. 7.2. As for the third height function, the following curves indicate the regions where $F_3 = 0$,

$$\begin{aligned} l_1 &= \{\alpha_2 = \alpha_1 + 2k\pi, k \in \mathbb{Z}\}, \text{ and} \\ l_2 &= \{\alpha_2 = \pi - \alpha_1 + 2k\pi, k \in \mathbb{Z}\}. \end{aligned}$$

The above lines are depicted by the solid curves in Fig. 7.2. Note how these lines partition the base space into regions where the height function is either positive (dark shades) or negative (light shades) in Fig. 7.2. Moreover, note that the third height function is odd about the l_1 set of lines. Thus, using the rules we devised in Section 6.2.1, we propose the gaits given in Table 7.2.

ϕ_1	:	$\alpha_1 =$	$\frac{\pi\,(-1+2\,\cos(t)+\sin(t))}{4}$
		$\alpha_2 =$	$\frac{\pi\,(1+2\,\cos(t)-\sin(t))}{4}$
ϕ_2	:	$\alpha_1 =$	$\alpha_1 = \frac{-(\pi\,(\sin(t)+\sin(2\,t)))}{2}$
		$\alpha_2 =$	$\frac{\pi\,(\sin(t)-\sin(2\,t))}{2}$

Table 7.2: Purely kinematic gaits for the floating three link snake.

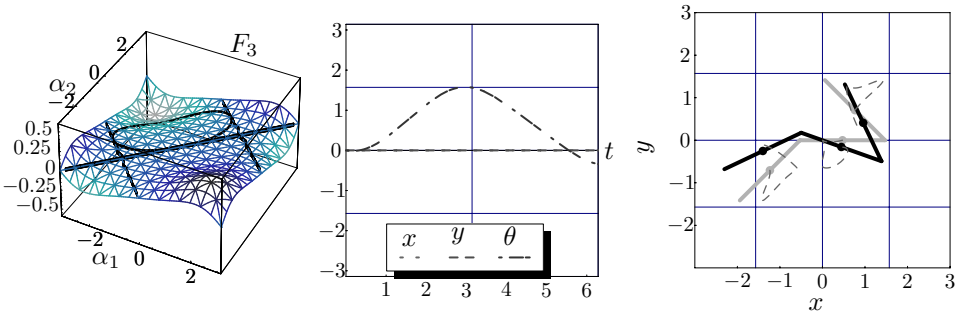

Figure 7.3: The time simulation of the gait, ϕ_1, for the floating three link snake.

One can clearly see that the first gait, ϕ_1, lies entirely in the negative region of F_3 as shown in the first plot of Fig. 7.3. Thus, we expect the integral of the third height function to yield a non-zero negative value, that is,

$$I^3_{GEO} = \int\int_{\phi_1} F_3(r)dr < 0.$$

Moreover, note that for the Lie group $SE(2)$, $I^3_{GEO} = \Delta\theta$, that is, the volume under the third height function actually computes the absolute change in orientation of the entire

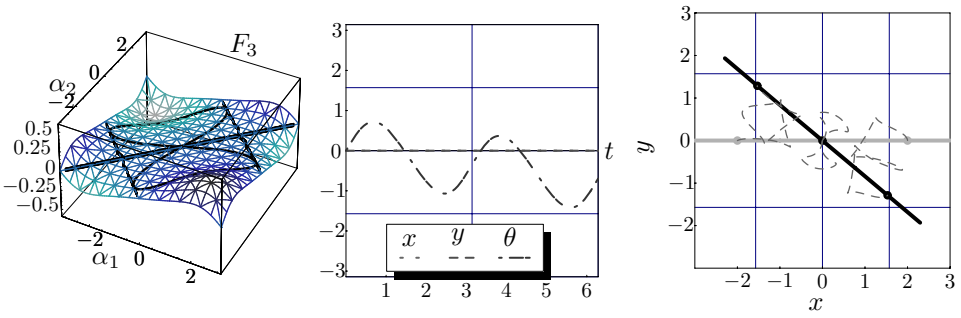

Figure 7.4: The time simulation of the gait, ϕ_2, for the floating three link snake.

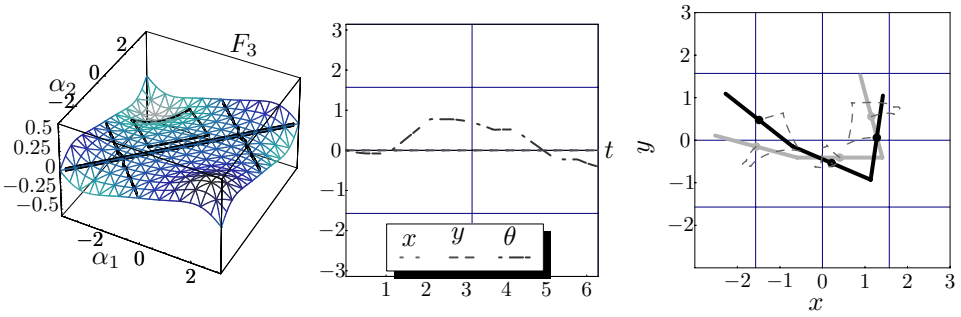

Figure 7.5: The time simulation of a non-sinusoidal square gait for the floating three link snake.

mechanical system after the completion of each gait. Thus, we expect the gait ϕ_1 to rotate the robot in a clock-wise direction after each cycle. We have simulated this gait, and, indeed as expected, the floating three link snake robot changes its orientation at the end of the gait, ϕ_1, as shown Fig. 7.3.

Similarly, we simulate the second gait, ϕ_2, depicted in the second row of Table 7.2 as shown in Fig. 7.4. Note that for ϕ_2, we utilized the fact that the third height function is odd about the line, l_1, hence, the figure-eight type curve which is symmetric with respect to l_1 must yield a non-zero negative orientation change. The time simulation of this gait verifies our expected orientation change as shown in Fig. 7.4.

Finally, we would like to note that, even though the proposed gaits for this floating three link snake are sinusoidal, other types of gaits are still allowable. In fact, we just chose to simulate the sinusoidal gaits as they simplify the numeric time simulations. We actually, designed a non-sinusoidal gait which is shown in Fig. 7.5. The square gait depicted in Fig. 7.5 lies entirely in the negative region of the third height function, thus, as expected it orients the three link snake robot in a clock-wise direction.

7.1.2 Pivoting Dynamic Model of RR-Robot

The *pivoting dynamic model* was first introduced by Balasubramanian *et al.* as a novel locomoting system [3, 4]. We are interested in this system because it is somewhat related to simpler systems studied in the prior work. However, we have opted to demonstrate our results on this novel system because it is more general than the prior systems and one can not simply make any educated guesses on what inputs could possibly locomote this system. This demonstrates the applicability of our gait generation technique.

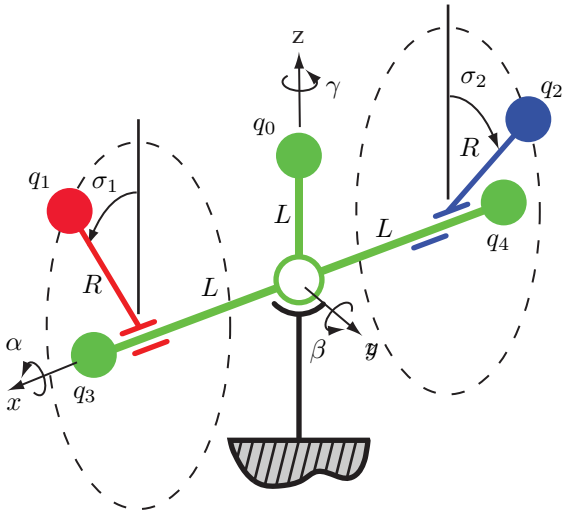

Figure 7.6: The pivoting dynamic model.

The pivoting dynamic model shown in Fig. 7.6 is composed of three rigid links. The outer two links are connected to the middle link via two revolute joints whose axes are coincident with the middle link. Thus, the outer two links lie in two parallel planes that are perpendicular to the middle link. The outer two links have mass, m, concentrated at their distal ends, while the middle link has three concentrated masses at each of its distal ends and one in the middle. The middle link is connected to the ground via a spherical joint at the link center. Finally we attach a body coordinate frame to the middle of the center link as shown in Fig. 7.6. The orientation of this body frame is represented by the three fiber variables, (α, β, γ), which denote the three rotations along the three frame axes. The two internal degrees of freedom are represented by the relative angle between the links (α_1, α_2).

Hence, the pivoting dynamic model has a five-dimensional, $(n = 5)$, configuration space $Q = G \times M$, where the associated Lie group fiber space is $G = SO(3)$, the three-dimensional special orthogonal group, denotes the robot's global orientation. The base space denoting the internal degrees of freedom is $M = \mathbb{S} \times \mathbb{S}$. The Lagrangian of the pivoting dynamic model in the absence of gravity is

$$L(q, \dot{q}) = \frac{1}{2} \sum_{i=1}^{5} \left(m_i \dot{x}_i^T \dot{x}_i \right) \tag{7.2}$$

where m_i represents the mass of each of the concentrated masses and each x_i represents the inertial position of these masses. Let the length of the middle link be $2L$ while the

length of the outer links be R. To simplify some expressions we will assume that all the masses are identical, that is, $m_i = m$.

We define the rotation matrices along the three axes in the usual way, that is,

$$
\begin{aligned}
R_x(\alpha) &= \begin{pmatrix} 1 & 0 & 0 \\ 0 & \cos(\alpha) & -\sin(\alpha) \\ 0 & \sin(\alpha) & \cos(\alpha) \end{pmatrix}, \\
R_y(\beta) &= \begin{pmatrix} \cos(\beta) & 0 & \sin(\beta) \\ 0 & 1 & 0 \\ -\sin(\beta) & 0 & \cos(\beta) \end{pmatrix}, \text{ and} \\
R_z(\gamma) &= \begin{pmatrix} \cos(\gamma) & -\sin(\gamma) & 0 \\ \sin(\gamma) & \cos(\gamma) & 0 \\ 0 & 0 & 1 \end{pmatrix}.
\end{aligned}
$$

Given that the fiber space has an $SO(3)$ group structure, we define the group action as $L_g = R_z(\gamma)R_y(\beta)R_x(\alpha)$[1]. Since $L_g \in SO(3)$, we can compute the lifted action as defined in [36], where $T_g L_{g^{-1}} = (L_g)^T \frac{d}{dt}(L_g)$. Then we can compute the lifted action in matrix form to arrive at

$$
\overbrace{\begin{pmatrix} \xi_\alpha \\ \xi_\beta \\ \xi_\gamma \end{pmatrix}}^{\xi} = \overbrace{\begin{pmatrix} 1 & 0 & -\sin(\beta) \\ 0 & \cos(\alpha) & \cos(\beta)\sin(\alpha) \\ 0 & -\sin(\alpha) & \cos(\alpha)\cos(\beta) \end{pmatrix}}^{T_g L_{g^{-1}}} \overbrace{\begin{pmatrix} \dot{\alpha} \\ \dot{\beta} \\ \dot{\gamma} \end{pmatrix}}^{\dot{g}}.
$$

The above equation allows us to verify the Lagrangian invariance by computing and comparing the quantities, $L((g,r),(\dot{g},\dot{r}))$ and $L((L_{g^{-1}}g,r),(T_g L_{g^{-1}}\dot{g},\dot{r}))$. After verifying the invariance of the Lagrangian we can compute the reduced Lagrangian and the reduced mass matrix. The components of the reduced mass matrix, as given in (3.19), are computed for the pivoting dynamic model where

[1]Note that the one could use different rotation matrices ordering as long as L_g is full rank. Different actions do not affect the computation of the reduced Lagrangian.

$$I = \begin{pmatrix} 2\left(L^2+2R^2\right) & 2LR\left(\cos(\alpha_2)-\cos(\alpha_1)\right) & 2LR\left(\sin(\alpha_2)-\sin(\alpha_1)\right) \\ 2LR\left(\cos(\alpha_2)-\cos(\alpha_1)\right) & \frac{5L^2+R^2}{0.5}-\frac{\cos(2\alpha_1)+\cos(2\alpha_2)}{R^{-2}} & -\left(R^2\left(\sin(2\alpha_1)+\sin(2\alpha_2)\right)\right) \\ 2LR\left(\sin(\alpha_2)-\sin(\alpha_1)\right) & -R^2\left(\sin(2\alpha_1)+\sin(2\alpha_2)\right) & \frac{4L^2+R^2}{0.5}+\frac{\cos(2\alpha_1)+\cos(2\alpha_2)}{R^{-2}} \end{pmatrix},$$

$$IA = \begin{pmatrix} 2R^2 & 2R^2 \\ -2LR\cos(\alpha_1) & 2LR\cos(\alpha_2) \\ -2LR\sin(\alpha_1) & 2LR\sin(\alpha_2) \end{pmatrix}, \text{ and } m = \begin{pmatrix} 2R^2 & 0 \\ 0 & 2R^2 \end{pmatrix}.$$

Note that as expected the reduced mass matrix depends solely on the base variables α_1 and α_2. We have already verified the invariance of the Lagrangian and there are no external forces acting on the pivoting dynamic model. Thus, if the system starts at rest, then all angular momentum variables will remain constant and equal to zero for all time. We conclude that the pivoting dynamic model is a *purely mechanical system.*

Now, we compute the local from of the mechanical connection, $A(r)$, by inverting $I(r)$ and post multiplying it by $I(r)A(r)$. Hence, $A(r)$ will have the following form

$$A(r) = \frac{R}{LD}\begin{pmatrix} \frac{L}{R}f_1^1(\alpha_1,\alpha_2) & \frac{L}{R}f_2^1(\alpha_1,\alpha_2) \\ f_1^2(\alpha_1,\alpha_2) & f_2^2(\alpha_1,\alpha_2) \\ f_1^3(\alpha_1,\alpha_2) & f_2^3(\alpha_1,\alpha_2) \end{pmatrix},$$

where f_j^i are the i^{th} row and j^{th} column of the mechanical connection which are analytic functions of the base variables (α_1, α_2). The expressions of the f_j^i functions are presented in Table 7.3.

Now we set the system's point mass values to 1, and the both parameters $L = 1$ and $R = 1$, then we compute the heights function by utilizing Green's theorem. The three height functions corresponding to the three fiber directions are shown in Fig. 7.7.

All three height functions have distinctive signed regions. The darker colors denote the positive regions while the lighter colors denote the negative regions. Note that none of the height functions has unbounded regions. In fact, this is a property of all purely mechanical systems as we proved in Lemma 9. The intuition behind why the height functions for purely mechanical systems are never unbounded is that for whatever base motion the robot is forced to do, the system always has bounded motion, that is a bounded volume under the height functions. In other words, there are no singularities of motion.

$$
\begin{aligned}
f_1^1 &= 31L^4 + 15L^2R^2 + R^4 + L^2\left(L^2+R^2\right)\cos(2\alpha_1) + L^2\left(9L^2+4R^2\right)\cos(\alpha_1-\alpha_2) \\
&\quad +R^2\left(-\left(\left(L^2+R^2\right)\cos\left(2\left(\alpha_1-\alpha_2\right)\right)\right) + L^2\cos(2\alpha_2)\right) - L^4\cos(\alpha_1+\alpha_2) \\
f_1^2 &= 31L^4 + 15L^2R^2 + R^4 + L^2R^2\cos(2\alpha_1) + L^2\left(9L^2+4R^2\right)\cos(\alpha_1-\alpha_2) \\
&\quad \left(L^2+R^2\right)\left(-\left(R^2\cos\left(2\left(\alpha_1-\alpha_2\right)\right)\right) + L^2\cos(2\alpha_2)\right) - L^4\cos(\alpha_1+\alpha_2) \\
f_2^1 &= -\left(\left(8L^4+10L^2R^2+3R^4\right)\cos(\alpha_1)\right) \\
&\quad R^2\left(\left(2L^2+R^2\right)\cos(\alpha_1-2\alpha_2) + \left(L^2+R^2\right)\cos(2\alpha_1-\alpha_2) + \left(7L^2+3R^2\right)\cos(\alpha_2)\right) \\
f_2^2 &= R^2\left(7L^2+3R^2\right)\cos(\alpha_1) + R^2\left(L^2+R^2\right)\cos(\alpha_1-2\alpha_2) \\
&\quad \left(2L^2+R^2\right)\left(R^2\cos(2\alpha_1-\alpha_2) + \left(4L^2+3R^2\right)\cos(\alpha_2)\right) \\
f_3^1 &= -\left(10L^4+12L^2R^2+3R^4\right)\sin(\alpha_1) \\
&\quad R^2\left(\left(L^2+R^2\right)\sin(2\alpha_1-\alpha_2) - \left(\left(2L^2+R^2\right)\sin(\alpha_1-2\alpha_2)\right) + 3\left(3L^2+R^2\right)\sin(\alpha_2)\right) \\
f_3^2 &= R^2\left(3\left(3L^2+R^2\right)\sin(\alpha_1) - \left(L^2+R^2\right)\sin(\alpha_1-2\alpha_2) + \left(2L^2+R^2\right)\sin(2\alpha_1-\alpha_2)\right) \\
&\quad \left(10L^4+12L^2R^2+3R^4\right)\sin(\alpha_2) \\
D &= \frac{40L^6+80L^4R^2+31L^2R^4+2R^6+2L^2R^2\left(L^2+R^2\right)\cos(2\alpha_1)}{R^2} \\
&\quad -\left(R^2\left(3L^2+2R^2\right)\cos\left(2\left(\alpha_1-\alpha_2\right)\right)\right) + 2L^2\left(L^2+R^2\right)\cos(2\alpha_2) - 2L^4\cos(\alpha_1+\alpha_2)
\end{aligned}
$$

Table 7.3: Components of the local form of the mechanical connection for the pivoting dynamic model.

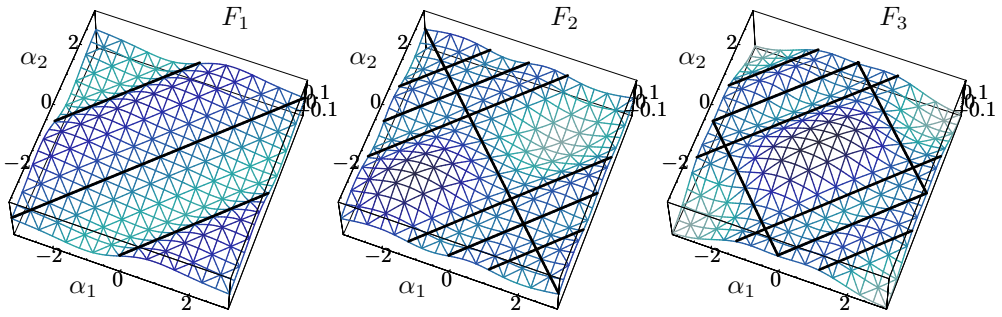

Figure 7.7: The height functions of the pivoting dynamic model.

Without loss of generality, we assume that we want to design a gait that rotates the robot *only* around the x axis. This means that we want to design a gait the envelops a non-zero volume *only* under the *first* height function in Fig. 7.7. To design such a curve, we should look carefully at the height functions properties. Note that the first height function in Fig. 7.7 is odd about the line $\alpha_2 = \alpha_1$ and even about the line $\alpha_2 = -\alpha_1$. The second height function is even about the line $\alpha_2 = \alpha_1$ and odd about the line $\alpha_2 = -\alpha_1$. Finally, the third height function is even about both lines. Thus, we can see that a figure-eight type of curve with the following properties will envelope volume only under the first height

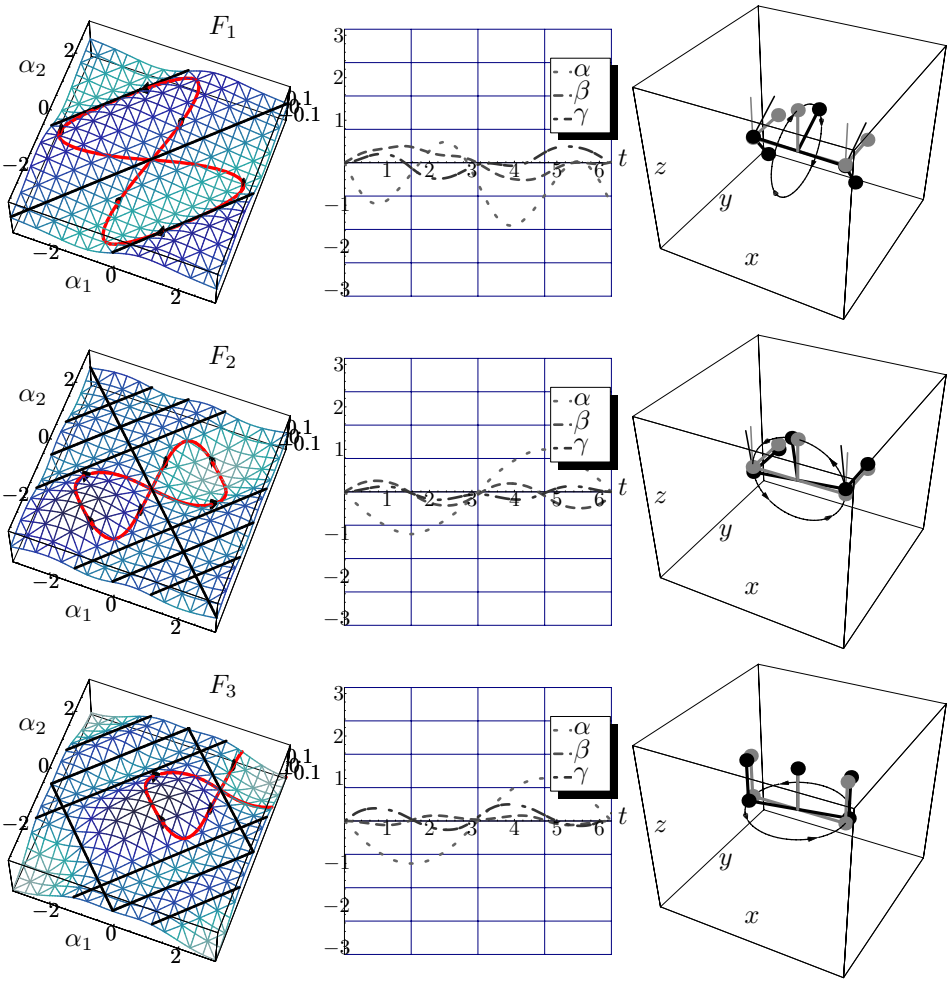

Figure 7.8: Time simulation of the three gaits, ϕ_1, ϕ_2, and ϕ_3, for the pivoting dynamic model. The first column depicts non-zero motion producing gaits superimposed over the height functions, the second column depicts the time evolution of the fiber variables, and the last column depicts snapshots of the mechanical system at the beginning and end of each gait.

function:

- The curve is centered at the origin of the base space.
- Both of the curve loops are on either side of the line $\alpha_2 = \alpha_1$.
- The curve is symmetric with respect to the two lines $\alpha_2 = \alpha_1$ and $\alpha_2 = -\alpha_1$.

ϕ_1	:	$\alpha_1 =$	$\frac{\pi}{2}(\sin(t) + \sin(2t))$
		$\alpha_2 =$	$\frac{\pi}{2}(-\sin(t) + \sin(2t))$
ϕ_2	:	$\alpha_1 =$	$\frac{\pi}{4}(2\sin(t) + \sin(2t))$
		$\alpha_2 =$	$\frac{\pi}{4}(-2\sin(t) + \sin(2t))$
ϕ_3	:	$\alpha_1 =$	$\frac{\pi}{4}(2 + 2\sin(t) + \sin(2t))$
		$\alpha_2 =$	$\frac{\pi}{4}(2 - 2\sin(t) + \sin(2t))$

Table 7.4: Purely kinematic gaits for the pivoting dynamic model.

- The curve is bounded by the two lines $\alpha_2 = \alpha_1 - \pi$ and $\alpha_2 = \alpha_1 + \pi$.

The curve ϕ_1 in the first row of Table 7.4 satisfies all the above conditions. Note that, referring to Section 6.2.1, we used the second rule on the first height function and the fourth rule on the second and third height functions. This curve is shown in the first row of Fig. 7.8. We have numerically simulated this gait and indeed as expected the robot rotated only around the x axis after one complete cycle. The rotations along all three axes is shown in the second column of the first row of Fig. 7.8. Note that there are no net rotations about other two axes, y and z, the end of the gait cycle.

Similarly, we can design two other gaits, ϕ_2 and ϕ_3, shown respectively in the second and third rows of Table 7.4, that will independently rotate the robot only around either the y and z axes. The time simulation of both gaits are shown in the second and third rows of Fig. 7.8.

Finally, we plotted the initial and final configurations of the pivoting dynamic model for each the three gaits as shown in the last column of Fig. 7.8, where the three independent rotations, $\Delta\alpha$, $\Delta\beta$, and $\Delta\gamma$ are depicted. The gray color indicates the initial configuration of the pivoting dynamic model while the back color indicates the robot's final configuration.

Hence, using our gait generation analysis we were able to easily design three gaits each of which moves the robot independently along one fiber direction.

7.1.3 Demonstrations of the Pivoting Three Link Snake

To demonstrate our gait generation techniques for purely mechanical systems, we built a simple robot using Lego blocks and hobby servos. Rather than building an actual floating three link snake or the pivoting dynamic model, we opted for a simpler planar version shown in Fig. 7.9 as it was much easier to construct and still demonstrates our techniques.

For this particular robot, which can be thought of as the pivoting (rather than floating)

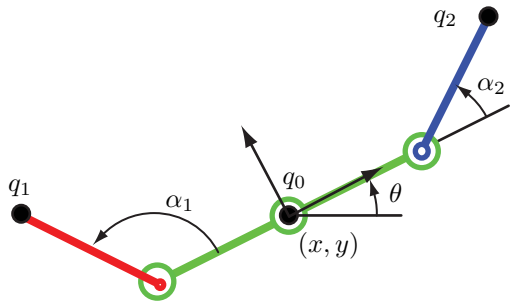

Figure 7.9: A depiction of the pivoting three link snake with its configuration variables.

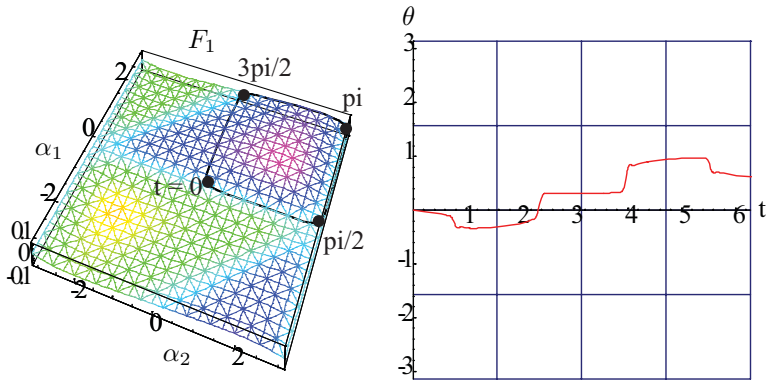

Figure 7.10: The height function and the time simulation of the pivoting three link snake.

ϕ_1	:	$\alpha_1 =$	$\frac{\pi}{2}\left(1+\sin(t)^{\frac{1}{5}}\right)$
		$\alpha_2 =$	$\frac{\pi}{2}\left(1+\sin(t)^{\frac{1}{5}}\right)$

Table 7.5: Proposed gait for the pivoting three link snake robot.

three link snake robot or the planar version of the pivoting dynamic model, the configuration space is $q = (\theta, \alpha_1, \alpha_2) \in Q = SO(2) \times \mathbb{S} \times \mathbb{S}$. This planar model has four concentrated masses, one at each of the distal ends of the outer links and two at each end of the middle link. Then we compute the reduced mass matrix from which we can compute the mechanical connection.

Specifically for this robot, since the fiber space $SO(2)$ is commutative, we can directly compute the change in the inertial angle, θ. Then integrating the connection we get

$$\Delta\theta = \frac{LR^2}{2} \int\int \frac{R\left(\sin(\alpha_1) + \sin(\alpha_2)\right) - L\sin(\alpha_1 - \alpha_2)}{\left(2L^2 + R^2 + LR\left(\cos(\alpha_1) - \cos(\alpha_2)\right)\right)^2} d\alpha_1 d\alpha_2$$

A plot of the above height function, the integrand, is shown in the first plot of Fig. 7.10.

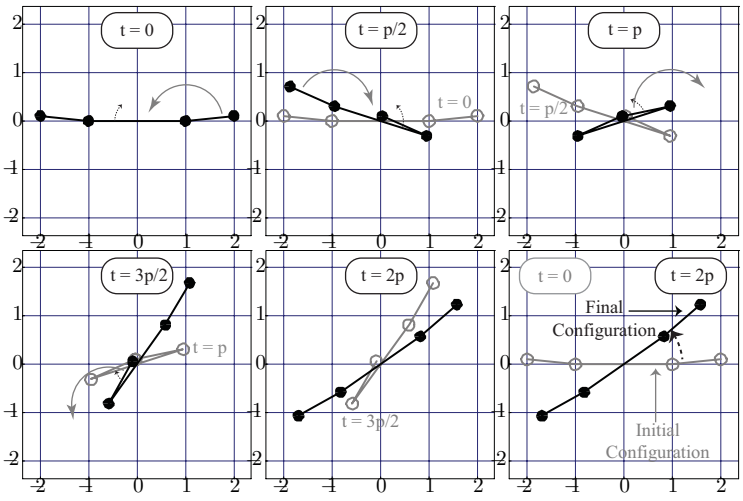

Figure 7.11: Snapshots of the pivoting three link snake as it performs the gaits ϕ_1

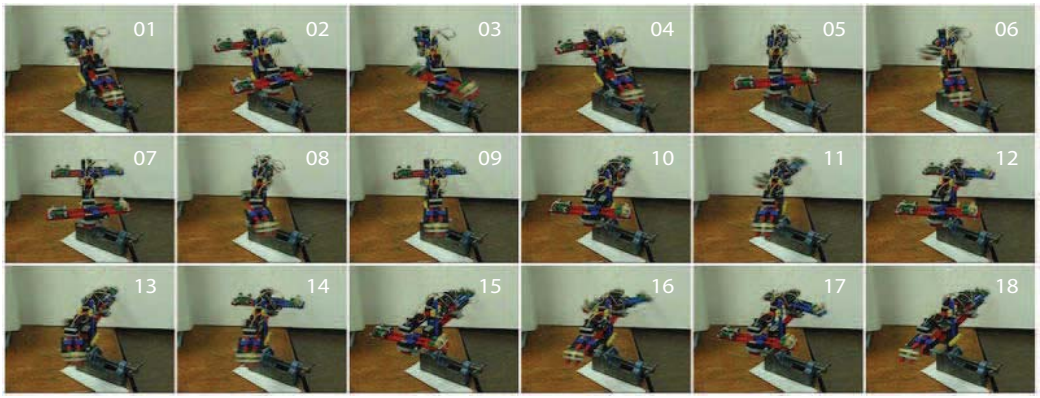

Figure 7.12: Snapshots of the actual pivoting three link snake as it performs the gaits ϕ_1.

Now, consider the base space curve given in Table 7.5. This particular curve, ϕ_1, encloses a large volume and remains in the same positive region, (Fig. 7.10). We have simulated this specific gait and plotted the change the fiber angle, θ, versus time as shown in the second plot of Fig. 7.10.

Finally, we plotted several snapshots of the pivoting three link snake at the beginning and end of specific intervals of the square gait, ϕ_1, as shown in Fig. 7.11. We have implemented this gait on our actual planar pivoting robot and indeed, as expected, the robot started rotating after each cycle as shown in Fig. 7.12. Nonetheless, the magnitudes of rotation of the actual robot did not match that of our model. The reasons for this mismatch we believe are due to the friction in the bearings around which the robot pivots

and the slight errors in computing the mass and inertia of the actual links.

7.2 Principally Kinematic Systems

Recall that principally kinematic systems are mechanical systems whose motion is entirely specified by the existence of a set of non-holonomic constraints. In other words, these are systems that have as many non-holonomic constraints as the dimension of the fiber space where the constraints, away from singularities, fully span the fiber space. In Chapter 4 we proved that the reconstruction equation for principally kinematic system has the simple form depicted in (4.9).

Next, we introduce the three link kinematic snake which, as we shall verify, belongs to the family of principally kinematic systems. We compute its principal kinematic connection, and the system's height functions. Then we utilize our geometric gait generation synthesis to generate gaits for the kinematic snake to locomote it in the plane.

7.2.1 Three Link Kinematic Snake

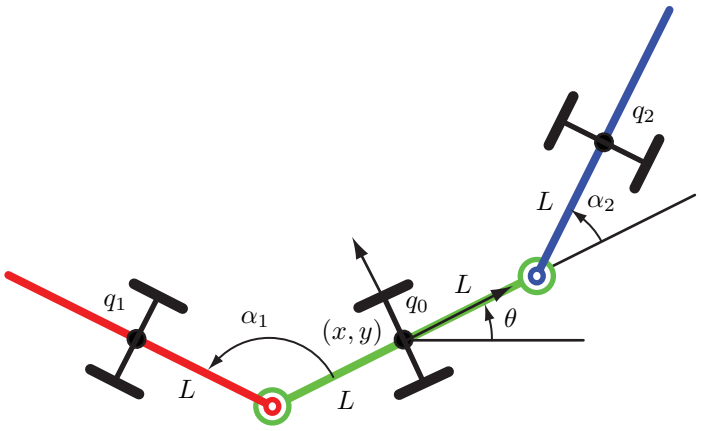

Figure 7.13: Kinematic three-link snake.

The kinematic snake robot is composed of three rigid links that are connected by two revolute joints and three passive wheel sets connected to each link as shown in Fig. 7.13. This robot is similar to the kinematic snake studied by Ostrowski in [40]. In our case, the wheel axes are rigidly held perpendicular to the links, however, Ostrowski actually controlled the angles between the wheel axes and the links, hence, increasing the dimension of the base space. Even though we fix the angles of the wheel axes with respect to the

links, we are still able to generate gaits to move the kinematic snake in the plane.

We attach a body coordinate frame to the middle of the center link as shown in Fig. 7.13. The position and orientation of this body frame is represented by the three fiber variables, (x, y, θ), which denote position of the origin of the body frame and its orientation in the plane. The two internal degrees of freedom are represented by the relative angle between the links (α_1, α_2).

The kinematic snake has a five dimensional, $(n = 5)$, configuration space $Q = G \times M$, where the associated Lie group fiber space denoting the robot's orientation in the plane is $G = SE(2)$, the special Euclidean group. The base space denoting the internal degrees of freedom is $M = \mathbb{S} \times \mathbb{S}$. Note that the mass and inertia values are irrelevant for this system since, as we shall show later, it is principally kinematic and all the momentum variable are annihilated. What this means, if we lock the base variables of the kinematic snake, away from singular base configuration, the kinematic snake can not move in any direction since the non-holonomic constraints fully span the fiber space. Thus, there are no allowable motions along which we can define any momentum variables.

There are three non-holonomic constraints acting on the kinematic snake. Each of them has the following form

$$\begin{pmatrix} \dot{x}_i & \dot{y}_i \end{pmatrix} \begin{pmatrix} \cos(\theta_i) \\ \sin(\theta_i) \end{pmatrix} = 0$$

where (x_i, y_i) is the global[2] position of the intersection point of the wheel axes and the snake links, and θ_i is the global orientation of the wheel axes.

Given that the fiber space has an $SE(2)$ group structure, we can compute the group action and lifted action. In particular, the matrix form of the lifted action is given in (7.1). Using this equation we can compute the non-holonomic constraints, $\omega(q)\dot{q} = 0$, in body coordinates. This is simply done by inverting (7.1) to get $\dot{g} = \left(T_g L_{g^{-1}}\right)^{-1} \xi$ and substituting for the fiber velocity, $\dot{g}$, by its body representation, ξ into $\omega(q)\dot{q} = 0$ as we did in Lemma 5. Then we verify that the constraints are independent of any fiber variables as shown in the following equation

[2]Recall that, global means that the position is represented in a fixed inertial frame.

$$\begin{pmatrix} -\sin(\sigma_1) & \cos(\sigma_1) & -R - L\cos(\sigma_1) \\ 0 & 1 & 0 \\ \sin(\sigma_2) & \cos(\sigma_2) & R + L\cos(\sigma_2) \end{pmatrix} \begin{pmatrix} \xi_1 \\ \xi_2 \\ \xi_3 \end{pmatrix} + \begin{pmatrix} -R & 0 \\ 0 & 0 \\ 0 & -R \end{pmatrix} \begin{pmatrix} \dot{\sigma}_1 \\ \dot{\sigma}_2 \end{pmatrix} = 0, \quad (7.3)$$

where indeed the reduced non-holonomic constraints independent of the fiber variables, $g = (x, y, \theta)$. Moreover, we know that away from singular configurations, the non-holonomic constraints are linearly independent. Thus, the number of the non-holonomic constraints is three which is equal to the dimension of the fiber space, $SE(2)$. Hence, the kinematic snake robot is a *principally kinematic* system. Now, we compute the kinematic connection which has the following form,

$$\mathbb{A}(r) = \frac{R}{D} \begin{pmatrix} R + L\cos(\alpha_2) & R + L\cos(\alpha_1) \\ 0 & 0 \\ -\sin(\alpha_2) & -\sin(\alpha_1) \end{pmatrix},$$

where $D = R\sin(\alpha_1) + L\sin(\alpha_1 - \alpha_2) - R\sin(\alpha_2)$ and again the components of the connection are functions of the base variables (α_1, α_2). Next, we use the components of the kinematic connection to compute the height functions for the kinematic snake to arrive at

$$\begin{aligned} F_1 &= \frac{2LR + \left(L^2 + R^2\right)\cos(\sigma_2) + \cos(\sigma_1)\left(L^2 + R^2 + 2LR\cos(\sigma_2)\right)}{-\frac{4}{R}\left(L\cos(\tfrac{\sigma_1-\sigma_2}{2}) + R\cos(\tfrac{\sigma_1+\sigma_2}{2})\right)^2 \sin(\tfrac{\sigma_1-\sigma_2}{2})^2}, \\ F_2 &= 0, \text{ and} \\ F_3 &= \frac{R\sin(\frac{\sigma_1+\sigma_2}{2})}{2\left(L\cos(\frac{\sigma_1-\sigma_2}{2}) + R\cos(\frac{\sigma_1+\sigma_2}{2})\right)\sin(\frac{\sigma_1-\sigma_2}{2})^2}. \end{aligned}$$

In particular, we choose the robot parameters to be $L = 1$ and $R = 1$. A plot of the three height functions for such a kinematic snake are shown in Fig. 7.14. The first two height functions correspond to ξ^1 and ξ^2 fiber motions while the third height function corresponds to ξ^3 fiber rotation. Note that the first height function is negative everywhere in the base space, the second is zero everywhere in the base space, while the third has distinctive negative regions (lighter shaded) separated from the positive (darker shaded) regions by the solid line $\alpha_1 = \alpha_2$. The second height functions is always zeros since we aligned the second axis of the body frame along the wheel axis of the middle link as shown in Fig. 7.13. This means for an observer sitting on the robot, there will never be any

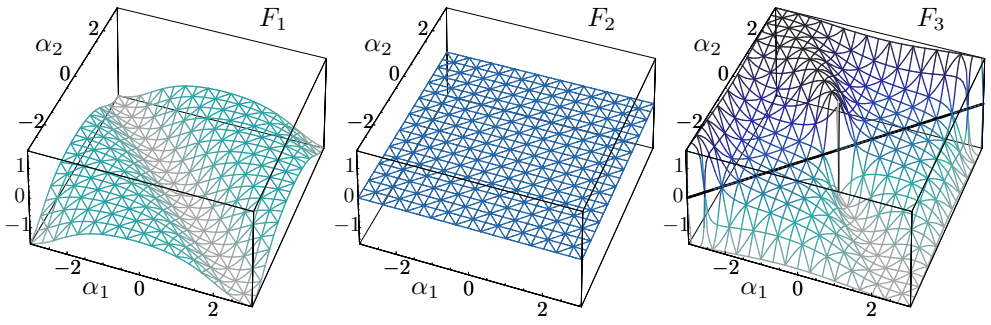

Figure 7.14: The three height functions of the kinematic snake. The darker shades indicate the positive regions which are separated from the lighter shaded negative regions by the solid lines.

motion along the wheel axis due to the no-sideways motion non-holonomic constraint.

Moreover, note that the first and third height functions have unbounded regions. To be able to plot these unbounded height regions, we used the "arctan" function to map the range of the height functions to the interval $[-\frac{\pi}{2}, \frac{\pi}{2}]$. The following lines, l_1 and l_3 denote the unbounded regions for the first and third hight functions, respectively.

$$\begin{aligned} l_1 &= \{\alpha_2 = \alpha_1 + 2k\pi, k \in \mathbb{Z}\} \\ l_3 &= \{\alpha_2 = \alpha_1 + 2k\pi, \alpha_1 = (2k+1)\pi, \text{ and } \alpha_2 = (2k+1)\pi, k \in \mathbb{Z}\} \end{aligned}$$

These regions are depicted in Fig. 7.14, where the graphs of the height functions approached the upper and lower bounds of plot range. These unbounded regions correspond to a singular configuration of the robot, where one, or more, of the non-holonomic constraints become a linear combination of the others. For example, consider the solid line $\alpha_2 = -\alpha_1$ in Fig. 7.14. At this line both the first and third height functions have infinite values which we plot at $\pm\frac{\pi}{2}$ using the "arctan" function. This line corresponds to snake configurations where all three wheel axes meet at a single point. It is intuitively clear that if the robot starts at such a configuration it can not change its configuration without breaking one of the non-holonomic constraint, that is, without one of the wheels sliding sideways.

On the other hand, consider a gait that contains a portion of the line $\alpha_2 = -\alpha_1$. The volume under the height function for such a gait will be unbounded, that is, for a finite

base variable change, the snake will have infinite motion. Such a gait is not feasible. Thus, not only these height function help us in designing gaits, but also depict singularity region in the base space.

Again, without loss of generality, assume we want to design a gait that will rotate the kinematic snake, that is move the system along the θ fiber direction. In other words, we want to design a curve that will envelope non-zero volume only under the third height function. Note that the first height function for the kinematic snake is even about both lines $\alpha_2 = \alpha_1$ and $\alpha_2 = -\alpha_1$, while the third height function is even about the line $\alpha_2 = -\alpha_1$ and odd about the line $\alpha_2 = \alpha_1$. So to move the robot in the θ direction we need figure-eight type of curve with the following properties:

1. The first height function is negative everywhere in the base space and it is even about all line $\alpha_2 = \alpha_1 + k$, where $k \in \mathbb{R}$. Thus, using the fourth rule in Section 6.2.1, we know that we need a curve that is self-intersecting and should be symmetric about the one of the lines, $\alpha_2 = \alpha_1 + k$. Such a curve will ensure zero volume under the first height functions.

2. The curve should not intersect any of the unbounded regions prescribed by the lines, l_1 and l_2.

3. Finally, since we need the curve to enclose a non-zero volume under the third height function, we use the second rule in Section 6.2.1 and ensure that the curve is symmetric about the line $\alpha_2 = \alpha_1$ about which the third height function is odd.

The curve ϕ_3 in the third row of Table 7.6 satisfies all the above conditions as shown in the third row of Fig. 7.15. We can easily see that such a curve envelopes non-zero volume only under the third height function. We numerically simulated such a gait and indeed we get a motion of the kinematic snake which after one complete cycle only rotates the robot. All fiber motions are plotted in the second column of the third row of Fig. 7.15. We also plot two snapshots of the kinematic snake at the beginning and end of the ϕ_3 gait. It is clear that the kinematic snake is rotating as shown in the last plot of the third row of Fig. 7.15.

Similarly we can design two other gaits, ϕ_1 and ϕ_2, shown respectively in the first and second rows of Table 7.6, that move the robot only in the x and y directions as shown in the first and second rows of Fig. 7.15. Note that both gaits have an identical curve, but different initial configurations. The initial configuration is denoted by the solid dot in the

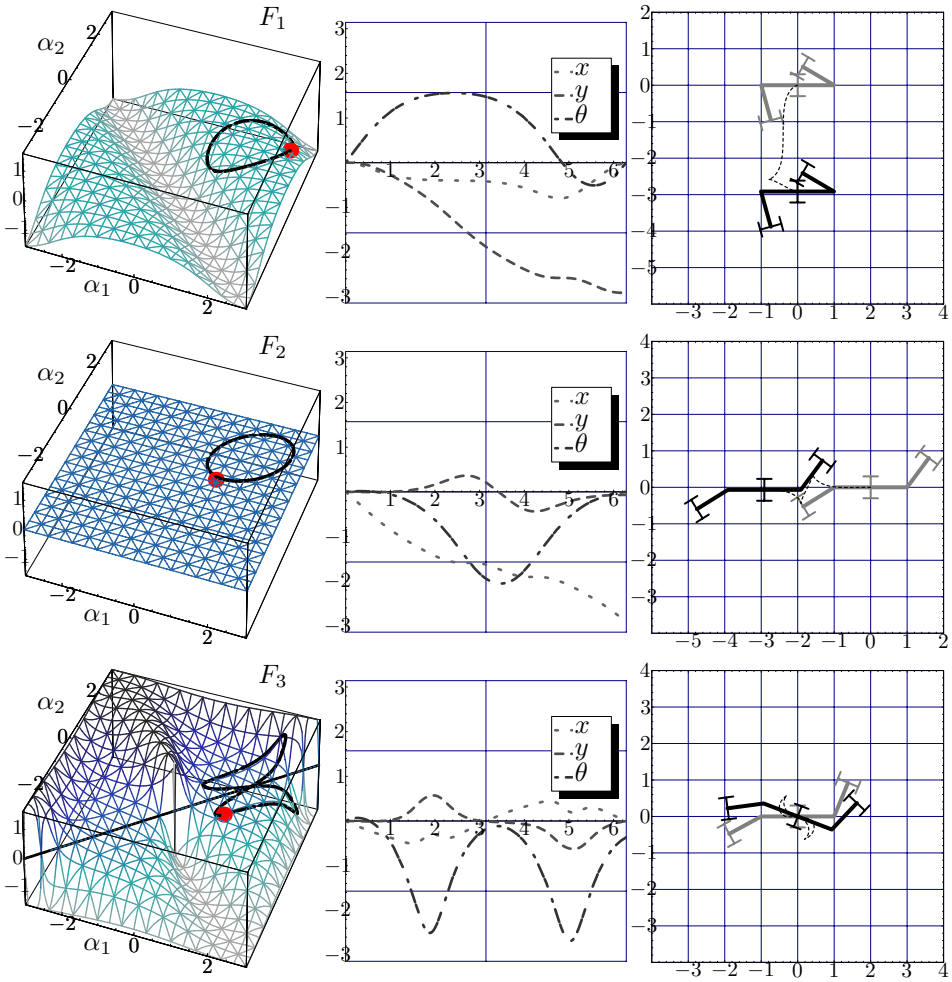

Figure 7.15: The time simulations of the three gaits ϕ_1, ϕ_2, and ϕ_3, for the kinematic three link snake. The first column depicts non-zero motion producing gaits superimposed over the height functions, the second column depicts the time evolution of the fiber variables, and the last column depicts snapshots of the mechanical system at the beginning and end of each gait.

first column of Fig. 7.15. The motion of the kinematic snake due to the above two gaits is depicted in the last column of the first and second row of Fig. 7.15. We can clearly see that the kinematic snake moves along the x direction while performing ϕ_1 and parallel parks or moves along the y direction while performing ϕ_2.

Note that both gaits produce identical geometric phase shift in body coordinates, that

ϕ_1	:	$\alpha_1 = \frac{\pi}{2} - 0.63778\cos(t) - 0.832148\sin(t)$
		$\alpha_2 = \frac{\pi}{2} - 1.01344\cos(t) + 0.268663\sin(t)$
ϕ_2	:	$\alpha_1 = \frac{\pi}{2} + 1.03919\cos(t) - 0.139003\sin(t)$
		$\alpha_2 = \frac{\pi}{2} + 0.271378\cos(t) - 1.01271\sin(t)$
ϕ_3	:	$\alpha_1 = \frac{\pi}{4}\left(2 + \frac{\pi(9\sin(4.1594+2t)+4\sin(2.0797+t))}{18\sqrt{2}}\right)$
		$\alpha_2 = \frac{\pi}{4}\left(2 + \frac{\pi(9\sin(4.1594+2t)-4\sin(2.0797+t))}{18\sqrt{2}}\right)$

Table 7.6: Purely kinematic gaits for the kinematic snake robot.

is, I^1_{GEO} = volume under the height function while $I^2_{GEO} = 0$. Nonetheless, due to the non-commutativity of the fiber Lie group, $SE(2)$, the same geometric phase shift is transferred entirely into Δx in the case of ϕ_1 and entirely into Δy in the case of ϕ_2.

7.2.2 Demonstration of the Three Link Kinematic Snake

To demonstrate our gait generation technique, we built a simple kinematic snake using Lego blocks and hobby servos. In this case we applied two sinusoidal gaits. The first gait we applied was similar in structure to ϕ_1, that is, the gait was a an elliptical non-intersecting gait that is symmetric with respect to the line $\alpha_1 = \alpha_2$. As expected, implementing this gait moved the kinematic snake along the same direction after each complete cycle. Snapshots of the actual robot are shown in Fig. 7.16(a).

We would like to note that we observed some sideways slipping of the wheels and the magnitude of the slipping was more significant as our gaits got closer to the line $\alpha_1 = -\alpha_2$. This observation does match our intuition, since we know from the height function analysis, that the line $\alpha_1 = -\alpha_2$ represents the singular configurations of the robot. Hence, according to our analysis, as the gaits got closer to the line $\alpha_1 = -\alpha_2$, they should envelop larger volumes, that is, the magnitudes of motion should get larger. Moreover, we know that as the gaits approach the singular line $\alpha_1 = -\alpha_2$, the constraint forces get larger in magnitudes. Nonetheless, since the wheels on our kinematic snake robots are not ideal, as the constraint forces became larger and overcame the sideways frictional forces, the wheels started slipping. So for gaits that approached the singular line $\alpha_1 = -\alpha_2$, rather than attaining larger magnitudes of motion, we observed wheel slipping.

In fact, we pushed this idea to an extreme where we implemented a circular gait that was centered at the origin of the base space, that is, the gait actually crosses the singular line $\alpha_1 = -\alpha_2$ twice per cycle. Even though we observed considerable slipping of the wheels

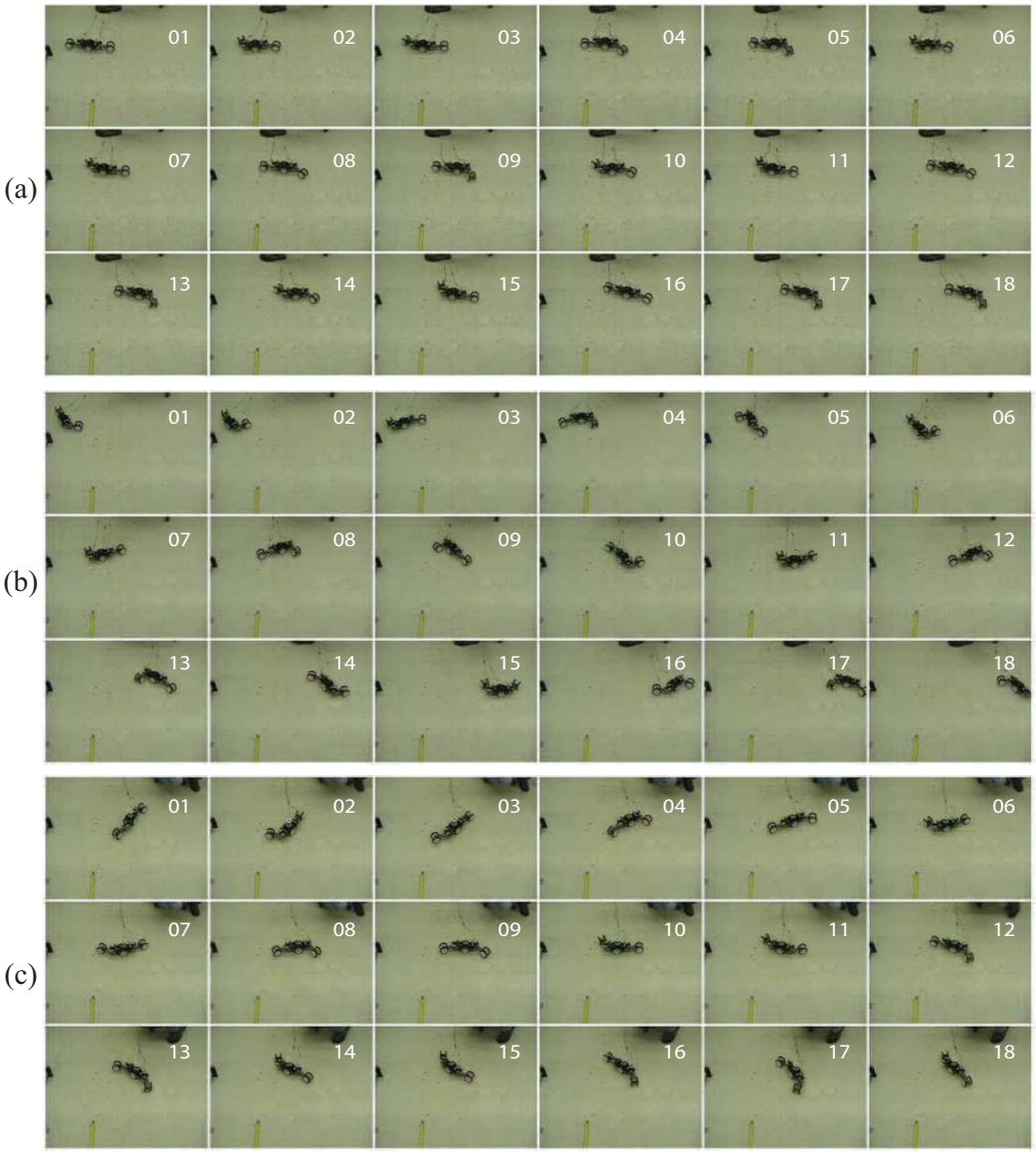

Figure 7.16: Snapshots of the actual kinematic three link snake as it performs two translational gaits in (a) and (b), and one rotational gait in (c).

each time the gait passed through the singular line, the actual magnitude of motion along the x direction was relatively large when compared the the gaits we implemented earlier as shown in Fig. 7.16(b). This is not an indication of a failure of our gait generation analysis which predicts infinite motion for such a gait, rather the actual model violated the non-holonomic constraints at these singular configuration and due to slip and modeling errors produced a large finite motion. Finally, we implemented a figure-eight type curve which,

as expected, rotated the kinematic snake in place as shown in Fig. 7.16(c).

7.3 Purely Dynamic Systems: Simplified Trikke

In this section, we generate gaits for purely dynamic systems, that is, systems whose height functions are null over the entire space. The simplest type of mechanical systems that belong to this family are systems that have a one-dimensional base space. The robo-trikke which was introduced and analyzed by Kumar and Chitta in [11, 45] is a purely dynamic system. Moreover, this system is similar to the roller racer system analyzed by Tsakiris *et al.* in [28]. Next we analyze and eventually generate gaits for a simplified Trikke system shown in Fig. 7.17

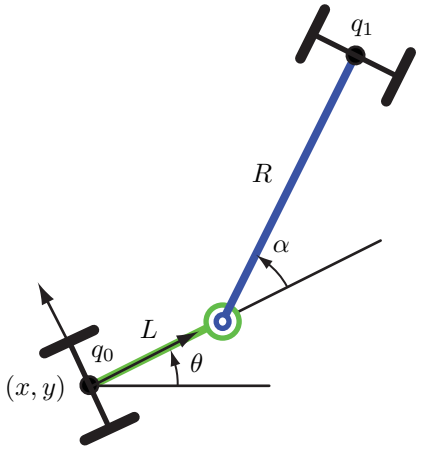

Figure 7.17: A schematic of the simplified Trikke.

A schematic of the simplified Trikke is shown in Fig. 7.17. It is composed of two rigid links that are connected by a revolute joint. Additionally, we have two passive wheel sets attached to the distal ends of the two link. The wheel axes are held rigidly perpendicular to the respective links. We attach a body coordinate frame to the intersection of one of the wheel axes and the links and we align the first axis of the body frame along that link as shown in Fig. 7.17. The position and orientation of the body frame is represented by the fiber variables, (x, y, θ), while the internal degree of freedom representing the inter link angle is denoted by the base variable, (α_1).

Hence, the simplified Trikke has a four-dimensional, $(n = 4)$, configuration space $Q = G \times M$, where the associated Lie group fiber space denoting the robot's position and orientation in the plane is $G = SE(2)$, the special Euclidean group. The base space

denoting the internal degree of freedom is $M = \mathbb{S}$. The Lagrangian of the simplified Trikke in the absence of gravity is

$$L(q, \dot{q}) = \frac{1}{2} \sum_{i=1}^{2} \left(m_i \dot{x}_i^T \dot{x}_i + j_i \dot{\theta}_i^2 \right) \tag{7.4}$$

where m_i and j_i represent the mass and inertia of each of the two links with the wheels attached to them, while x_i and θ_i represent the inertial position and orientation of the center of mass of these rigid bodies. Moreover, the two non-holonomic constraints, one for each wheel set, acting on the simplified Trikke are given by the following form

$$\frac{d}{dt} \begin{pmatrix} \tilde{x}_i & \tilde{y}_i \end{pmatrix} \begin{pmatrix} \cos(\tilde{\theta}_i) \\ \sin(\tilde{\theta}_i) \end{pmatrix} = 0$$

where $(\tilde{x}_i, \tilde{y}_i)$ is the global position of the intersection point of the wheel axes and the two links, and $\tilde{\theta}_i$ is the global orientation of the wheel axes. Let the length of the two links be L and R, their mass be M_L and M_R, and their inertias be J_L and J_R, respectively.

Given that the fiber space has an $SE(2)$ group structure, we utilize the lifted action given in (7.1) to compute the reduced Lagrangian and reduced non-holonomic constraints and thus verify that they are independent of any fiber variables. The matrices associated with the reduced Lagrangian and non-holonomic constraints for the simplified Trikke are given below in (7.5) through (7.7).

$$I = \begin{pmatrix} M_L + M_R & 0 & -(R\sin(\alpha_1) M_R) \\ 0 & M_L + M_R & (L + R\cos(\alpha_1))\, M_R \\ -(R\sin(\alpha_1) M_R) & (L + R\cos(\alpha_1))\, M_R & J_L + J_R + L^2 M_R + R^2 M_R + 2LR\cos(\alpha_1) M_R, \end{pmatrix} \tag{7.5}$$

$$IA = \begin{pmatrix} -(R\sin(\alpha_1) M_R) \\ R\cos(\alpha_1) M_R \\ J_R + R^2 M_R + LR\cos(\alpha_1) M_R \end{pmatrix}, \text{ and } m(r) = J_R + R^2 M_R, \tag{7.6}$$

where $I(r)$, the locked inertia tensor is the top left 3×3 sub-matrix of the reduced mass matrix, $\tilde{M}$. The non-holonomic constraints are expressed with

$$\bar{\omega}_\xi = \begin{pmatrix} 0 & 1 & 0 \\ -\sin(\alpha_1) & \cos(\alpha_1) & R + L\cos(\alpha_1) \end{pmatrix}, \text{ and } \bar{\omega}_r = \begin{pmatrix} 0 \\ R \end{pmatrix}, \tag{7.7}$$

where we have $\bar{\omega}_\xi \xi + \bar{\omega}_r \dot{r} = 0$. Now, we verify that the simplified Trikke belongs to the

mixed type of mechanical system. It has a *three-dimensional* base space, $SE(2)$. Moreover, it has *two* non-holonomic constraints, one for each wheel set. We have verified that these constraints are invariant with respect to the group action and we know that these non-holonomic constraints are linearly independent away from singular configurations. Thus, we conclude that the simplified Trikke is a *mixed system*.

Having computed the reduced Lagrangian and non-holonomic constraints for the simplified Trikke in (7.5) through (7.7), we can easily compute the generalized non-holonomic momentum using (4.3) to get

$$\begin{aligned} p &= \left(L\cot(\alpha_1)\left(M_L+M_R\right)+\frac{R\csc(\alpha_1)\left(2M_L+M_R+\cos(2\alpha_1)M_R\right)}{2}\right)\xi_1 \\ &\quad +\left(L+R\cos(\alpha_1)\right)M_R\xi_2+\left(J_L+J_R+L^2M_R+LR\cos(\alpha_1)M_R\right)\xi_3+J_R\dot{\alpha}_1. \end{aligned} \tag{7.8}$$

Now, to simplify some expressions, we make the following substitutions of the parameters for the simplified Trikke, where we set $M_L=\lambda_M, M_R=1, J_L=\lambda_J, J_R=1, L=\lambda_L$, and $R=1$. As for the reconstruction equation, we can easily compute it by solving the system of equations (4.5) and (4.6) for ξ. Then for the simplified Trikke we compute the mixed connection and the matrix multiplying the generalized momentum are shown in (7.9) and (7.10), respectively.

$$\mathbf{A}(r) = \frac{1}{D_a}\begin{pmatrix} -2\sin(\alpha_1)\left(\lambda_J+{\lambda_L}^2\right) \\ 0 \\ 2\left(1+\cos(\alpha_1)\lambda_L\right)\left(1+\lambda_M\right) \end{pmatrix}, \text{ and} \tag{7.9}$$

$$\Gamma(r) = \frac{1}{D_a}\begin{pmatrix} 2\sin(\alpha_1)\left(1+\cos(\alpha_1)\lambda_L\right) \\ 0 \\ \sin(\alpha_1)^2 \end{pmatrix}, \text{ where} \tag{7.10}$$

$$D_a = 2\left(1+\sin(\alpha_1)^2\lambda_J+2\cos(\alpha_1)\lambda_L+{\lambda_L}^2+\left(1+\cos(\alpha_1)\lambda_L\right)^2\lambda_M\right). \tag{7.11}$$

For the simplified Trikke, the generalized momentum evolution equation is given by

$$\begin{aligned}\dot{p} &= -\frac{\left(2\cos(\alpha_1)+\lambda_L\left(3+\cos(2\alpha_1)+2\cos(\alpha_1)\lambda_L\right)\right)\left(1+\lambda_M\right)}{\sin(\alpha_1)D_a}\dot{\alpha}_1 p \\ &\quad +\frac{2\lambda_L\left(1+\lambda_M-\sin(\alpha_1)^2{\lambda_L}^2\lambda_M+\cos(\alpha_1)\lambda_L\left(1+\lambda_M\right)\right)}{\sin(\alpha_1)D_a}\dot{\alpha}_1^2 \\ &\quad -\frac{\lambda_J\left(2\cos(\alpha_1)\left(1+\lambda_M\right)+\lambda_L\left(1+\cos(2\alpha_1)+2\lambda_M\right)\right)}{\sin(\alpha_1)D_a}\dot{\alpha}_1^2.\end{aligned}$$

Now, we compute the integrating factor, $h(r)$, of the above first order differential equation to get $h(\alpha_1)=\sin(\alpha_1)/\sqrt{D_a}$. Hence, rewriting the momentum evolution equation in terms of the scaled momentum variable, ρ, to arrive at

$$\begin{aligned}\dot{\rho} &= \frac{2\cos(\alpha_1)\left(-\lambda_J+{\lambda_L}^2\right)\left(1+\lambda_M\right)+\lambda_L}{D_a^{\frac{3}{2}}}\dot{\alpha}_1^2 \\ &\quad +\frac{\lambda_L\left(2+\left(2-2\sin(\alpha_1)^2{\lambda_L}^2\right)\lambda_M-\lambda_J\left(1+\cos(2\alpha_1)+2\lambda_M\right)\right)}{D_a^{\frac{3}{2}}}\dot{\alpha}_1^2. \qquad (7.12)\end{aligned}$$

The latter equation is much simpler than the original momentum evolution equation since the right hand side is composed only of one term multiplying the square of the base velocity variable, $\dot{\alpha}_1$. Thus, the new reconstruction equations, expressed in terms of the scaled momentum variable has the from

$$\xi=-\mathbf{A}(\alpha_1)\dot{\alpha}_1+\bar{\Gamma}(\alpha_1)\rho,$$

where $\mathbf{A}(\alpha_1)$ is given in (7.9) and $\bar{\Gamma}(\alpha_1)=\frac{\sqrt{D_a}}{\sin(\alpha_1)}\Gamma(r)$ where $\Gamma(r)$ is given in (7.10). We can compute the height functions using the mixed connection terms, however, for the simplified Trikke all the height functions are zero since $m=1$ in (6.6). Thus, we can conclude that the simplified Trikke is a *purely dynamic* mechanical system.

As for the gamma functions, they are simply the components of the matrix $\bar{\Gamma}(\alpha_1)$ given above. Setting the simplified Trikke parameters to $\lambda_M=1/3, \lambda_J=3$, and $\lambda_L=2$, we plot the height and gamma functions for the simplified Trikke as shown in Fig. 7.18. Note that, as expected, all the height function are zero. Moreover, note that the first gamma function, G_1, is even about the point $\alpha_1=0$ while the third gamma function, G_3, is odd about this point. Moreover, note that the first gamma function, G_1, is equal to zero at $\alpha_1=\pm 2\pi/3$ while the third gamma function, G_3, is equal to zero at $\alpha_1=k\pi$, where

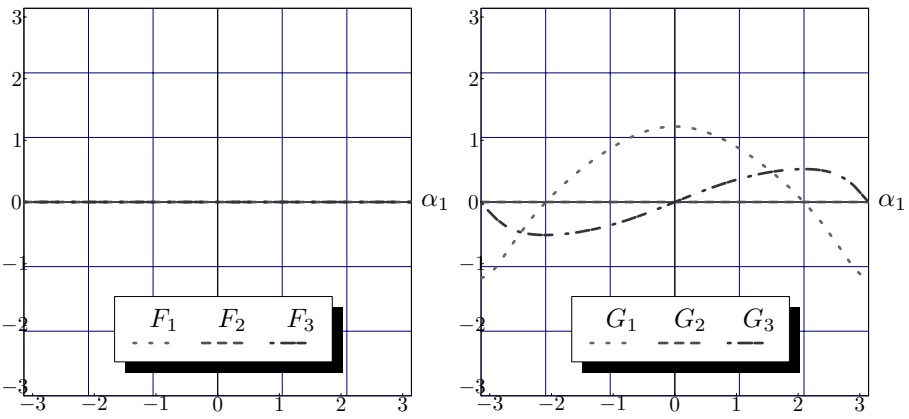

Figure 7.18: The three height and gamma functions for the simplified Trikke.

$k \in \mathbb{Z}$.

All gaits for the simplified Trikke are necessarily purely dynamic since it is a purely dynamic system as was shown in Fig. 6.1. To generate purely dynamic gaits, we have to study the properties of the gamma functions as well as the right hand side of momentum evolution equation expressed in terms of the scaled momentum. We have already computed the and analyzed the properties the gamma function in the prior section. Now, we analyze the right hand side of the scaled momentum evolution equation to eventually generate purely dynamic gaits for the simplified Trikke.

Recall that, for purely dynamic gaits, we require that the scaled momentum is sign definite as we explained in Section 6.2.2. Hence, for the simplified Trikke, we should ensure that the right hand side of (7.12) is never zero. The scaled momentum evolution equation, (7.12), has the simple form

$$\dot{\rho} = \frac{\sigma(\alpha_1)}{\sqrt{D_a^3}} \dot{\alpha}_1^2.$$

Since, the simplified Trikke parameters are all positive, we can verify that the denominator $\sqrt{D_a^3}$ given in (7.11)is always positive. Hence, to ensure that $\dot{\rho} \neq 0$, we have to analyze the numerator, $\sigma(\alpha_1)$, which, after utilizing some trigonometric identities, we can verify to be a quadratic expression in the variable $\cos(\alpha_1)$, that is, $\sigma(\alpha_1) = a\cos(\alpha_1)^2 + b\cos(\alpha_1) + c$, where a, b and c are functions of the Trikke parameters, $(\lambda_M, \lambda_J, \lambda_L)$. Thus, we have to ensure that this quadratic expression has no roots, that is, the term $\Delta = b^2 - 4ac$

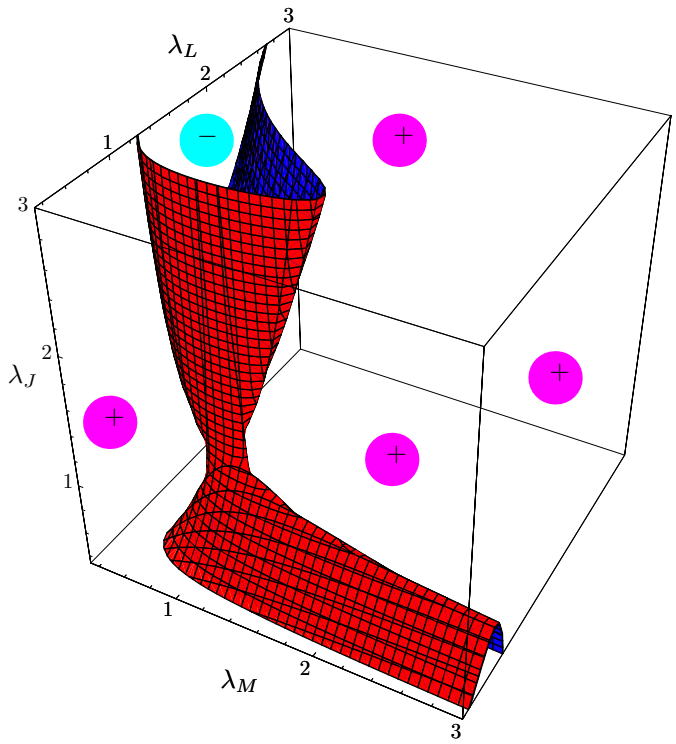

Figure 7.19: Surface partitioning the simplified Trikke parameter space.

is less than zero. If the numerator has no root, and we already proved that the denominator is always positive, then we can conclude that the right hand side of (7.12) is never zero. For the simplified Trikke, we have

$$\Delta = \left(\lambda_J - {\lambda_L}^2\right)^2 (1+\lambda_M)^2 + 4{\lambda_L}^2 \left(-\lambda_J + {\lambda_L}^2 \lambda_M\right) \left(-1 + \left(-1 + \lambda_J + {\lambda_L}^2\right) \lambda_M\right).$$

In Fig. 7.19 we plotted the surface where $\Delta = 0$ which partitions the parameter space for all simplified Trikkes into two regions: $\Delta < 0$ and $\Delta > 0$. Hence, for designing purely dynamic gaits for the simplified Trikke, we have to ensure that the Trikke parameters belong to a negative region as depicted in Fig. 7.19. In fact, the Trikke parameters we used earlier to plot the height and gamma functions, $(\lambda_M = 1/3, \lambda_J = 3, \lambda_L = 2)$, were picked from the negative region. It is interesting to note that for simplified Trikke whose parameters are picked from the negative regions, the scaled momentum is sign definite regardless of the base input, α_1.

Having picked parameters for the simplified Trikke that ensure that the scaled mo-

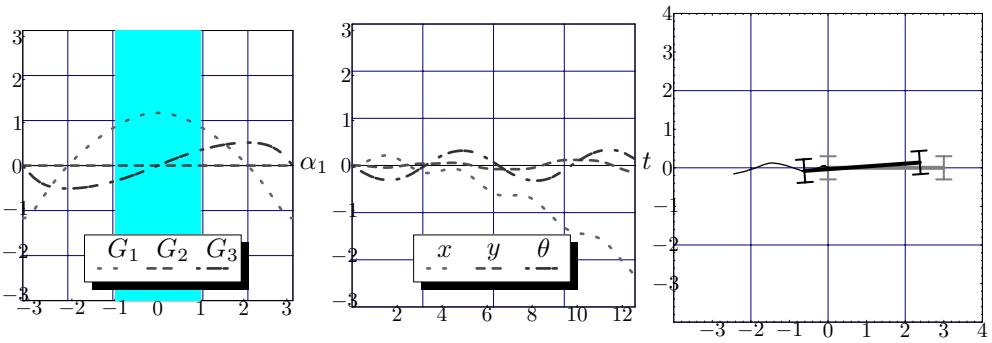

Figure 7.20: Simulation of a translational gait, ϕ_1, for the simplified Trikke.

ϕ_1	:	$\alpha_1(t) = \sin(t)$
ϕ_2	:	$\alpha_1(t) = 2\frac{\pi}{3} + \frac{\pi}{6}\sin(t)$

Table 7.7: Purely dynamic gaits for the simplified Trikke.

mentum is never zero, we can go ahead and design purely dynamic gaits by analyzing the gamma functions depicted in Fig. 7.18.

Without loss of generality, lets assume that we want to design a gait that moves the simplified Trikke along the ξ^1 direction. Thus, we have to ensure that the gait remains entirely within a positive region of the first gamma function, G_1. Moreover, we have to ensure that the gait is symmetric with respect to an odd point of the third gamma function G_3. Thus, we conclude that a gait that is centers about the origin of the base space, $\alpha_1 = 0$, will yield a non-zero dynamic phase shift only along the ξ^1 direction. The gait ϕ_1 in the first row of Table 7.7 satisfies all the above requirements.

We have simulated the gait ϕ_1 and presented the results in Fig. 7.20. This first plot in Fig. 7.20 depicts the gait ϕ_1 superimposed on top of the gamma function. We can see that this particular gait lies entirely in a positive region of the first gamma function, G_1; moreover, this gait is symmetric about an odd point, $(\alpha_1 = 0)$, of the third gamma function, G_3, as depicted by the shaded region in the first plot of Fig. 7.20. The second plot in Fig. 7.20 depicts a time simulation of the gait ϕ_1, where we can see the evolution of the fiber variables, (x, y, θ). The final plot depicts two snapshots of the simplified Trikke at the beginning and end of the gait ϕ_1 where we can see that the Trikke is moving along the x direction.

Similarly, we propose another gait, ϕ_2 in the second row of Table 7.7, that ensures that the dynamic phase shift is non-zero only along the ξ^3 direction. We designed this gait, to

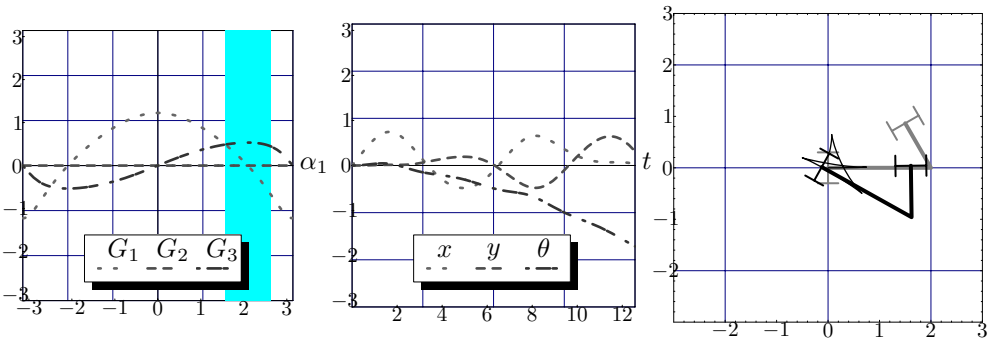

Figure 7.21: Simulation of a rotational gait, ϕ_2, for the simplified Trikke.

lie entirely in a positive region of the third gamma function, G_3 while it spans two regions of opposite signs of the first gamma function as depicted by the shaded region of the first plot in Fig. 7.21. We simulated this gait and we can see that it rotates the Trikke as shown in the second plot of Fig. 7.21. Finally, the last plot in Fig. 7.21 depicts two snapshots of the simplified Trikke at the beginning and end of the gait, ϕ_2, where we can clearly see that the Trikke has indeed rotated.

7.4 Mixed Systems

In this Section, we generate gaits for two mixed systems. The first of which is the Snakeboard[3] which was extensively studied in the literature in [8,40]. The second mixed system is a novel mechanical system which we term the *variable inertia snakeboard*. We introduce the variable inertia snakeboard which, as the name suggest, is a variable inertia system as opposed to the constant inertia original snakeboard. Applying our gait generation tools to this novel system, allows us to prove the generality and applicability of our techniques. Since both snakeboards, as we shall prove, are mixed systems, we will generate three types of gaits for each system as we prescribed in Fig. 6.1.

7.4.1 Snakeboard

A schematic of the original snakeboard is shown in Fig. 7.22. It is composed of one rigid link, a rotor pivoting around the center of the link and two passive wheel sets pivoting at the each of the distal ends of the link. The no sideways slippage of these two sets of wheels provide the two non-holonomic constraints. We attach a body coordinate frame to

[3]We shall refer to the system as the original snakeboard in the rest of this document.

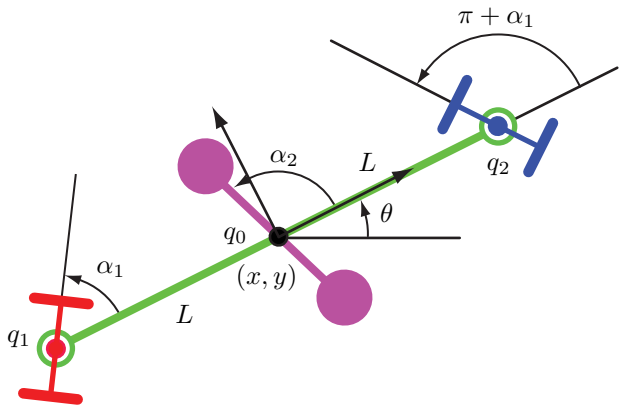

Figure 7.22: A schematic of the original Snakeboard.

the middle of the center link as shown in Fig. 7.22. The position and orientation of the body frame is represented by the fiber variables, (x, y, θ), while the two internal degrees of freedom representing the wheel axes and rotor angles are denoted by the base variables, (α_1, α_2). Note that, just as was the case in the prior work, we have coupled the wheel axes rotation to be equal in magnitude but opposite in direction.

Hence, the original snakeboard has a five-dimensional, $(n = 5)$, configuration space $Q = G \times M$, where the associated Lie group fiber space denoting the robot's position and orientation in the plane is $G = SE(2)$, the special Euclidean group. The base space denoting the internal degrees of freedom, the coupled wheel angles and the rotor angle, is $M = \mathbb{S} \times \mathbb{S}$. The Lagrangian of the pivoting dynamic model in the absence of gravity is

$$L(q, \dot{q}) = \frac{1}{2} \sum_{i=1}^{3} \left(m_i \dot{x}_i^T \dot{x}_i + j_i \dot{\theta}_i^2 \right) \tag{7.13}$$

where m_i and j_i represent the mass and inertia of each of the rigid bodies: the center link, the rotor, and the wheels, while x_i and θ_i represent the inertial position and orientation of these rigid bodies. Moreover, two non-holonomic constraints act on the system are given by the following form

$$\frac{d}{dt} \begin{pmatrix} \tilde{x}_i & \tilde{y}_i \end{pmatrix} \begin{pmatrix} \cos(\tilde{\theta}_i) \\ \sin(\tilde{\theta}_i) \end{pmatrix} = 0$$

where $(\tilde{x}_i, \tilde{y}_i)$ is the global position of the intersection point of the wheel axes and the middle link, and $\tilde{\theta}_i$ is the global orientation of the wheel axes. Let the length of the middle link be $2L$ and the mass and inertia of the entire system be denoted by M and

J, respectively. The rotor and wheel inertias are denoted by J_r and J_w, respectively. To simplify some expressions we will assume that $J + J_r + 2J_w = ML^2$.

Given that the fiber space has an $SE(2)$ group structure, we utilize the group action and lifted action given in (7.1) to compute the reduced Lagrangian and non-holonomic constraints and verify that they are independent of any fiber variables. The matrices associated with the reduced Lagrangian and non-holonomic constraints for the original snakeboard are given below in (7.14) through (7.16).

$$\tilde{M} = \left(\begin{array}{ccc|cc} M & 0 & 0 & 0 & 0 \\ 0 & M & 0 & 0 & 0 \\ 0 & 0 & ML^2 & 0 & J_r \\ \hline 0 & 0 & 0 & 2J_w & 0 \\ 0 & 0 & J_r & 0 & J_r \end{array}\right) \tag{7.14}$$

where $I(r)$, the locked inertia tensor is the top left 3×3 sub-matrix of $\tilde{M}$. The non-holonomic constraints are expressed with

$$\bar{\omega}_\xi = \left(\begin{array}{ccc} -\sin(\alpha_1) & \cos(\alpha_1) & L\cos(\alpha_1) \\ -\sin(\alpha_1) & -\cos(\alpha_1) & L\cos(\alpha_1) \end{array}\right) \tag{7.15}$$

$$\bar{\omega}_r = \left(\begin{array}{cc} 0 & 0 \\ 0 & 0 \end{array}\right) \tag{7.16}$$

Note the *constant* reduced mass matrix for the original snakeboard. This actually simplifies the problem of gait generation. In fact, this is one of the reasons we are introducing the variable inertia snakeboard, which does not have a constant reduced mass matrix.

Now, we verify that the original snakeboard belongs to the mixed type of mechanical system. It has a *three-dimensional* base space, $SE(2)$. Moreover, it has *two* non-holonomic constraints, one for each wheel set. We have verified that these constraints are invariant with respect to the group action and we know that these non-holonomic constraints are linearly independent away from singular configurations. Thus, we conclude that the original snakeboard is a *mixed system*.

Having computed the reduced Lagrangian and non-holonomic constraints for the original snakeboard in (7.14) through (7.16), we can easily compute the generalized non-

holonomic momentum using (4.3) to have

$$p = LM\cot(\alpha_1)\xi^1 + L^2M\xi^3 + Jr\dot{\alpha}_2. \tag{7.17}$$

As for the reconstruction equation, we can easily compute it by solving the system of equations (4.5) and (4.6) for ξ. Then for the original snakeboard we have

$$\mathbf{A}(r) = \frac{J_r}{ML^2}\begin{pmatrix} 0 & \frac{L}{2}\sin(2\alpha_1) \\ 0 & 0 \\ 0 & \sin(\alpha_1)^2 \end{pmatrix}, \text{ and} \tag{7.18}$$

$$\Gamma(r) = \frac{1}{ML^2}\begin{pmatrix} \frac{L}{2}\sin(2\alpha_1) \\ 0 \\ \sin(\alpha_1)^2 \end{pmatrix}. \tag{7.19}$$

For the original snakeboard, the generalized momentum evolution equation is rather simple and it is given by

$$\dot{p} = -\cot(\alpha_1)\dot{\alpha}_1 p + J_r\cot(\alpha_1)\dot{\alpha}_1\dot{\alpha}_2.$$

This equation allows us to compute the integrating factor, $h(r) = \exp(\int \cot\alpha_1\dot{\alpha}_1 dt) = \sin(\alpha_1)$. Then (5.8), the new evolution equation, expressed using the scaled momentum variable for the original snakeboard becomes

$$\dot{\rho} = -\frac{Jr}{2}\begin{pmatrix} \dot{\alpha}_1 \\ \dot{\alpha}_2 \end{pmatrix}^T \overbrace{\begin{pmatrix} 0 & \cos(\alpha_1) \\ \cos(\alpha_1) & 0 \end{pmatrix}}^{\bar{\Sigma}(r)} \begin{pmatrix} \dot{\alpha}_1 \\ \dot{\alpha}_2 \end{pmatrix}. \tag{7.20}$$

Now we compute the height functions for the original snakeboard. Using the mixed connection, we can compute the exterior derivative of each row. Hence using (6.6), the height functions will have the following expressions

$$\begin{aligned} F_1 &= \frac{J_r}{ML}\cos(2\alpha_1), \\ F_2 &= 0 \text{ , and} \\ F_3 &= \frac{J_r}{ML^2}\sin(2\alpha_1). \end{aligned}$$

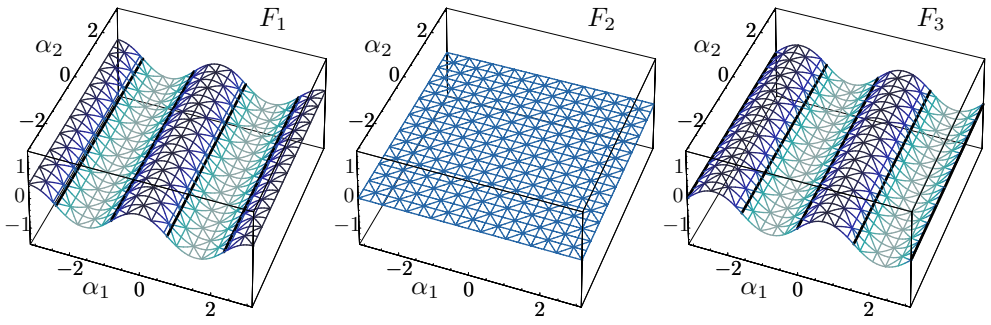

Figure 7.23: The three height functions for the original snakeboard.

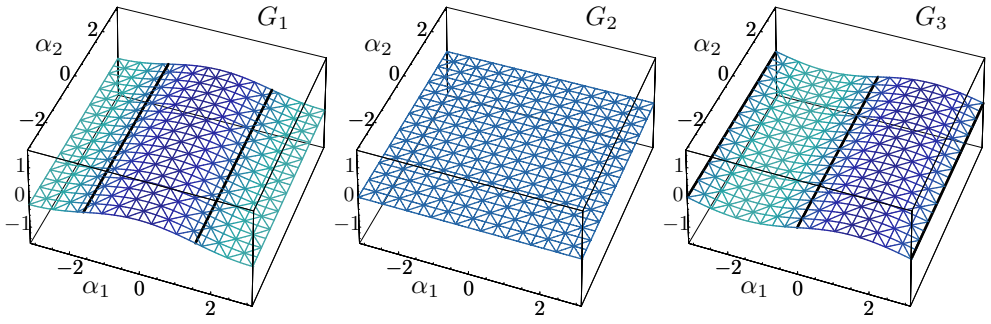

Figure 7.24: The three gamma functions for the original snakeboard.

These height functions are shown in Fig. 7.23. As for the gamma functions, since the original snakeboard has only one generalized momentum variable, we simply divide the Γ functions in (7.19) by the integrating factor to get

$$\begin{aligned} G_1 &= \frac{1}{ML}\cos(\alpha_1), \\ G_2 &= 0 \text{ , and} \\ G_3 &= \frac{1}{ML^2}\sin(\alpha_1). \end{aligned}$$

The gamma functions for the original snakeboard are depicted in Fig. 7.24. Hence, it is self-evident from the expressions of the height and gamma functions that they do not depend on α_2, the rotor angle. This explains why the graphs of the original snakeboard height and gamma functions are extrusions (Fig. 7.23) and (Fig. 7.24).

Referring to Fig. 7.23, note the following properties of the height functions for the

original snakeboard.

- $F_1 = 0$ for $\{\alpha_1 = (2k+1)\frac{\pi}{4}, k \in \mathbb{Z}\}$,
- $F_2 = 0$ for all $\{\alpha_1, \alpha_2\}$,
- $F_3 = 0$ for $\{\alpha_1 = k\frac{\pi}{2}, k \in \mathbb{Z}\}$,
- F_1 is even about the lines $\alpha_1 = k\frac{\pi}{2}, k \in \mathbb{Z}\}$,
- F_1 is odd about the lines $\alpha_1 = (2k+1)\frac{\pi}{4}, k \in \mathbb{Z}\}$,
- F_3 is even about the lines $\alpha_1 = (2k+1)\frac{\pi}{4}, k \in \mathbb{Z}\}$,
- F_3 is odd about the lines $\alpha_1 = k\frac{\pi}{2}, k \in \mathbb{Z}\}$.

Referring to Fig. 7.24, note the following properties of the gamma functions for the original snakeboard.

- $G_1 = 0$ for $\{\alpha_1 = (2k+1)\frac{\pi}{2}, k \in \mathbb{Z}\}$,
- $G_2 = 0$ for all $\{\alpha_1, \alpha_2\}$,
- $G_3 = 0$ for $\{\alpha_1 = k\pi, k \in \mathbb{Z}\}$,
- G_1 is even about the lines $\alpha_1 = k\pi, k \in \mathbb{Z}\}$,
- G_1 is odd about the lines $\alpha_1 = (2k+1)\frac{\pi}{2}, k \in \mathbb{Z}\}$,
- G_3 is even about the lines $\alpha_1 = (2k+1)\frac{\pi}{2}, k \in \mathbb{Z}\}$,
- G_3 is odd about the lines $\alpha_1 = k\pi, k \in \mathbb{Z}\}$.

Purely Kinematic Gaits

Recall that for purely dynamic gaits, we want to solve for base space curves for which $I_{GEO} \neq 0$ while $I_{DYN} = 0$. Hence, we first solve the scaled momentum differential equation such that the momentum is zero for all time. This is done by setting the right hand side of (7.20) equal to zero. In general, the right hand side of (7.20) is a quadratic expression with four unknowns, $(\alpha_1, \alpha_2, \dot{\alpha}_1, \dot{\alpha}_2)$. However, for the original snakeboard, (7.20) has a simple form where

$$\dot{\rho} = -J_r \cos(\alpha_1)\dot{\alpha_1}\dot{\alpha_2}.$$

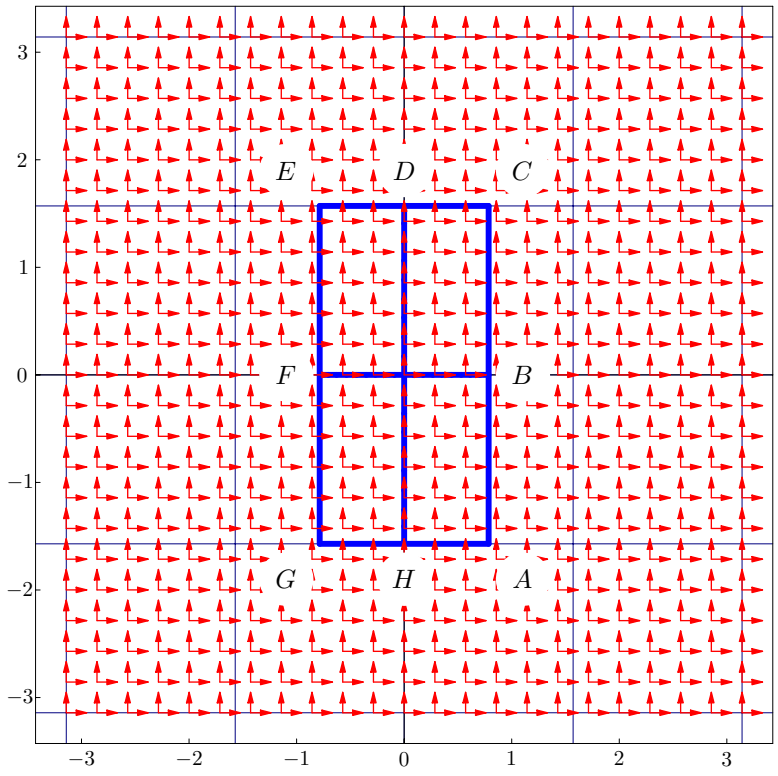

Figure 7.25: Vector field defining the purely kinematic gaits of the 'original snakeboard.

The right hand side has a single term which has a product of the two base velocities, $\dot{\alpha_1}$ and $\dot{\alpha_2}$. Thus, it is clear that if we ensure that at least of the base velocities is zero at any given time, then we must have $\dot{\rho} = 0$. Additionally, if we assume that we are starting from zero initial momentum, that is, $p = \rho = 0$, then any base space curve that has at least one of the base velocities is zero is a candidate for a purely kinematic gait for the original snakeboard.

Hence, for the original snakeboard we plot two vector fields, $\dot{\alpha_1} = 0$ and $\dot{\alpha_2} = 0$, over the entire base space as shown in Fig. 7.25, where any part of the integral curves of these vector fields can be used to construct a purely kinematic gait. The integral curves of the vector fields are the following lines

$$\begin{aligned} l_1 &= \{\alpha_1 = k, k \in \mathbb{R}\}, \\ l_2 &= \{\alpha_2 = k, k \in \mathbb{R}\}. \end{aligned}$$

Then we can easily construct purely kinematic gaits for the original snakeboard by flowing along the above lines. Flowing along the above lines means that we can change only one base variable at a time, so either change the rotor angle or the wheel angles and not both at the same time. These gaits are structurally similar to the gaits proposed by Bullo *et al.* in [8]. In Figure 7.25 we have plotted a subset of these integral lines (solid lines). Now we can easily design purely kinematic gaits which are given in Table 7.8.

${}^{PK}\phi_1$	:	$A - C - E - G - A$
${}^{PK}\phi_2$	:	$A - B - F - E - C - B - F - G - A$
${}^{PK}\phi_3$	:	$A - C - D - H - G - E - D - H - A$

Table 7.8: Purely kinematic gaits for the original snakeboard.

In designing the above gaits, we have carefully chosen along which integral lines to flow. The motions due to these three gaits are depicted in Fig. 7.26. For instance, consider the first gait, ${}^{PK}\phi_1$, which is a rectangle centered at the origin of the base space. Such a curve envelops a non-zero volume only under the first height function shown in the first row of Fig. 7.26. For this particular gait, we limited the wheel angles to $-\frac{\pi}{4} \leq \alpha_1 \leq \frac{\pi}{4}$. This ensures that we do not include any negative volume under the first height function as shown in the first plot in the first row of Fig. 7.26. Actually we have simulated this gait and depicted the time simulation in the second and third plots of the first row of Fig. 7.26. Note, that for ${}^{PK}\phi_1$, $\rho = 0$ for all time as shown in the second plot of the first row of Fig. 7.26. The third plot in the first row of Fig. 7.26 depicts the fiber variables versus time while the last plot in the first row depicts two snapshots of the original snakeboard at the beginning and end of the gait, ${}^{PK}\phi_1$. Note the net motion along the x direction.

Actually, we simulated the other gaits, ${}^{PK}\phi_2$ and ${}^{PK}\phi_3$, given in Table 7.8 as shown in the second and third rows of Fig. 7.26, respectively. Note that the gait ${}^{PK}\phi_2$ moves the original snakeboard along the y direction while the gait ${}^{PK}\phi_3$ rotates the original snakeboard.

Purely Dynamic Gaits

Purely dynamic gaits are relatively easier to design. The designed curves should enclose zero volume under all height functions simultaneously. For example, purely dynamic sinusoidal gaits are usually gaits in which the frequencies of all inputs are identical. We designed three purely dynamic gaits for the original snakeboard which are given in Ta-

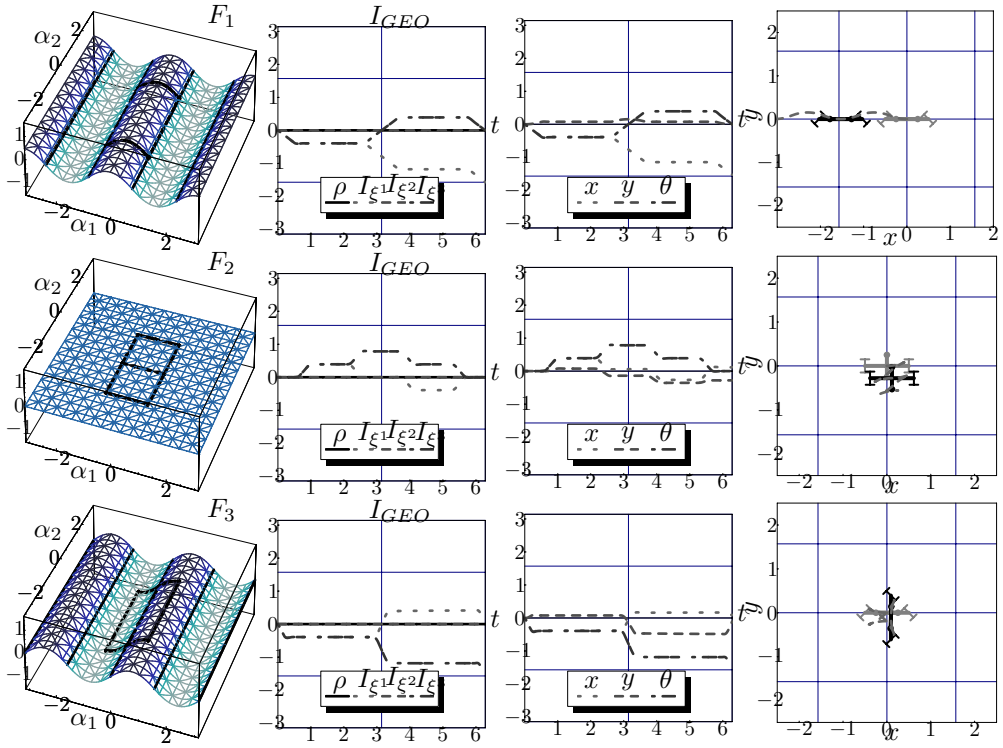

Figure 7.26: Simulation of the three purely kinematic gaits, ${}^{PK}\phi_1$, ${}^{PK}\phi_2$, and ${}^{PK}\phi_3$, for the original snakeboard. The first column depicts non-zero motion producing purely kinematic gaits superimposed over the height functions, the second column depicts the evolution of the scaled momentum and the geometric phase shift along the fiber directions, the third column depicts the time evolution of the fiber variables, and the last column depicts snapshots of the mechanical system at the beginning and end of each gait.

${}^{PD}\phi_1$	:	$\alpha_1 = \frac{\pi}{5}(1 - 2\sin^2(t))$ $\alpha_2 = \frac{\pi}{3}\sin(t)$
${}^{PD}\phi_2$	:	$\alpha_1 = \frac{5\pi}{11}\sin(t)$ $\alpha_2 = \frac{5\pi}{11}(1 - 2\sin^2(t))$
${}^{PD}\phi_3$	:	$\alpha_1 = \frac{\pi}{5}(1 - 2\sin^2(t)) + \frac{\pi}{4}$ $\alpha_2 = \frac{\pi}{3}\sin(t)$

Table 7.9: Purely dynamic gaits for the original snakeboard.

ble 7.9.

The motions of the original snakeboard due to the above gaits are depicted in Fig. 7.27.

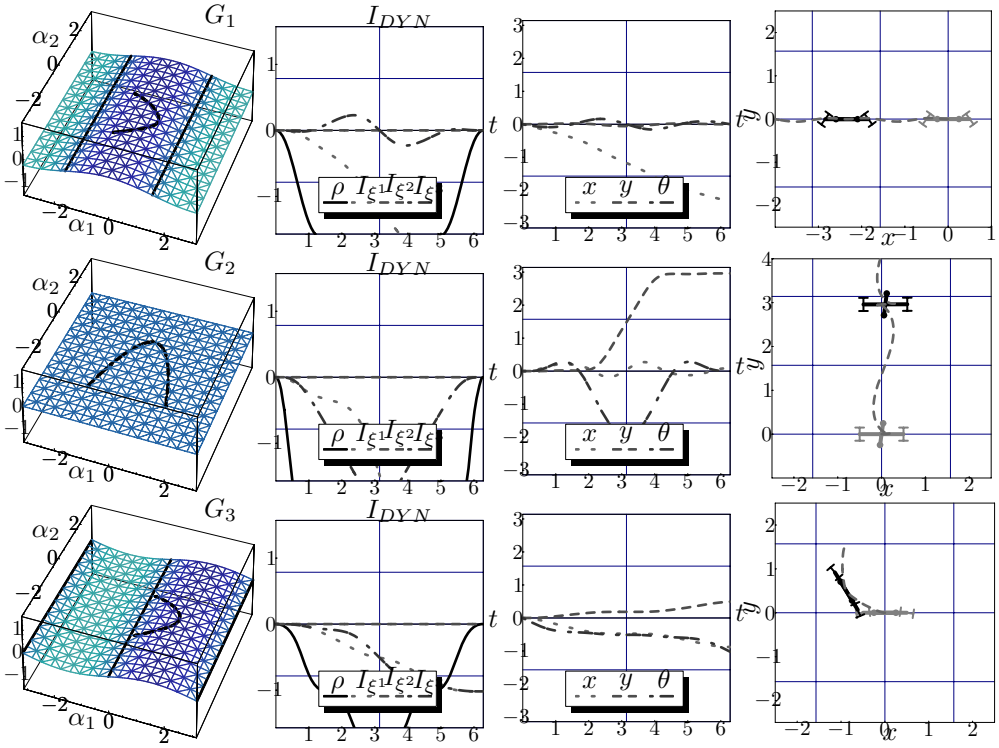

Figure 7.27: Simulation of the three purely dynamic gaits, ${}^{PD}\phi_1$, ${}^{PD}\phi_2$, and ${}^{PD}\phi_3$, for the original snakeboard. The first column depicts non-zero motion producing purely dynamic gaits superimposed over the gamma functions, the second column depicts the evolution of the scaled momentum and the dynamic phase shift along the fiber directions, the third column depicts the time evolution of the fiber variables, and the last column depicts snapshots of the mechanical system at the beginning and end of each gait.

Consider the first gait, ${}^{PD}\phi_1$, which is depicted in the first row of Fig. 7.27. As expected this gait encloses zero volume in the base space. For this particular gait, we numerically verified that $\rho \leq 0$ for all time as shown in the second plot in the first row of Fig. 7.27. Moreover, we placed the curve in a base space region where only the first gamma function is positive as shown in the first plot of the first row of Fig. 7.27, and we ensured that the curve is symmetric about the line $\alpha_1 = 0$, which is an odd line for the third gamma function. Then we numerically simulated this gait and computed the values of I_{DYN} along the fiber directions, (ξ^1, ξ^2, ξ^3), as shown in the second plot of the first row of Fig. 7.27. Observe that only I^{DYN} along the ξ^1 direction is non-zero after the first cycle of the gait. Then, we numerically compute the three fiber variables, (x, y, θ), of the original snakeboard and plot

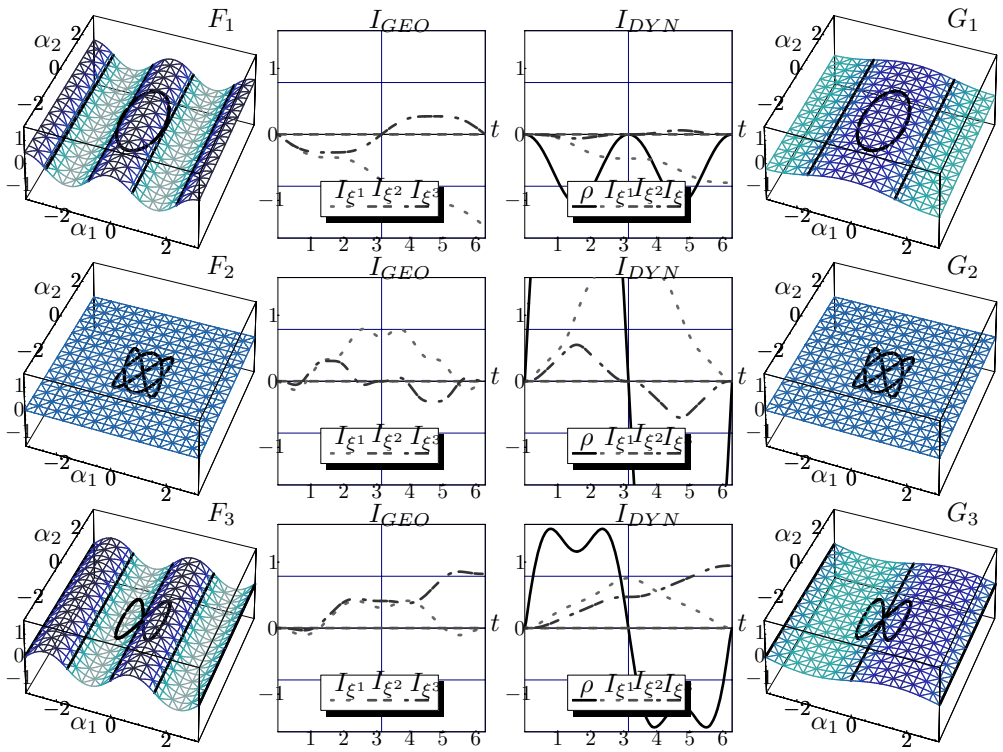

Figure 7.28: Simulation of the three kino-dynamic gaits, ${}^{KD}\phi_1$, ${}^{KD}\phi_2$, and ${}^{KD}\phi_3$, for the original snakeboard. The first and last columns depict non-zero motion producing kino-dynamic gaits superimposed over the height and gamma functions, respectively, the middle columns depict the evolution of the scaled momentum and the geometric and dynamic phase shifts along the fiber directions.

them versus time as show in the third plot in the first row of Fig. 7.27. As expected, this gait moves the original snakeboard only along the ξ^1 direction[4]. Finally, the last plot in the first row of Fig. 7.27 depicts to snapshots of the original snakeboard at the beginning and end of the gait, ${}^{PD}\phi_1$, where the motion along the x direction can be seen.

Similarly, we design two gaits, ${}^{PD}\phi_2$ and ${}^{PD}\phi_3$, which respectively encloses non-zero volume under the second and third gamma functions as shown in the second and third rows of Fig. 7.27. These two gaits move the original snakeboard along the y direction or rotates it along the θ fiber direction.

[4]For this particular gait, the motion along the ξ^1 direction, is mapped almost entirely to motion along the x direction.

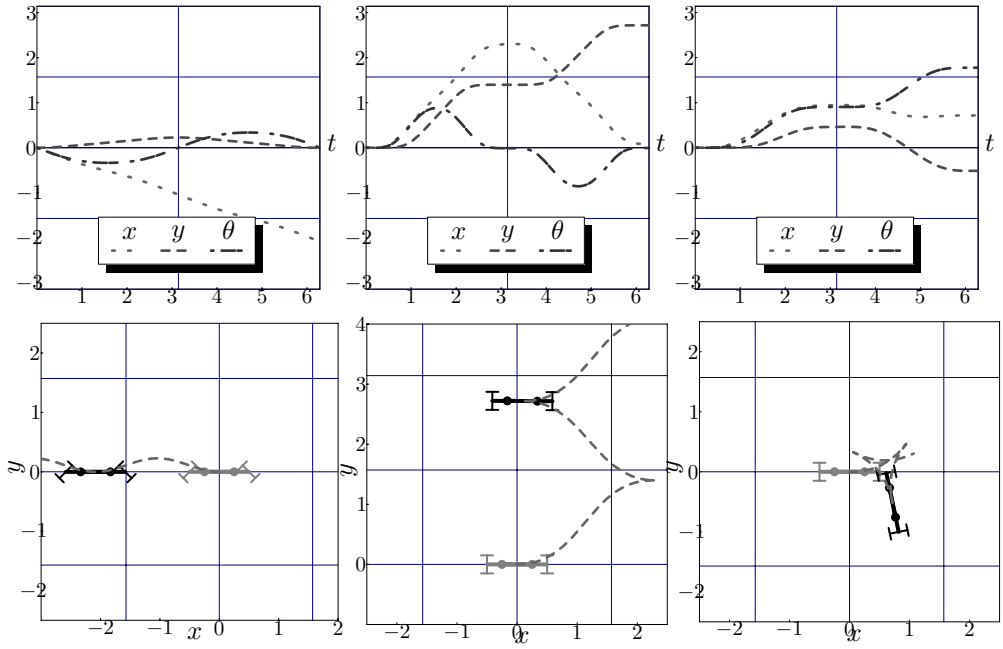

Figure 7.29: The motion of the original snakeboard as it performs the three kino-dynamic gaits, ${}^{KD}\phi_1$, ${}^{KD}\phi_2$, and ${}^{KD}\phi_3$.

Kino-dynamic Gaits

As we mentioned earlier, kino-dynamic gaits are gaits for which both the geometric and dynamic phase shift contribute to the systems motion. For these gaits, we start with the volume analysis of the geometric gaits. For example, to design a gait that moves the original snakeboard in the ξ^1 direction, we design a curve that encloses a non-zero volume only under the first height function shown in the first row of Fig. 7.28. We can easily conclude that a curve with the following properties is a possible candidate.

- Closed non-intersecting curve.
- Symmetric about the line $\alpha_1 = k\pi/2$, $k \in \mathbb{Z}$.
- The curve is bounded by the two lines, $k\pi/4 \leqslant \alpha_1 \leqslant (k+1)\pi/4$, $k \in \mathbb{Z} - \{0\}$.

The gait given in the first row of Table 7.10 satisfies all the above properties. We have simulated this gait as shown in the first row of Fig. 7.28. The first and last plots depict the gait in the base space superimposed on top of the height and gamma functions, respectively, where we verify that it satisfies the above requirements. We simulated this

gait and plotted the values of I_{GEO} and I_{DYN} versus time in the second and third plots of the first row of Fig. 7.28. Note the non-zero value of the I_{GEO} and I_{DYN} along the ξ^1 direction at the end of the cycle. Moreover, note that at the end of each cycle, both the geometric and dynamic phase shifts have the same sign and additively contribute to the total motion. Finally, we plot the actual fiber variables versus time and the initial and final configurations of the original snakeboard as shown in the first column of Fig. 7.29. Note that this particular gait moves the original snakeboard solely along the global x direction.

${}^{KD}\phi_1$	:	$\alpha_1 = \frac{\pi}{4}\cos(t)$
		$\alpha_2 = \frac{\pi}{2}\sin(t)$
${}^{KD}\phi_2$	:	$\alpha_1 = \frac{\pi}{4}\sin(2t)$
		$\alpha_2 = \frac{\pi}{3}\sin(3t)$
${}^{KD}\phi_3$	:	$\alpha_1 = \frac{\pi}{4}\sin(t)$
		$\alpha_2 = \frac{\pi}{3}\sin(2t)$

Table 7.10: Kino-dynamic gaits for the original snakeboard.

Similarly we generate two other gaits given in the second and third rows of Table 7.10 that move the original snakeboard along the y and θ directions. We have simulated both gait, ${}^{KD}\phi_2$ and ${}^{KD}\phi_3$, which are shown in the second and third rows of Fig. 7.28. Note that for ${}^{KD}G_2$ both I_{GEO} and I_{DYN} are always zero in the ξ^2 direction. However, the gait still produced a net y motion as shown in the second column Fig. 7.29. This is due to the non-commutativity of the group fiber, $SE(2)$. The third gait, ${}^{KD}\phi_3$, rotated the original snakeboard along the θ fiber direction as shown in the last column of Fig. 7.29. We have plotted snapshots of the original snakeboard at the beginning and end of each of the above gaits in the second row of Fig. 7.29.

7.4.2 Variable Inertia Snakeboard

In this section we introduce the *variable inertia snakeboard* example which is somewhat related to the original snakeboard but as we shall see it is a rather more complicated system. The variable inertia snakeboard shown in Fig. 7.30 is composed of three rigid links that are connected by two revolute joints. The outer two links have mass, m, concentrated at the distal ends and an inertia, j, while the middle link is massless. Moreover, attached to the distal ends of the outer two links is a set of passive wheels whose axes are perpendicular to the robot's links. The no sideways slippage of these two sets of wheels provide the two

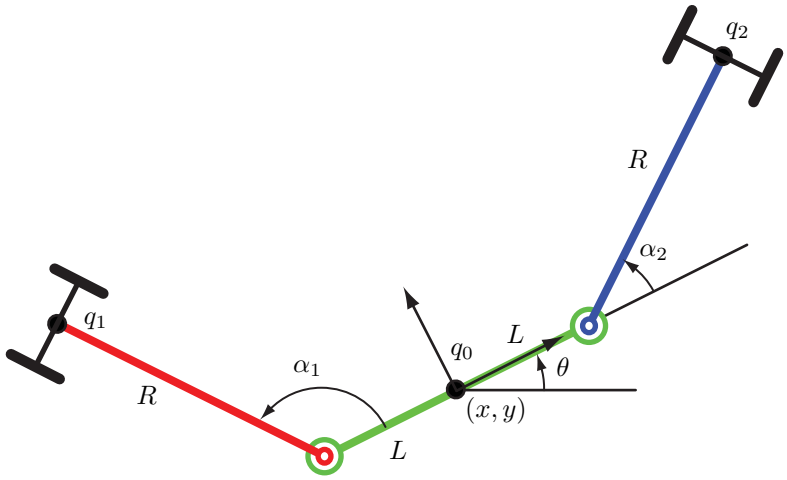

Figure 7.30: Variable inertia Snakeboard.

non-holonomic constraints which act on the system. We attach a body coordinate frame to the middle of the center link and align its first axis along that link. The location of the origin of this body-attached frame is represented the configuration variables (x, y) while its global orientation is represented by the variable θ. The two internal degrees of freedom are represented by the relative angle between the links (α_1, α_2).

Hence, the variable inertia snakeboard has a five dimensional, $(n = 5)$, configuration space $Q = G \times M$, where the associated Lie group fiber space denoting the robot's position and orientation in the plane is $G = SE(2)$, the special Euclidean group. The base space denoting the internal degrees of freedom is $M = \mathbb{S} \times \mathbb{S}$. The Lagrangian of the variable inertia snakeboard in the absence of gravity is computed using (7.13).

Let $2L$ and R be the length of the middle link and the outer links, respectively. To simplify some expressions we will assume that the mass and inertia of the two distal links are identical, that is, $m_i = m$ and $j_i = j = mR^2$. Given that the fiber space has an $SE(2)$ group structure, we can compute the group lifted action as shown in (7.1). The lifted action allows us to verify the Lagrangian invariance and to compute the reduced Lagrangian and the component of the reduced mass matrix associated with it are given by

$$
\begin{aligned}
I &= mR\begin{pmatrix} \frac{2}{R} & 0 & -\sin(\alpha_1)+\sin(\alpha_2) \\ 0 & \frac{2}{R} & \cos(\alpha_1)-\cos(\alpha_2) \\ -\sin(\alpha_1)+\sin(\alpha_2) & \cos(\alpha_1)-\cos(\alpha_2) & 2\left(\frac{L^2+2R^2}{R}+\frac{\cos(\alpha_1)+\cos(\alpha_2)}{1/L}\right) \end{pmatrix}, \\
IA &= mR\begin{pmatrix} -\sin(\alpha_1) & \sin(\alpha_2) \\ \cos(\alpha_1) & -\cos(\alpha_2) \\ 2R+L\cos(\alpha_1) & 2R+L\cos(\alpha_2) \end{pmatrix}, \text{ and } m(r)=\begin{pmatrix} 2mR^2 & 0 \\ 0 & 2mR^2 \end{pmatrix}
\end{aligned}
$$

Note that the reduced mass matrix for the variable inertia snakeboard depends solely on the base variables α_1 and α_2 and is *not constant* as was the case for the original snakeboard which was studied in the prior work. Similarly we can write the non-holonomic constraints with respect to the body coordinate frame for the variable inertia snakeboard as

$$
\bar{\omega}_\xi = \begin{pmatrix} -\sin(\alpha_1) & \cos(\alpha_1) & R+L\cos(\alpha_1) \\ \sin(\alpha_2) & -\cos(\alpha_2) & R+L\cos(\alpha_2) \end{pmatrix} \tag{7.21}
$$

$$
\bar{\omega}_r = \begin{pmatrix} R & 0 \\ 0 & R \end{pmatrix} \tag{7.22}
$$

Now, we verify that the variable inertia snakeboard belongs to the mixed type of mechanical system. It has a *three-dimensional* base space, $SE(2)$. Moreover, it has *two* non-holonomic constraints, one for each wheel set. We can verify that these constraints are invariant with respect to the group action and we know that these non-holonomic constraints are linearly independent away from singular configurations. Thus, we conclude that the variable inertia snakeboard is a *mixed system*.

Similarly, we can compute the generalized non-holonomic momentum which is given by

$$
p = \frac{m\left(p_{\xi^1}\xi^1 + p_{\xi^2}\xi^2 + p_{\xi^3}\xi^3 + p_\alpha(\dot{\alpha}_1+\dot{\alpha}_2)\right)}{2\sin(\alpha_1-\alpha_2)}, \tag{7.23}
$$

where p_{ξ^i} and p_α are analytic functions of the base variables which are shown in Table 7.11. As for the mixed connection, it is given by

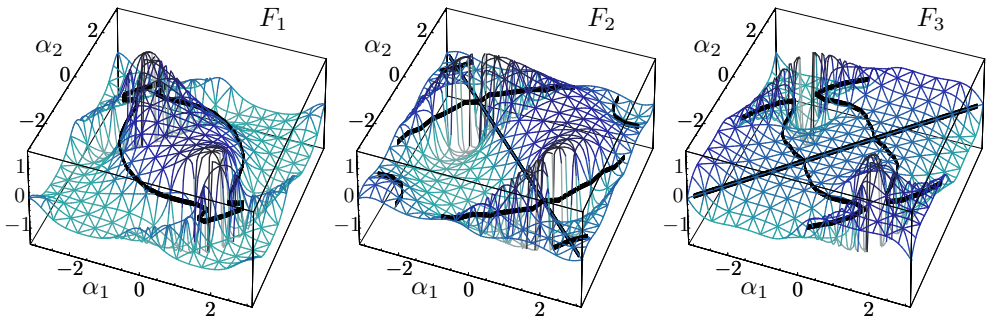

Figure 7.31: The three height functions for the variable inertia snakeboard. The darker shades indicate the positive regions which are separated from the lighter colored regions by the solid curves.

$$\mathbf{A}(r) = \frac{1}{2D_a} \begin{pmatrix} \mathbf{A}_1^1 & \mathbf{A}_2^1 \\ \mathbf{A}_1^2 & \mathbf{A}_2^2 \\ \mathbf{A}_1^2 & \mathbf{A}_3^2 \end{pmatrix} \tag{7.24}$$

where $\mathbf{A}_j^i$ and D_a are also analytic functions of the base variables which are shown in Table 7.11. Note how complex are the expressions for the generalized non-holonomic momentum and the mixed connection for the variable inertia snakeboard are in comparison to those of the fixed-inertia original snakeboard.

Similarly, we can compute the integrating factor for the variable inertia snakeboard and then the momentum evolution equation of the scaled momentum variable is given by

$$\dot{\rho} = \frac{2mR}{D_s} \begin{pmatrix} \dot{\alpha}_1 \\ \dot{\alpha}_2 \end{pmatrix}^T \overbrace{\begin{pmatrix} \bar{\Sigma}_{11} & \bar{\Sigma}_{12} \\ \bar{\Sigma}_{21} & \bar{\Sigma}_{22} \end{pmatrix}}^{\bar{\Sigma}(r)} \begin{pmatrix} \dot{\alpha}_1 \\ \dot{\alpha}_2 \end{pmatrix}, \tag{7.25}$$

where $\bar{\Sigma}_{ij}$ and D_s are analytic functions of the base variables which are shown in Table 7.11.

Using the mixed connection and coefficients multiplying the scaled momentum in the reconstruction equations, we can respectively compute the height and gamma functions for the variable inertia snakeboard. The expressions for this particular system are rather complicated and we will not present them here; however, we encourage the reader to compute these terms as an exercise. We depict the graphs of the three height functions and three gamma functions in Fig. 7.31 and Fig. 7.32, respectively. Referring to Fig. 7.31, note the following properties of the height functions for the variable inertia snakeboard.

$$
\begin{array}{lcl}
p_{\xi_1} & = & 3R\cos(\alpha_1) + R\cos(\alpha_1 - 2\alpha_2) + 4L\cos(\alpha_1 - \alpha_2) \\
 & & +R\cos(2\alpha_1 - \alpha_2) + 3R\cos(\alpha_2) + 4L\cos(\alpha_1 + \alpha_2) \\
p_{\xi_2} & = & 3R\sin(\alpha_1) - R\sin(\alpha_1 - 2\alpha_2) + R\sin(2\alpha_1 - \alpha_2) + 3R\sin(\alpha_2) + 4L\sin(\alpha_1 + \alpha_2) \\
p_{\xi_3} & = & 2\sin(\alpha_1 - \alpha_2)\left(2\left(L^2 + R^2\right) + LR\cos(\alpha_1) + LR\cos(\alpha_2)\right) \\
p_{\alpha} & = & 2\sin(\alpha_1 - \alpha_2)R^2 \\
\hline
\mathbf{A}_1^1 & = & -2\left(\left(L^2 + R^2 + 2LR\cos(\alpha_2) + L^2\cos(2\alpha_2)\right)\sin(\alpha_1)\right) \\
 & & -2\left(+R\left(R + L\left(\cos(\alpha_1) + \cos(\alpha_2)\right)\right)\sin(\alpha_2)\right) \\
\mathbf{A}_2^1 & = & 2\left(R\left(R + L\left(\cos(\alpha_1) + \cos(\alpha_2)\right)\right)\sin(\alpha_1)\right) \\
 & & 2\left(+\left(L^2 + R^2 + 2LR\cos(\alpha_1) + L^2\cos(2\alpha_1)\right)\sin(\alpha_2)\right) \\
\mathbf{A}_1^2 & = & 2R\cos(\alpha_2)\left(R + L\cos(\alpha_2)\right) + \cos(\alpha_1)\left(3L^2 + 2R^2 + 6LR\cos(\alpha_2) + L^2\cos(2\alpha_2)\right) \\
 & & -L^2\sin(\alpha_1)\sin(2\alpha_2) \\
\mathbf{A}_2^2 & = & -2LR\cos(\alpha_1)^2 - \left(3L^2 + 2R^2\right)\cos(\alpha_2) - 2R\cos(\alpha_1)\left(R + 3L\cos(\alpha_2)\right) \\
 & & -L^2\cos(2\alpha_1 + \alpha_2) \\
\mathbf{A}_1^3 & = & 3L\cos(\alpha_1) + L\cos(\alpha_1 - 2\alpha_2) + 2R\left(1 + \cos(\alpha_1 - \alpha_2)\right) \\
\mathbf{A}_2^3 & = & 2R + 2R\cos(\alpha_1 - \alpha_2) + L\cos(2\alpha_1 - \alpha_2) + 3L\cos(\alpha_2) \\
D_a & = & R\left(2\left(L^2 + R^2\right) + 3LR\cos(\alpha_1) + L^2\cos(2\alpha_1) + L^2\cos(2\alpha_2)\right) \\
 & & +R^2\left(2R\cos(\alpha_1 - \alpha_2) + L\left(\cos(\alpha_1 - 2\alpha_2) + \cos(2\alpha_1 - \alpha_2) + 3\cos(\alpha_2)\right)\right) \\
\hline
\bar{\Sigma}_1^1 & = & 2R\cos(\alpha_1)\left(\left(R + L\cos(\alpha_2)\right)\left(3 + \cos(2\alpha_2)\right) + 2\left(R + 2L\cos(\alpha_2)\right)\sin(\alpha_1)\sin(\alpha_2)\right) \\
 & & +2\sin(\alpha_1)\left(-2\left(\left(2L^2 + R^2\right)\cos(\alpha_2) + LR\left(2 + \cos(2\alpha_2)\right)\right)\sin(\alpha_1)\right) \\
 & & -2\sin(\alpha_1)\left(2LR\sin(\alpha_2)^3 + R^2\sin(2\alpha_2)\right) \\
\bar{\Sigma}_2^1 & = & -4\left(\cos(\alpha_1) - \cos(\alpha_2)\right)\left(R\left(R + L\left(\cos(\alpha_1) + \cos(\alpha_2)\right)\right) - L^2\sin(\alpha_1)\sin(\alpha_2)\right) \\
\bar{\Sigma}_1^2 & = & \bar{\Sigma}_2^1 \\
\bar{\Sigma}_2^2 & = & -2\left(R\left(R + L\cos(\alpha_1)\right)\left(3 + \cos(2\alpha_1)\right)\cos(\alpha_2)\right) \\
 & & -4R\sin(\alpha_1)\left(R\cos(\alpha_2) + \cos(\alpha_1)\left(R + 2L\cos(\alpha_2)\right) - L\sin(\alpha_1)^2\right)\sin(\alpha_2) \\
 & & +4\left(\left(2L^2 + R^2\right)\cos(\alpha_1) + LR\left(2 + \cos(2\alpha_1)\right)\right)\sin(\alpha_2)^2 \\
D_s & = & {D_a}^{3/2}
\end{array}
$$

Table 7.11: Expression of the components of the generalized momentum, mixed connection, and the evolution equation for the variable inertia snakeboard.

- $F_2 = 0$ for $\alpha_1 = \alpha_2$,
- $F_3 = 0$ for $\alpha_1 = -\alpha_2$,
- F_1 is even about both lines $\alpha_1 = \alpha_2$ and $\alpha_1 = -\alpha_2$,
- F_2 is even about $\alpha_1 = \alpha_2$ and odd about $\alpha_1 = -\alpha_2$,
- F_3 is even about $\alpha_1 = -\alpha_2$ and odd about $\alpha_1 = \alpha_2$.

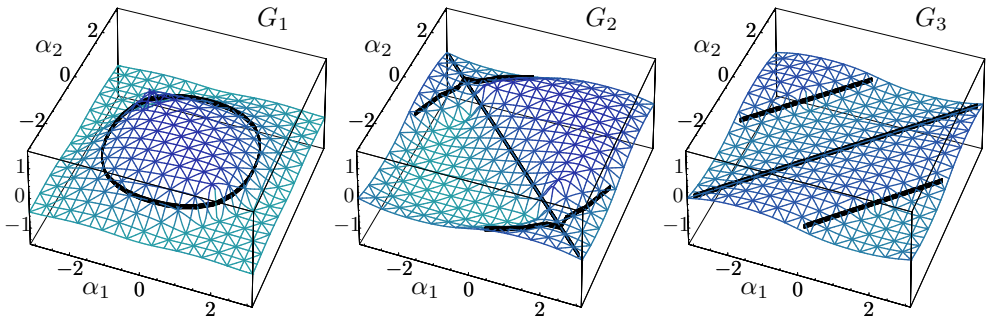

Figure 7.32: The three gamma functions for the variable inertia snakeboard. The darker shades indicate the positive regions which are separated from the lighter colored regions by the solid curves.

There are additional curves in the base space for which the height functions are zero. These curves are depicted by the solid curves in Fig. 7.31. Referring to Fig. 7.32, note the following properties of the gamma functions for the variable inertia snakeboard.

- $G_2 = 0$ for $\alpha_1 = \alpha_2$,
- $G_3 = 0$ for $\alpha_1 = -\alpha_2$,
- G_1 is even about both lines $\alpha_1 = \alpha_2$ and $\alpha_1 = -\alpha_2$,
- G_2 is even about $\alpha_1 = \alpha_2$ and odd about $\alpha_1 = -\alpha_2$,
- G_3 is even about $\alpha_1 = -\alpha_2$ and odd about $\alpha_1 = \alpha_2$.

There are additional curves in the base space for which the gamma functions are zero. These curves are depicted by the solid curves in Fig. 7.32.

Purely Kinematic Gaits

For the variable inertia snakeboard, we can design purely kinematic gaits by setting the right hand side of (7.25) equal to zero. However, in the case of the variable inertia snakeboard, the right hand side does not simplify to a single term as was the case of the original snakeboard. In fact, for the variable inertia snakeboard, the right hand side of (7.25) has the following quadratic expression

$$\dot{\rho} = \frac{2mR}{D_s}\left(\Sigma_1^1\dot{\alpha}_1^2 + 2\Sigma_2^1\dot{\alpha}_1\dot{\alpha}_2 + \Sigma_2^2\dot{\alpha}_2^2\right), \tag{7.26}$$

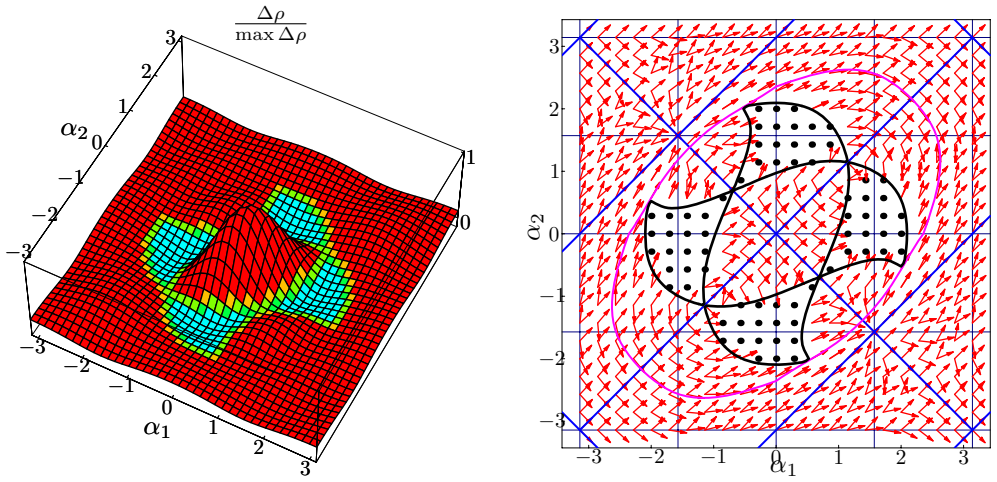

Figure 7.33: A plot of the $\Delta\rho$ function and a plot of the vector fields that define the purely kinematic gaits for the variable inertia snakeboard.

where Σ^i_j and D_s are analytic functions of the base variables given in Table 7.11. Thus, to ensure that the right hand side of (7.26) is equal to zero we have to consider the term

$$\Delta\rho(\alpha_1, \alpha_2) = \Sigma^1_2\Sigma^1_2 - \Sigma^1_1\Sigma^2_2,$$

where we have to ensure that $\Delta\rho \geq 0$; otherwise, the right hand side of (7.26) will not have roots, that is, it will never be zero. A plot of a $\Delta\rho/\max(\Delta\rho)$ is shown in the first plot in Fig. 7.33. The light colored regions indicate that $\Delta\rho(\alpha_1, \alpha_2) < 0$, that is, we can never compute any velocities for which $\dot{\rho} = 0$. In other words, we should avoid these regions of the base space while designing purely kinematic gaits.

Note that while designing purely kinematic gaits for the original snakeboard, we never knew that such regions existed. This was due to the simplicity of the momentum evolution equation governing the motion of the original snakeboard. We only realized the existence of these regions when we analyzed the more general variable inertia snakeboard.

Now, that we identified regions in the base space where the right hand side of (7.26) is equal to zero and has a solution, we can go ahead and design purely kinematic gaits for the variable inertia snakeboard. The right hand side of (7.26) has four unknowns, $(\alpha_1, \alpha_2, \dot{\alpha}_1, \dot{\alpha}_2)$. Thus, at each point in the base space, that is, fixing (α_1, α_2), we need to solve the velocities $(\dot{\alpha}_1, \dot{\alpha}_2)$ for which the right hand side is zero. Since, we have two unknowns and one equation, we solve for the ratios, $\frac{\dot{\alpha}_1}{\dot{\alpha}_2}$ and $\frac{\dot{\alpha}_2}{\dot{\alpha}_1}$ for which the right hand side is zero. This has the effect of ignoring the magnitudes of the base velocities, $(\dot{\alpha}_1, \dot{\alpha}_2)$;

the two ratios $\frac{\dot{\alpha}_1}{\dot{\alpha}_2}$ and $\frac{\dot{\alpha}_2}{\dot{\alpha}_1}$ define the slopes of vectors at each point in the base space which we use to define vector fields over the entire base space. A plot of these directions in the base space is seen in the second plot of Fig. 7.33. Note that the vector fields are defined everywhere on the base space except for the regions where $\Delta\rho(\alpha_1, \alpha_2) < 0$.

Thus, any part of the integral curves of the above vector fields is necessarily a purely kinematic gait. For example, the following families of lines are the simplest integral curves we could define for the above vector field,

$$\begin{aligned} l_1 &= \{\alpha_2 = \alpha_1 + k\pi, k \in \mathbb{Z}\} \\ l_2 &= \{\alpha_2 = -\alpha_1 + 2k\pi, k \in \mathbb{Z}\} \end{aligned}$$

These lines are depicted as solid lines in the second plot of Fig. 7.33. We did not use the above families of lines to design purely kinematic gaits since upon inspection we recognized that such gaits would pass through singular shapes of the variable inertia snakeboard, $(\alpha_1, \alpha_2) = \{(\frac{\pi}{2}, -\frac{\pi}{2}), (-\frac{\pi}{2}, \frac{\pi}{2})\}$, (Fig. 7.31). Alternatively, we can solve for other closed integral curves that do not pass through singular shape configurations. We depict such an integral curve (gray color) which is has an overall elliptical shape shown in the second plot of Fig. 7.33.

To design a purely kinematic gait that moves the variable inertia snakeboard along say the ξ^1 direction, we pick and closed integral curve that will enclose a non-zero volume solely under the first height function. Similarly we can pick integral curves that will move the robot in the other two fiber direction.

Rather than numerically solving for these integral curves and selecting the ones that enclose the non-zero volume under the desired height function, which is a tedious process, we chose to propose an approximate purely kinematic set of gaits. After inspecting the vector fields around the center of the base space, we can clearly see that the integral curves are almost straight lines as shown in Fig. 7.34. So we shall expect a change in the scaled momentum value as we traverse these gaits since they are approximate solutions. Thus, using the properties of the variable inertia snakeboard height functions, we propose the purely kinematic gaits given in Table 7.12.

The first gait, ${}^{PK}\phi_1$ envelopes a non-zero volume solely under the first height function, nonetheless, we should expect a small magnitude of motion as this gait has a small area in the base space. We simulated this gait which is depicted in the first row of Fig. 7.35.

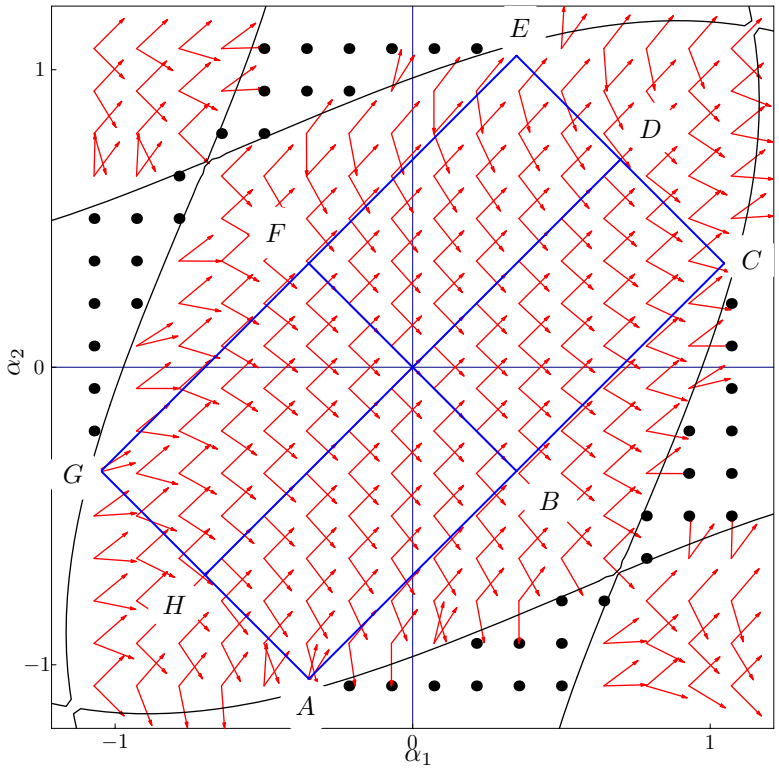

Figure 7.34: A plot of the three purely kinematic gaits, ${}^{PK}\phi_1$, ${}^{PK}\phi_2$, and ${}^{PK}\phi_3$, for the variable inertia snakeboard.

${}^{PK}\phi_1$	:	$A - C - E - G - A$
${}^{PK}\phi_2$	:	$A - B - F - E - C - B - F - G - A$
${}^{PK}\phi_3$	:	$A - C - D - H - G - E - D - H - A$

Table 7.12: Purely kinematic gaits for the variable inertia snakeboard.

In the first plot, we can see that the gait envelope non-zero volume under the first height function, moreover, in the second plot of the the first row of Fig. 7.35, we can see, as expected, that the scaled momentum is not exactly zero. The third plot in the first row of Fig. 7.35 depict the time simulation of the fiber variables as the variable inertia snakeboard performs the gait ${}^{PK}\phi_1$, while the forth plot depicts two snapshots of the snakeboard at the beginning (gray color) and end (black color) of this particular gait.

Similarly, we simulated the other two gaits, ${}^{PK}\phi_2$ and ${}^{PK}\phi_3$, given in the second and third rows of Table 7.12 to envelope volume only under the second and third height functions, respectively. For example consider the gait, ${}^{PK}\phi_2$. This particular gait has

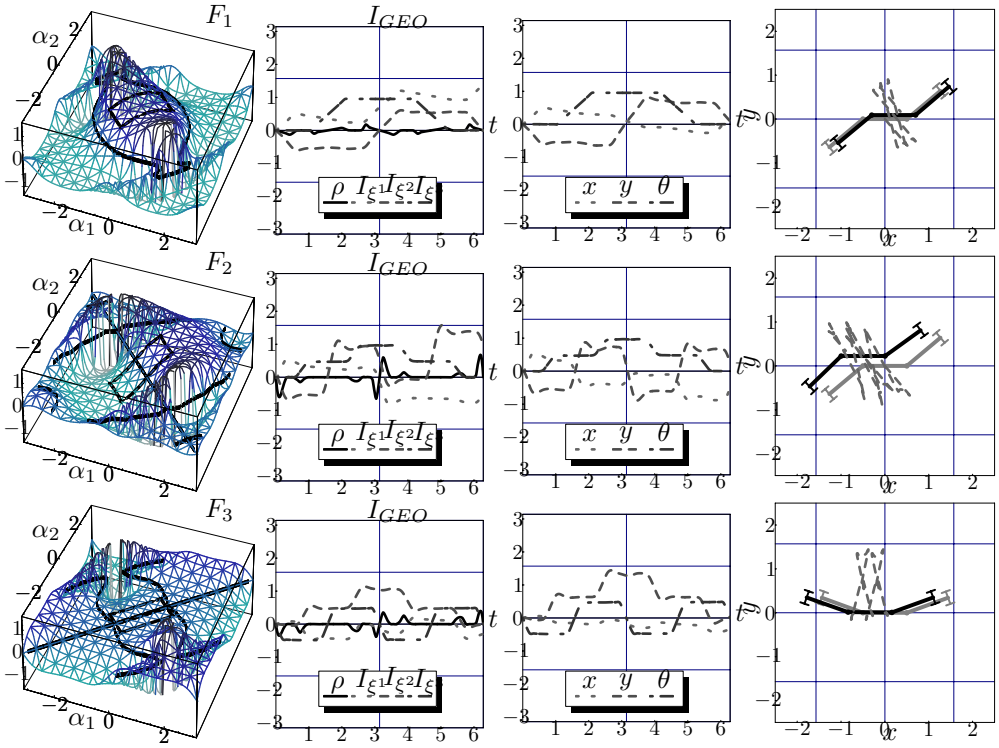

Figure 7.35: Simulation of the three purely kinematic gaits, ${}^{PK}\phi_1$, ${}^{PK}\phi_2$, and ${}^{PK}\phi_3$, for the variable inertia snakeboard. The first column depicts non-zero motion producing purely kinematic gaits superimposed over the height functions, the second column depicts the evolution of the scaled momentum and the geometric phase shift along the fiber directions, the third column depicts the time evolution of the fiber variables, and the last column depicts snapshots of the mechanical system at the beginning and end of each gait.

two similar rectangular loops of opposite orientation on each side of the line $\alpha_1 = -\alpha_2$. Since both the first and the third height functions are even about this line, the positive and negative volumes under the two loops will cancel out. Whereas, the second height function is odd about that line, hence, the volumes of the two rectangular loops add up. This proves that this gait will definitely have a non-zero geometric phase shift only along ξ^2. Indeed, we have simulated this particular gait and the results can be seen in the second row of Fig. 7.35. The results for the third gait, ${}^{PK}\phi_3$, can be seen in the third row of Fig. 7.35, which slightly rotates the variable inertia snakeboard.

Purely Dynamic Gaits

As for purely dynamic gaits for the variable inertia snakeboard, we analyze the systems gamma functions depicted in Fig.7.32. So to construct a gait that yields a zero I_{GEO} and a non-zero I_{DYN} along say the ξ^1 direction, we need curve that encloses zero area in the base space, stays in a same signed regions of the first gamma function, and be centered about odd points of the other two gamma functions. The base space curve, ${}^{PD}\phi_1$, given in the first row of Table 7.13 satisfies all these requirements.

${}^{PD}\phi_1$:	$\alpha_1 =$	$\frac{\pi}{4}(1 - \sin(t) - 2\sin^2(t))$
	$\alpha_2 =$	$\frac{\pi}{4}(1 + \sin(t) - 2\sin^2(t))$
${}^{PD}\phi_2$:	$\alpha_1 =$	$\frac{\pi}{10}(2\sin(3t) - 5)$
	$\alpha_2 =$	$\frac{\pi}{6}(\sin(t) - 3)$
${}^{PD}\phi_3$:	$\alpha_1 =$	$\frac{\pi}{4}(2\sin(t) + 1)$
	$\alpha_2 =$	$\frac{\pi}{4}(2\sin(t) - 1)$

Table 7.13: Purely dynamic gaits for the variable inertia snakeboard.

We have simulated the gait ${}^{PD}G_1$ and depicted the results in the first row of Fig. 7.36. The gait is superimposed on top of the first gamma function where we can see that the curve lies entirely in the positive region of the first gamma function. The second plot in depicts the values of the dynamic phase shift, I_{DYN}, along the three fiber directions, where we can see that this particular gait yields a non-zero I_{DYN} only along ξ^1. The third plot depicts the values of the fiber variables as the variable inertia snakeboard performs the gait ${}^{PD}G_1$. We see that this particular gait moves the snakeboard along the x direction. The final plot in Fig. 7.36 depicts two snapshots of the variable inertia snakeboard at the beginning (gray color) and end (black color) of the gait ${}^{PD}G_1$.

Similarly, we proposed two other gaits, ${}^{PD}G_2$ and ${}^{PD}G_3$, given in the second and third rows of Table 7.13 that are supposed to yield non-zero I_{DYN} along the ξ^2 and ξ^3 directions, respectively. We depicted these two gaits in the the second and third row of Fig. 7.36. Note that the gait ${}^{PD}G_2$ translates the variable inertia snakeboard along the y direction while the gait ${}^{PD}G_3$ rotates the snakeboard.

Kino-dynamic Gaits

For the variable inertia snakeboard, we can generate kino-dynamic gaits by using the volume integration analysis to produce candidate gaits. For example, to generate a gait

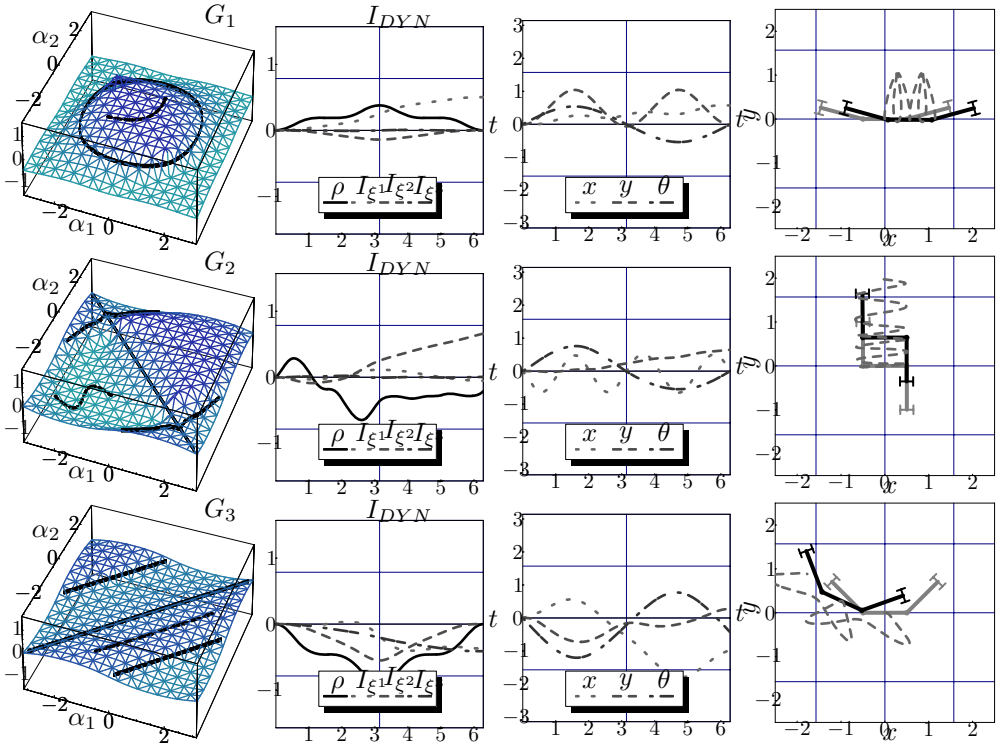

Figure 7.36: Simulation of the three purely dynamic gaits, ${}^{PD}\phi_1$, ${}^{PD}\phi_2$, and ${}^{PD}\phi_3$, for the variable inertia snakeboard. The first column depicts non-zero motion producing purely dynamic gaits superimposed over the gamma functions, the second column depicts the evolution of the scaled momentum and the dynamic phase shift along the fiber directions, the third column depicts the time evolution of the fiber variables, and the last column depicts snapshots of the mechanical system at the beginning and end of each gait.

that rotates the variable inertia snakeboard in place, we start by designing a curve in the base space that envelopes a non-zero volume only under the third height function of the variable inertia snakeboard. A curve with the following properties is a possible candidate:

- Figure-eight type curve.
- Each loop of the figure-eight curve lies on the opposite side of the line $\alpha_1 = \alpha_2$.
- The orientation of the loops should be in opposite directions.

The curve, ${}^{KD}\phi_3$, given in the third row of Table 7.14 satisfies all the above requirements. A plot of the curve superimposed over the height functions of the variable inertia

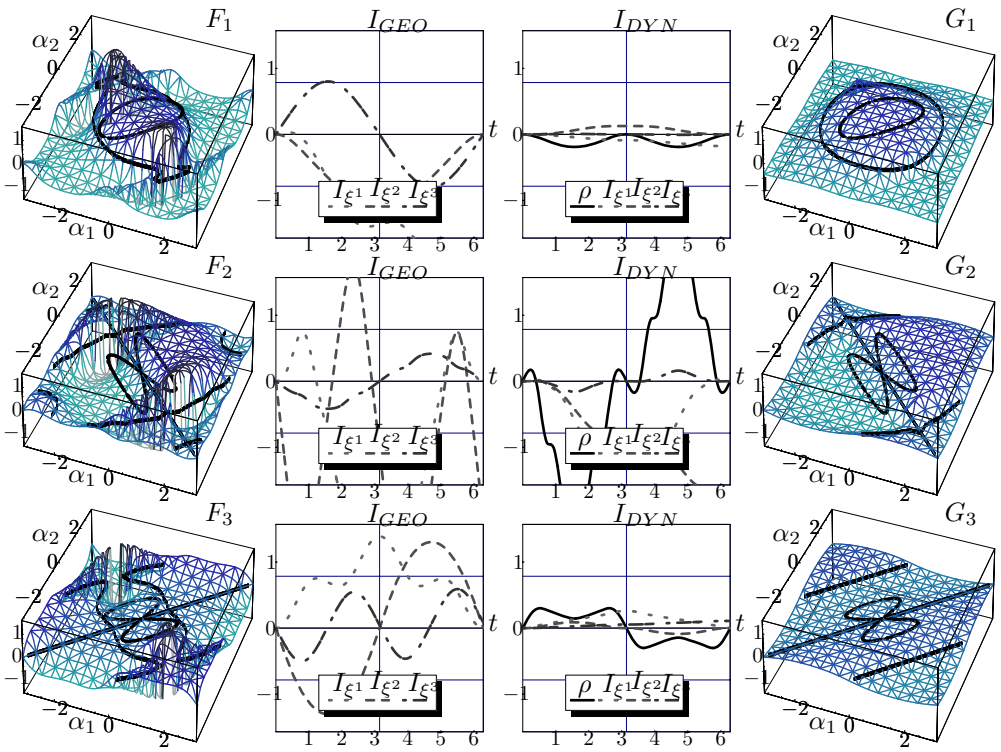

Figure 7.37: Simulation of the three kino-dynamic gaits, ${}^{KD}\phi_1$, ${}^{KD}\phi_2$, and ${}^{KD}\phi_3$, for the variable inertia snakeboard. The first and last columns depict non-zero motion producing kino-dynamic gaits superimposed over the height and gamma functions, respectively, the middle columns depict the evolution of the scaled momentum and the geometric and dynamic phase shifts along the fiber directions.

snakeboard is shown in the first plot of the third row of Fig. 7.37. We can clearly see that this gait is symmetric about the line $\alpha_2 = \alpha_1$, where it has two loops of opposite direction at either side of the line. Moreover, we know that only the third height function is odd about this line. Thus, we should expect a non-zero I_{GEO} only along the ξ^3 direction, which we can clearly see in the second plot of the third row of Fig. 7.37. Moreover, the last plot of the first figure depicts the gait superimposed on top of the first gamma function. We can see that this gait should yield a non-zero I_{DYN} only under along the ξ^3 direction as shown in the third plot of the third row of Fig. 7.37. Finally, we plot the global motion of the variable inertia snakeboard in the third column of Fig. 7.38 where we can see that the gait ${}^{KD}\phi_3$ actually rotates the variable inertia snakeboard.

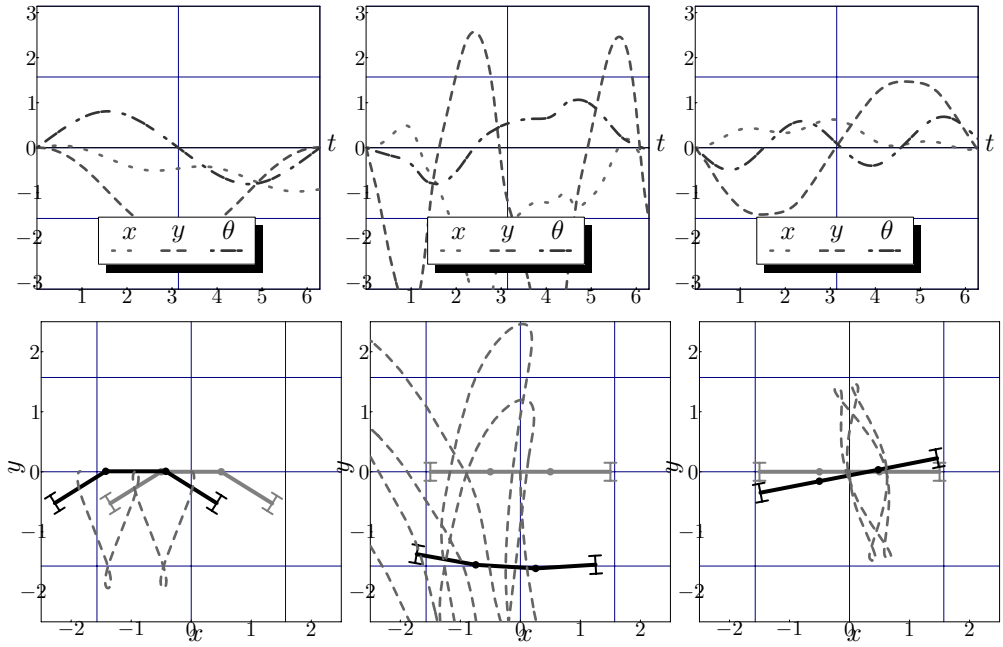

Figure 7.38: The motion of the variable inertia snakeboard as it performs the three kino-dynamic gaits, ${}^{KD}\phi_1$, ${}^{KD}\phi_2$, and ${}^{KD}\phi_3$.

${}^{KD}\phi_1$	:	$\alpha_1 = -\frac{1}{\sqrt{2}}\left(\frac{\pi}{2}\sin(t) + \frac{\pi}{4}\cos(t)\right)$ $\alpha_2 = \frac{1}{\sqrt{2}}\left(-\frac{\pi}{2}\sin(t) + \frac{\pi}{4}\cos(t)\right)$
${}^{KD}\phi_2$	:	$\alpha_1 = \frac{1}{\sqrt{2}}\left(\frac{\pi}{2}\sin(2t) + \frac{\pi}{4}\sin(t)\right)$ $\alpha_2 = -\frac{1}{\sqrt{2}}\left(\frac{\pi}{2}\sin(2t) - \frac{\pi}{4}\sin(t)\right)$
${}^{KD}\phi_3$	:	$\alpha_1 = \frac{1}{\sqrt{2}}\left(\frac{\pi}{3}\sin(2t) + \frac{\pi}{3}\sin(t)\right)$ $\alpha_2 = \frac{1}{\sqrt{2}}\left(-\frac{\pi}{3}\sin(2t) + \frac{\pi}{3}\sin(t)\right)$

Table 7.14: Kino-dynamic gaits for the variable inertia snakeboard.

Similarly, we can design two other curves that envelope volumes under the first and second height functions to move the variable inertia snakeboard in the x and y directions. Curves ${}^{KD}\phi_1$ and ${}^{KD}\phi_2$ given in the first and second rows of Table 7.14 are such possible candidates. The first and last plots of the first and second rows of Fig. 7.37 depict the two curves superimposed over the height and gamma functions of the variable inertia snakeboard. Moreover, we can see that for the gait ${}^{KD}\phi_1$, both I_{GEO} and I_{DYN} are non-zero along the ξ^1 direction at the end of each cycle and they have the same sign as shown in the second and third plot of the second row of figure Fig. 7.37 while both I_{GEO} and

I_{DYN} are non-zero along the ξ^2 direction at the end of each cycle for the gait ${}^{KD}\phi_2$.

We have simulated both gaits curves and as expected, ${}^{KD}\phi_1$ generates motion along the x direction and the gait ${}^{KD}\phi_2$ generates motion along y direction as shown in the first and second columns of Fig. 7.38, respectively.

Chapter 8

Experiments

In this section we implement our gait generation techniques on a variable inertia snakeboard system which was specifically constructed the applicability of our proposed gaits. We will propose several gaits to move this robot along specified direction and compare our simulated results the actual motion executed by the real robot.

We designed and constructed a variable inertia snakeboard as shown in Fig. 8.1. For this specific robot, we placed the wheel axes on the distal links such that the distant between the wheel axes and the revolute joints is identical to the length of the middle link. Moreover, we rigidly attached two sprockets to the two ends of the middle link. We also

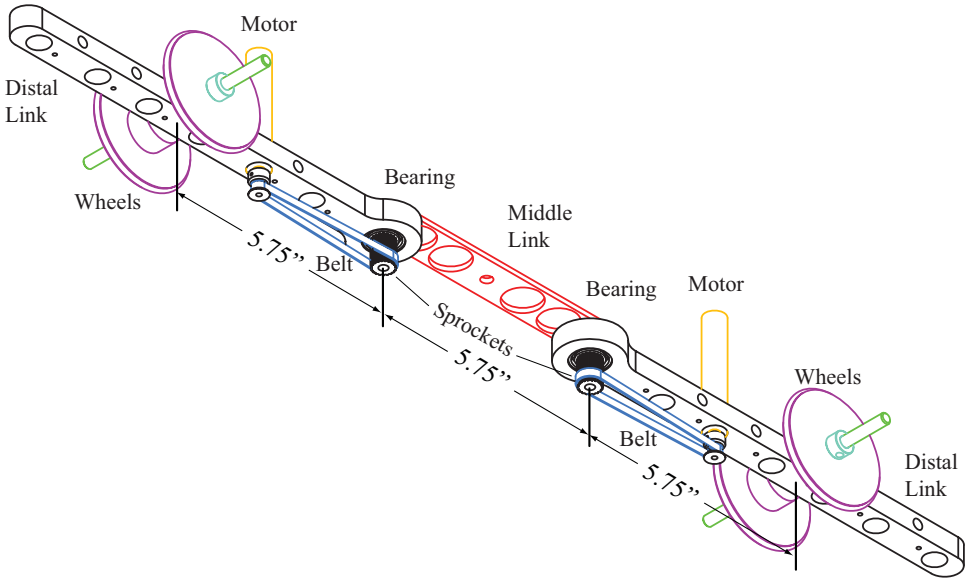

Figure 8.1: The variable inertia snakeboard

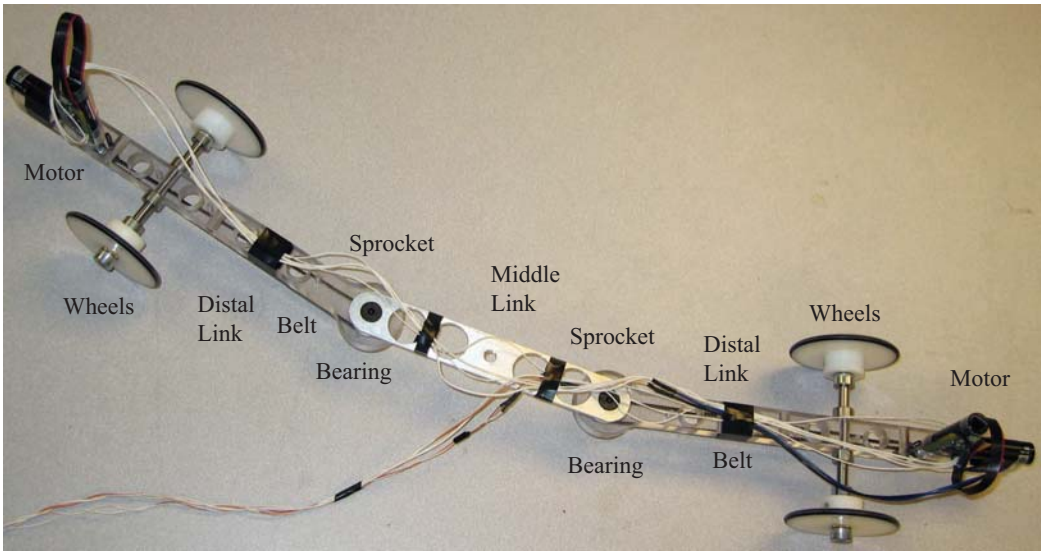

Figure 8.2: The variable inertia snakeboard

rigidly attached two motors to each of the distal links. These motors drive the sprockets on the middle link via timing belts. Thus, using the motors, this simple planar robot can only actuate independently the inter-link angles, that is, the robot's base variable. A photo of the assembled variable inertia snakeboard is depicted in Fig. 8.2.

Even though, we wanted to generate a gait of each of the three types of gaits to locomote the variable inertia snakeboard, we quickly realized the purely kinematic gaits produced relatively smaller magnitudes. We believe that the reason behind this is the fact that the purely dynamic gaits we generated for the variable inertia snakeboard in Section 7.4.2 produced small magnitudes of motion due to the small enclosed volume under the height functions. We also believe that the mechanical imperfections of the system also played a counter productive role and reduced the expected magnitudes of motion even further.

${}^{PD}\phi$:	$\alpha_1 =$	$\frac{3\pi}{4}\sin(t)$
	$\alpha_2 =$	$\sin(t)$
${}^{PD}\phi$:	$\alpha_1 =$	$\frac{\pi}{5}\sin(3t) - \frac{\pi}{2}$
	$\alpha_2 =$	$\frac{\pi}{6}\sin(t) - \frac{\pi}{2}$
${}^{KD}\phi$:	$\alpha_1 =$	$\frac{1}{\sqrt{2}}\left(\frac{\pi}{3}\sin(2t) + \frac{\pi}{3}\sin(t)\right)$
	$\alpha_2 =$	$\frac{1}{\sqrt{2}}\left(\frac{\pi}{3}\sin(2t) - \frac{\pi}{3}\sin(t)\right)$

Table 8.1: Implemented gaits for the variable inertia snakeboard.

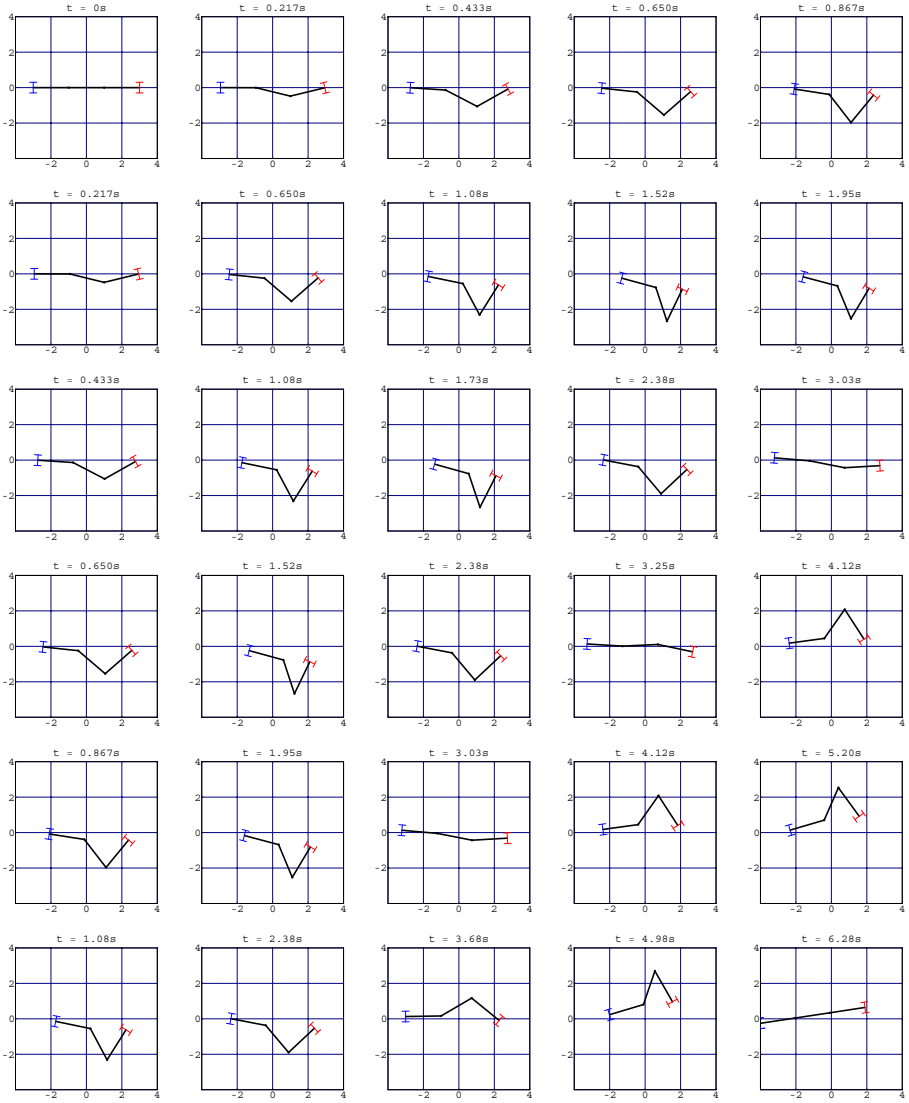

Figure 8.3: The time simulation of the purely dynamic gait, ${}^{PD}\phi$, that moves the variable inertia snakeboard along the x direction.

Thus, we generate three gaits for the variable inertia snake two of which belong to the purely dynamic gaits family and another that belongs to the kino-dynamic gaits family. Moreover, we designed the gaits such that each of them will move the variable inertia snakeboard along each of the fiber variables, (x, y, θ). These gaits are given in Table 8.1.

The first gait we implemented is a purely dynamic gait given in the first row of Table 8.1. This particular gait moves the variable inertia snakeboard along the x direction. We

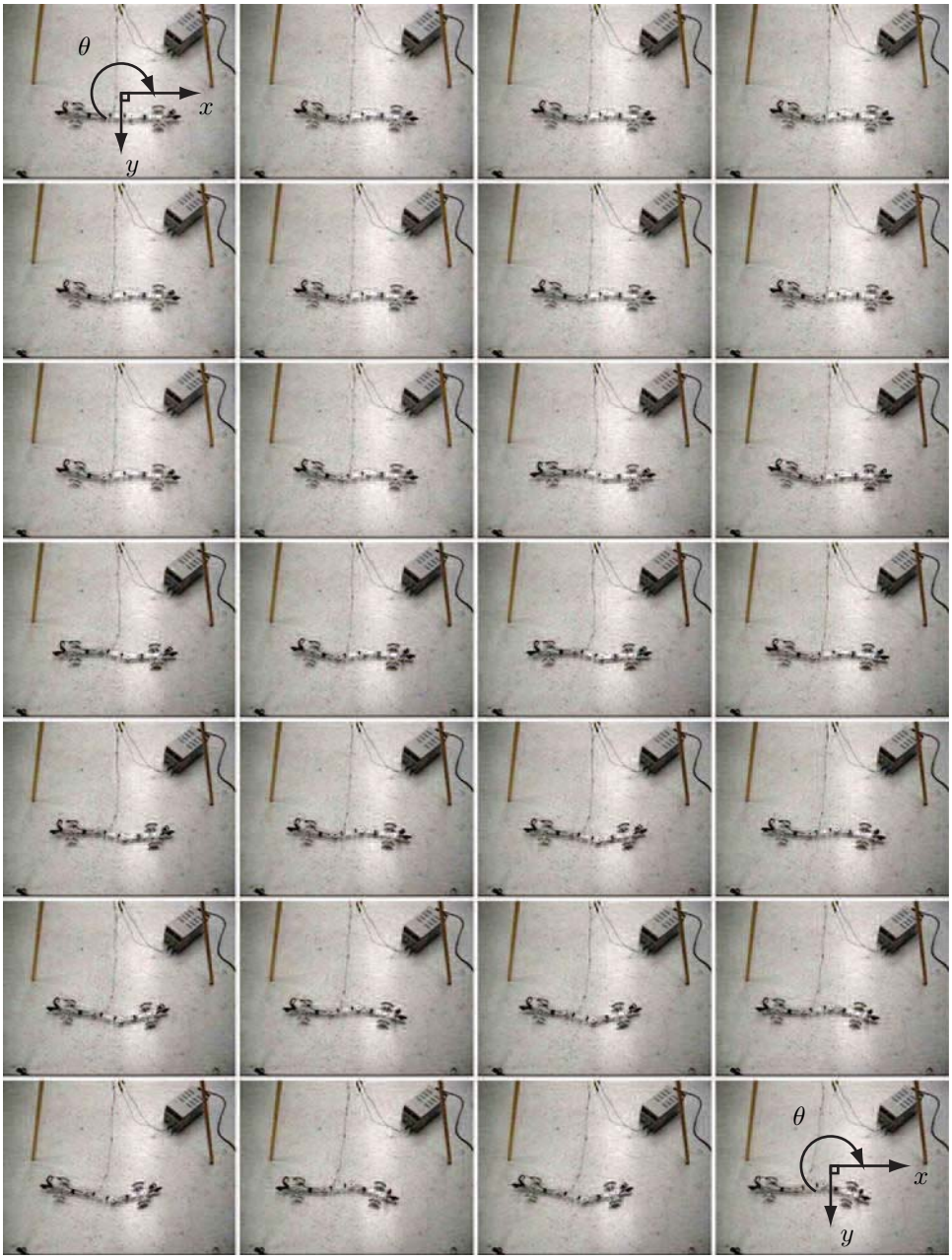

Figure 8.4: The actual motion of the variable inertia snakeboard while performing the purely dynamic gait, ${}^{PD}\phi$. The frames are one second apart.

simulated this gait numerically and plotted snapshots of the variable inertia snakeboard as it performed this gait in Fig. 8.3. One can clearly see that this mixed system is moving along the negative x direction.

We implemented this gait on the real variable inertia snakeboard and, as expected, the

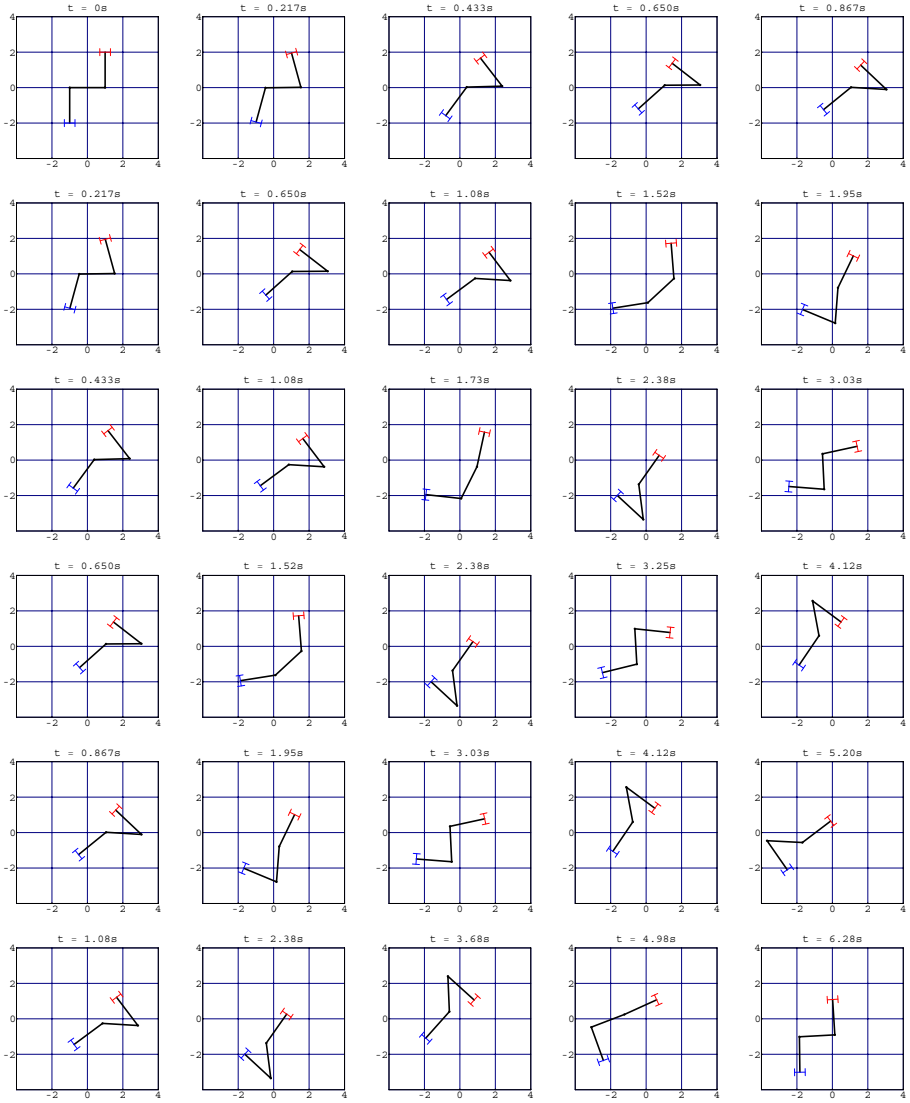

Figure 8.5: The time simulation of the purely dynamic gait, ${}^{PD}\phi$, that moves the variable inertia snakeboard along the y direction.

system started locomoting along the negative x direction. In Fig. 8.4 we depict snapshots which are one second apart of the variable inertia snakeboard performing the purely dynamic gait, ${}^{PD}\phi$. It is clear that the variable inertia snakeboard is moving towards the left side of the individual frames. Moreover, the intermediate motions of the variable inertia snakeboard closely match the motions of the simulated system depicted in Fig. 8.3.

The second gait we implemented was another purely dynamic gait, ${}^{PD}\phi$, given in the

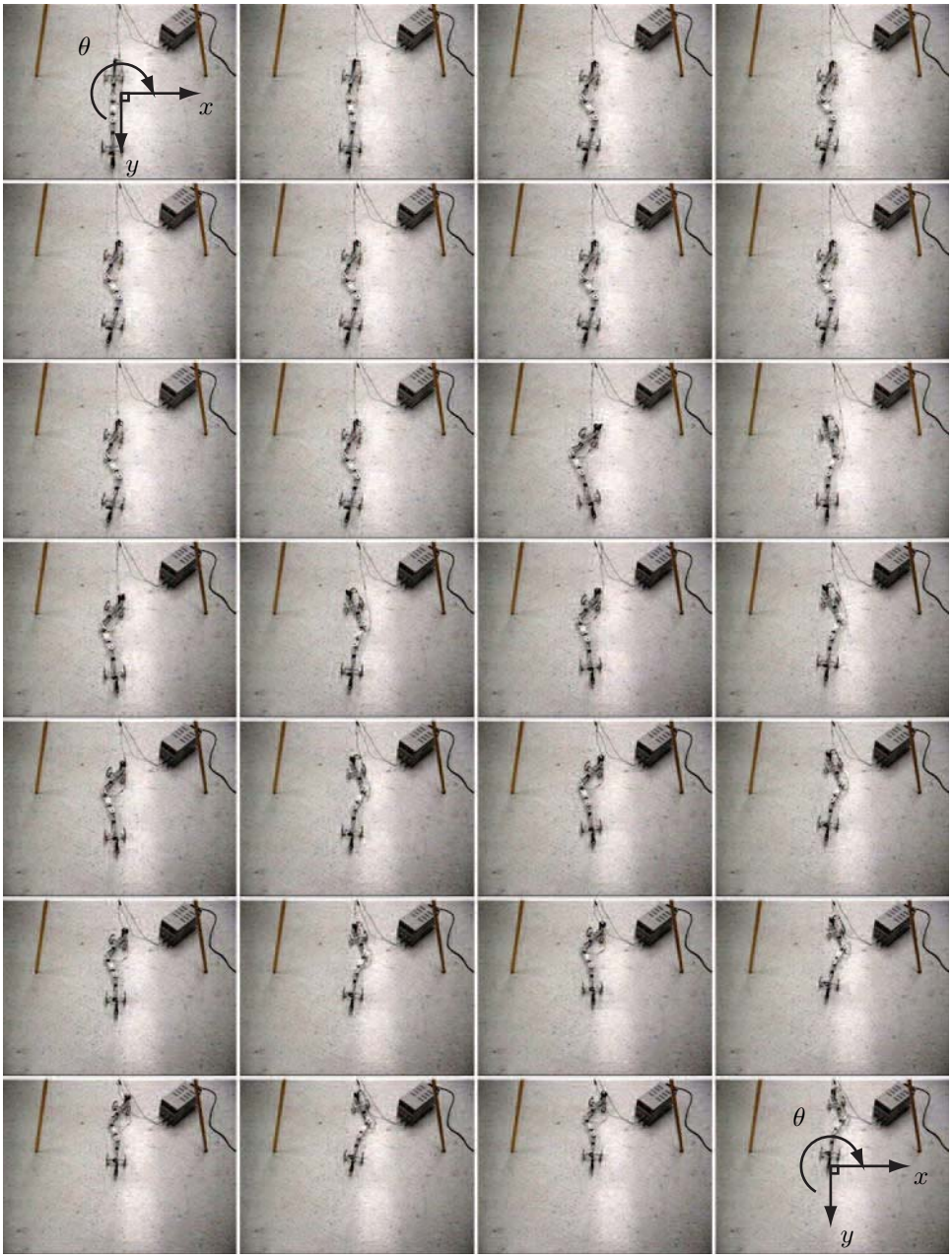

Figure 8.6: The actual motion of the variable inertia snakeboard while performing the purely dynamic gait, ${}^{PD}\phi$. The frames are one second apart.

second row of Table 8.1. This is a polygonal gait whose vertices are depicted in Fig. 7.34. Utilizing our gait generation techniques, we proposed this particular gait to move the variable inertia snakeboard along the y direction. This result was verified by the numerical time simulation shown in Fig. 8.5. We implemented this gait on the actual variable inertia

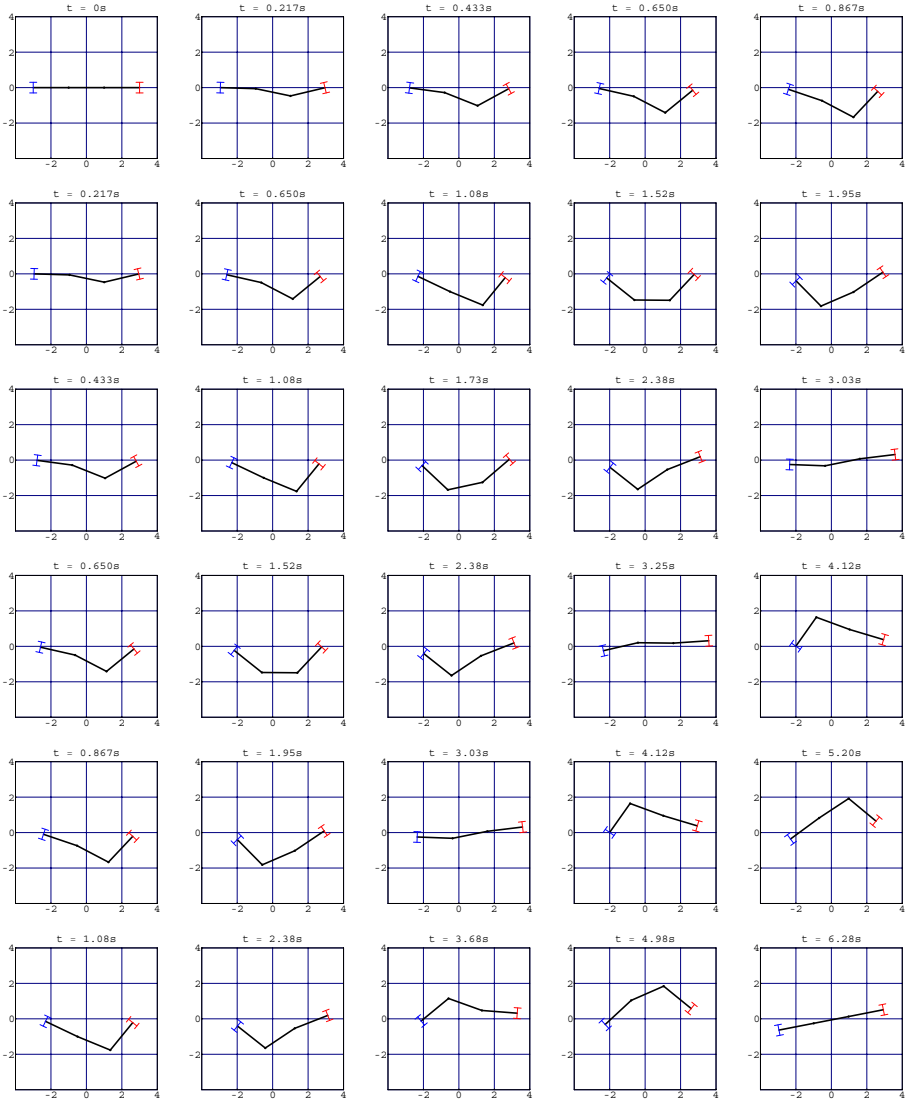

Figure 8.7: The time simulation of the kino-dynamic gait, ${}^{KD}\phi$, that rotates the variable inertia snakeboard along the θ direction.

snakeboard and we can clearly see that the system's motion closely resembles the numeric time simulation as shown in Fig. 8.6. In both cases the variable inertia snakeboard moves in the negative y direction.

The last gait we implement is of the kin-dynamic type and is depicted in the last row of Table 8.1. This is the same gait that we proposed in the previous chapter to rotate the variable inertia snakeboard. In Fig. 8.7, we depict snapshots of the numeric time

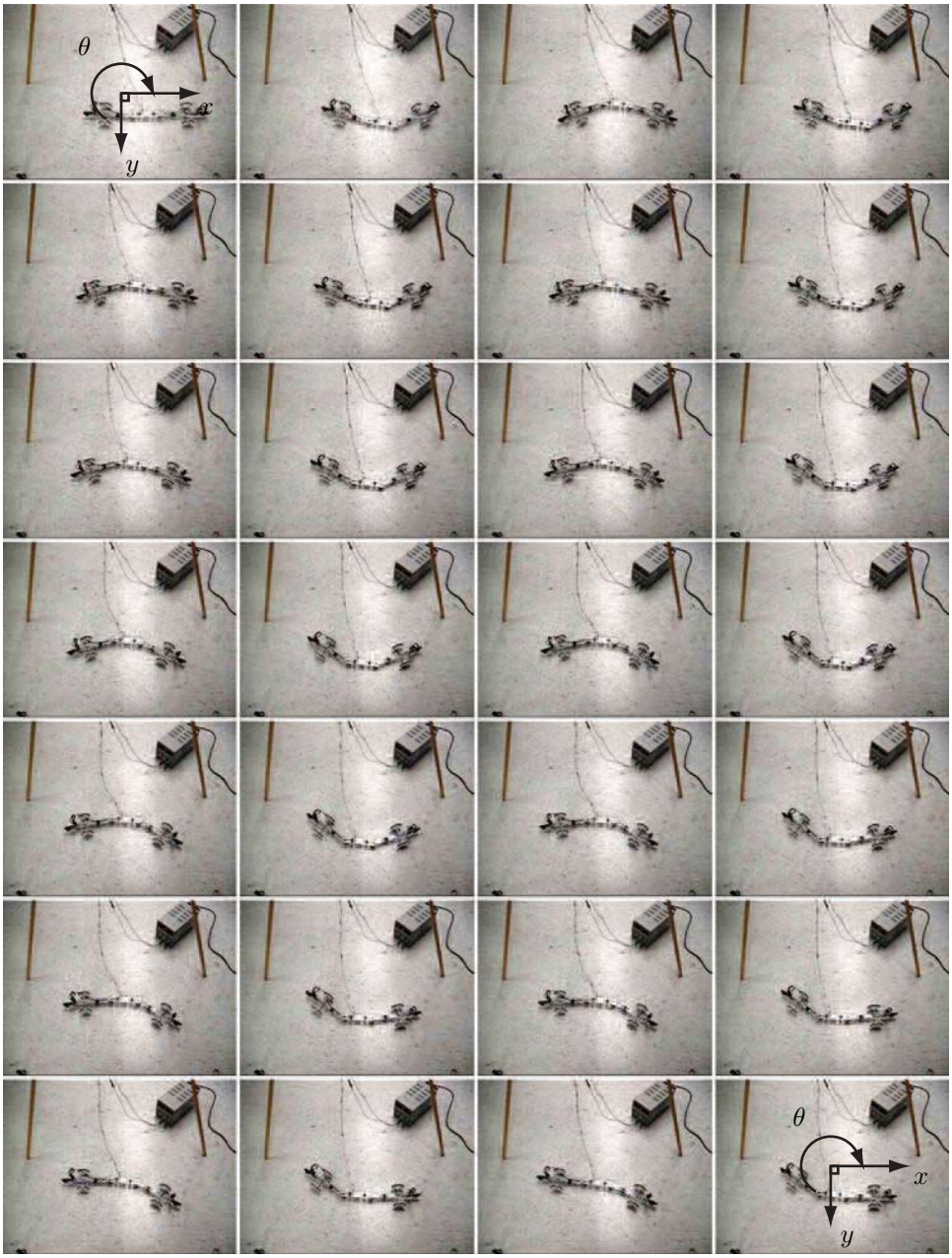

Figure 8.8: The actual motion of the variable inertia snakeboard while performing the kino-dynamic gait, ${}^{KD}\phi$. The frames are one second apart.

simulation of this particular gait, ${}^{KD}\phi$. We can see that this gait rotates the variable inertia snakeboard along the positive θ direction. We implemented this kino-dynamic gait on the actual variable inertia snakeboard and depicted one second apart frames of the actual motion of the system in Fig. 8.8. The snakeboard move along the positive θ fiber

direction. This rotation is clearly seen by comparing the first and last frames in Fig. 8.8.

We would like to shed some more light on the above experiments. Even though the gait design process was straight forward, getting the actual system to perform the proposed gait was more challenging. The cause of the miss-match between the simulation and experimental results is due to the inaccurate model we used for the simulation. In fact, in our models, we assumed that the middle link of the variable inertia snakeboard is massless which is not the case for the real robot. Intuitively, due to this additional mass in the system, we expected the magnitudes of motion to be smaller than the simulated results. Indeed, this was the case and to counteract the effect of the additional mass of the middle link, we added concentrated masses on the extremities of the outer link, thus, effectively increasing the mass and inertia of the outer links with are directly related to the magnitudes of motion.

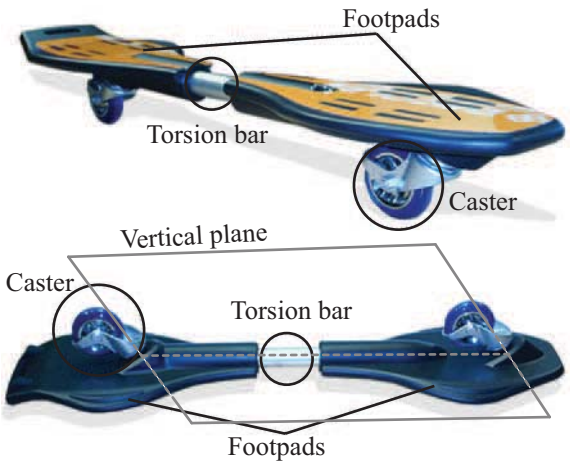

Figure 8.9: The *Essboard*. http://www.essboard.com

Finally, it is worth noting that we found a special skateboard whose free body diagram is almost identical to that of the variable inertia snakeboard. This toy is referred to as the *Wave-board* or the *Essboard* which is shown in Fig. 8.9. This particular skateboard has two casters are mounted on two footpads which are connected by a torsion bar. The axes around which the casters rotate are not vertical, they are slopped in such a way that the casters have an equilibrium position. If the footpads are parallel to the ground, the caster axes belong to a vertical plane containing the torsion bar. As the rider pitches the footpads, the casters rotate about their respective axes which are no longer in the vertical plane.

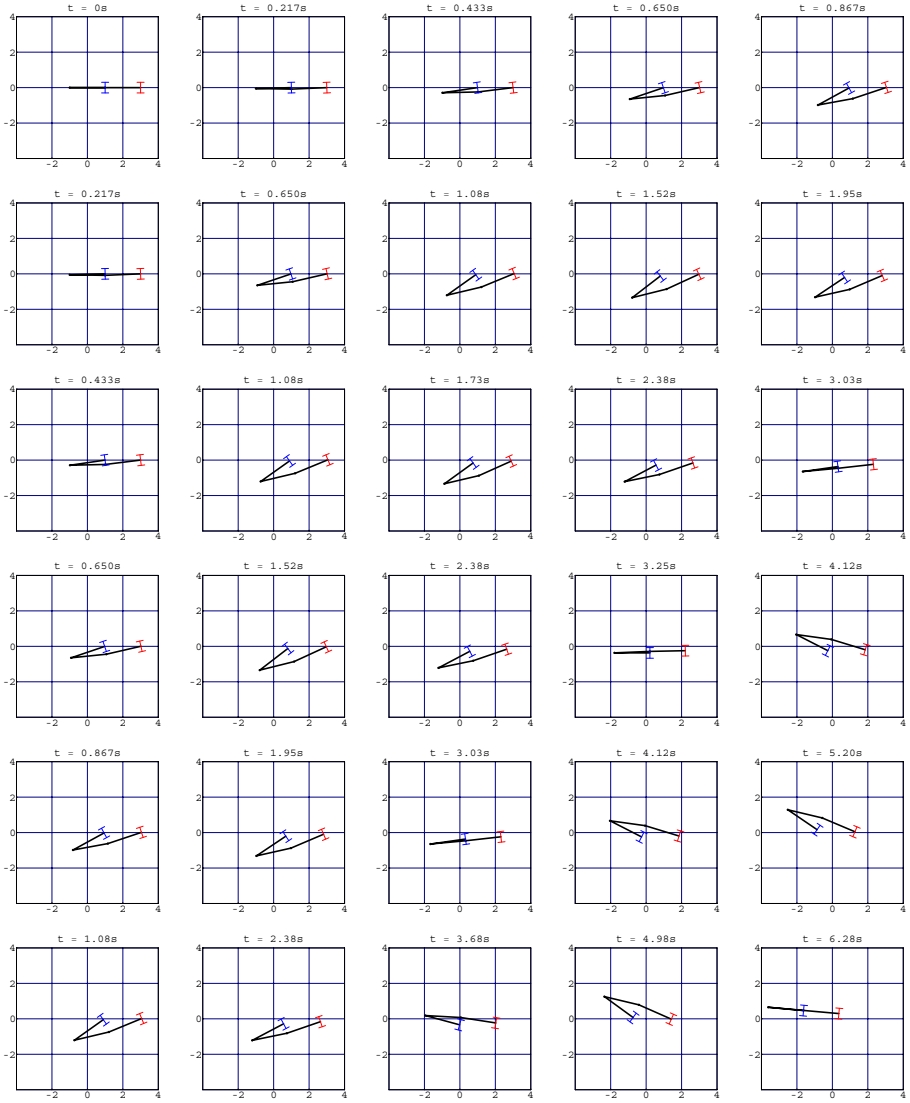

Figure 8.10: A time simulation of a gait that resembles gaits used by riders of the Essboard.

A top view of the Essboard will have the same schematic as that of the variable inertia snakeboard shown in Fig. 7.30. In the case of the Essboard, pitching the footpads causes the casters contact points to follow an arc which can be represented by the base angles of the variable inertia snakeboard.

Watching videos of riders using the Essboard to travel in a straight line, it is clear that the casters are in phase and that they are always almost parallel. We implemented such a *purely dynamic* gait on the our model and indeed we can clearly see that the variable

inertia snakeboard locomotes along the x direction as shown in Fig. 8.10. We did not implement this gait on the actual variable inertia snakeboard since such a gait will cause interference between the motors and the middle link.

Another interesting fact about riding the Essboard is that the riders always yaw their bodies with respect to the middle link of the board. This means that the riders are "transferring" momentum from their bodies to the system in a similar way that the rotor of the original snakeboard "transfers" momentum to the snakeboard. As a future work problem, we would like to investigate how adding a rotor to the variable inertia snakeboard will affect our gait generation techniques.

Chapter 9

Future Work

In this Chapter we present several of the future work problems that we think are worthy of pursuing. Next, we present several problems in which we will try and define the future work directions.

9.1 Higher-dimensional Base Spaces

Throughout this thesis document we have generated gaits for numerous examples. Even though, as per Assumption 3, most of these examples had at most a two-dimensional base space, we claim that our geometric gait synthesis tool is still valid in higher dimensions.

Recall that the reconstruction equation for the generalized mixed mechanical system type is given in (4.12), where $\xi = -\mathbf{A}(r)\dot{r} + \Gamma(r)p^T$. A higher-dimensional base space does means that the components of the mixed connection, $\mathbf{A}(r)$, as well as the gamma functions, $\Gamma(r)$, are still functions mapping the base space to the reals. In this section we analyzed how higher dimensional base spaces affect the kinematic part of the reconstruction equation. Recall that, integrating each row the kinematic part of the reconstruction equation, is equivalent to evaluating a line integral of an m-dimensional one-form along a base space curve, that is,

$$\int_t^\tau \mathbf{A}^i(r)\dot{r}dt = \oint_\phi \mathbf{A}^i(r)dr_i.$$

Recall that we require our gaits to be cyclic, that is, $\phi(0) = \phi(\tau)$. Thus, we can use Stokes' theorem to convert the above line integral to a volume integral given by

$$\int\int_{\Phi} \bar{\mathbf{A}}^{ij}(r) dr_i dr_j,$$

where the integrand is an m-dimensional two-form such that $i < j$, $i \neq j$, and $i, j = 1, \cdots, m$. Here, Φ is an arbitrary smooth two-surface embedded in the base space whose boundary is ϕ. Finally, since $\mathbf{A}^i(r)dr_i$ is an m-dimensional one-form, we know that the two-form, $\bar{\mathbf{A}}^{ij}(r)dr_i dr_j$, has $\frac{m}{2}(m-1)$ components.

For example, in the two-dimensional base space case, we had one height function for each of the fiber direction. For three-dimensional base space, we will have three height functions for each of the fiber direction. Thus, if we are dealing with systems that have l-dimensional fiber spaces, we need and analyze $l(m-1)\frac{m}{2}$ height functions simultaneously, which is a tedious process.

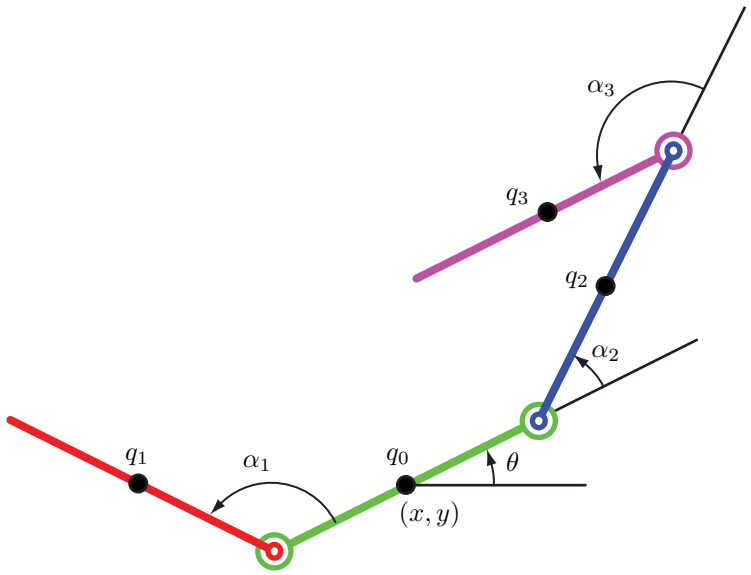

Figure 9.1: Floating four-link snake.

Consider a four-link floating snake as shown in Fig. 9.1. This example is an extension of the three link floating snake we studied in the previous chapter. We compute the reduced Lagrangian in a similar way from which we can solve for the local form of the mechanical connection. Note that since we attached the body frame to the system's center of mass, we know that the components of the first two rows of the mechanical connection are zeroes. Moreover, assuming zero initial momentum we can compute the change in orientation using the following equation

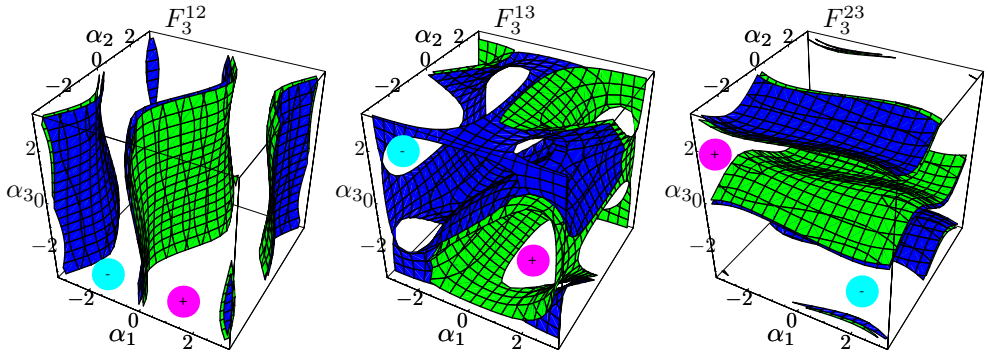

Figure 9.2: The three height functions along the θ direction for the four link snake robot.

$$\Delta\theta = 8\left(\int\int_{\Phi}\frac{F_3^{12}}{D^2}d\alpha_1 d\alpha_2 + \int\int_{\Phi}\frac{F_3^{13}}{D^2}d\alpha_1 d\alpha_3 + \int\int_{\Phi}\frac{F_3^{23}}{D^2}d\alpha_2 d\alpha_3\right),$$

where F_3^{ij} are the three eight functions associated with the θ fiber direction. These height functions have the following expressions

$$\begin{aligned}
F_3^{12} &= 5\sin(\alpha_1) - 3\sin(\alpha_2) + \sin(\alpha_1 - \alpha_3) + \sin(\alpha_1 + \alpha_3) - \sin(\alpha_2 + \alpha_3),\\
F_3^{13} &= 2\sin(\alpha_1) + \sin(\alpha_1 - \alpha_2) + \sin(\alpha_1 - \alpha_3) - 2\sin(\alpha_3) - \sin(\alpha_2 + \alpha_3),\\
F_3^{23} &= -(\cos(\alpha_2)\sin(\alpha_1)) + (3 + \cos(\alpha_1))\sin(\alpha_2) + (5 + 2\cos(\alpha_1))\sin(\alpha_3)\ , \text{and}\\
D &= 22 + 5\cos(\alpha_1) + 3\cos(\alpha_1 - \alpha_2) + 9\cos(\alpha_2)\\
&\quad + \cos(\alpha_1 - \alpha_2 - \alpha_3) + 5\cos(\alpha_3) + 3\cos(\alpha_2 + \alpha_3).
\end{aligned}$$

A plot of all three height function is depicted in Fig. 9.2 where for each height function, we plot the two-surface zero level set, $F_3^{ij} = 0$, that partitions the entire base space into positive and negative regions.

Having identified the positive and negative regions of the base space, we can go ahead and generate gaits using the tools we presented in Chapter 6; however, we have to simultaneously analyze three height functions for each fiber direction. The simplest gait we can construct is a non-intersection closed curve that lies entirely within a positive region of all three height functions.

The curve ϕ_1 given in the first row of Table 9.1 is such a curve which belong to the positive regions of all three height functions as shown in the first plot of Fig. 9.3. Recall,

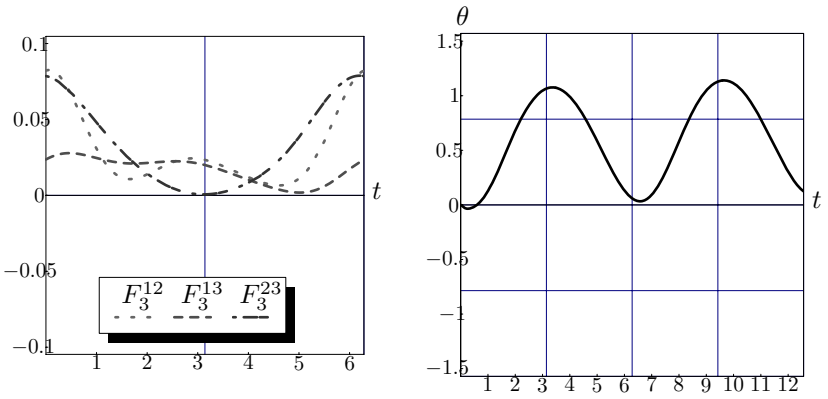

Figure 9.3: A non-intersecting gait for the four link snake robot.

		α_1	$=$	$\frac{\pi}{2}(\sin(t)+2)$
ϕ_1	:	α_2	$=$	$\frac{\pi}{2}(\cos(t)+2)$
		α_3	$=$	$\frac{\pi}{12}\cos(t)$
		α_1	$=$	$\frac{3\pi}{2}\sin(t)-\frac{\pi}{9}\sin(2t)$
ϕ_2	:	α_2	$=$	$\frac{3\pi}{2}\sin(t)+\frac{\pi}{9}\sin(2t)$
		α_3	$=$	π

Table 9.1: Purely kinematic gaits for the floating four link snake robot.

that each height function maps the entire three-dimensional base space to the reals. Thus, if we ensure that the entire curve in lies within a positive region of the height function, then there should exist a smooth two-surface that lies entirely within the positive region of the height function such that the designed curve is the boundary of that surface. Hence, we are integrating a two-from over an entirely positive surface, which must yield a non-zero positive value. Moreover, if this curve is in the same signed region of the three height function, then the three surface integrals must yield non-zero values with the same sign. Thus, we conclude that such a gait must yield a non-zero rotation of the entire robot. We have simulated the gait ϕ_1 which belongs to the positive regions of all three height function and indeed, as expected, it rotated the four link snake after each cycle as shown in the second plot of Fig. 9.3.

Similarly, we designed another self-intersecting gait, ϕ_2, given in the second row of Table 9.1. However, for this particular gait, we ensured that the intersection occurs at the zero level set for all three height functions. Moreover, we ensured that the curve belongs to the positive regions of all three height functions for the first half cycle and it belongs

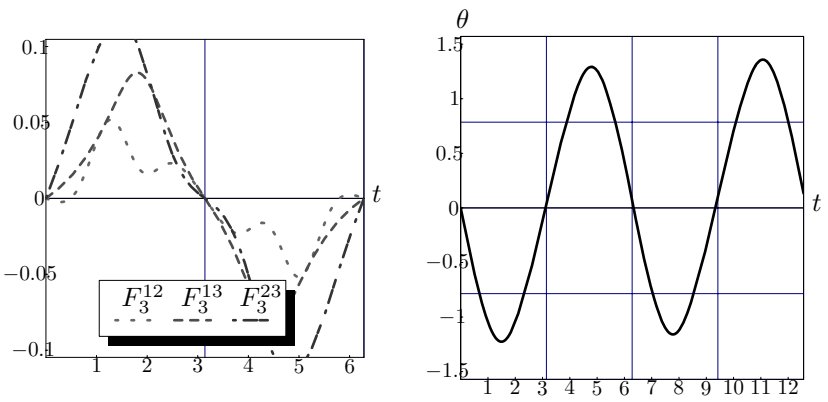

Figure 9.4: A self-intersecting gait for the four link snake robot.

to the negative regions of the three height functions for the second half cycle as shown in the first plot of Fig. 9.4. Thus, using the second rule in Section 6.2.1 we know that such a gait should yield non-zero values along all three height functions.

The intuition behind this reasoning is that each loop of the self-intersecting curve belongs to the same signed regions of all height functions. Thus, there should exist a smooth two-surface that lies entirely within those regions whose boundary is the curve itself such that the integral of the components of the two-form, that is the height functions, is non-zero. Moreover, since the two loops of the gait ϕ_2 have opposite orientation and belong to regions of opposite signs we know for fact that the integral along the entire cycle is non-zero. We actually simulated the gait ϕ_2 and indeed, as expected, it rotates the entire four link snake after each cycle as shown in the second plot of Fig. 9.4.

Thus far, we analyzed the geometric phase shift for systems with higher-dimensional base spaces. As for the dynamic phase shift, the second term in the right hand side of the reconstruction equation, our analysis which we presented in Section 6.2.2 is still valid. The only difference is the fact that the Γ functions are m-dimensional. Thus, we have to solve for the $m-1$ dimensional surfaces that separate the positive and negative regions of the Γ functions. The second part of the dynamic phase shift is the scaled momentum variable which we analyze in the next section.

9.2 Higher-dimensional Generalized Momentum

Another main assumption, Assumption 1, for this dissertation was to set, for mixed systems, the number of constraints to be at most one less than the dimension of the fiber

space, that is, $l-k=1$ where l is dimension of the fiber space and k is the number of non-holonomic constraints acting on the system. This assumption lead us to verify that the generalized momentum evolution equation is first order and it has an integrating factor. Utilizing this integration factor we were able to introduce the scaled momentum variable which simplified the expression of the dynamic phase shift and eventually allowed us to generate purely dynamic gaits.

Thus, we would like to analyze systems that have at least two generalized momentum variables, that is, $l-k>1$. For such systems, the evolution of the momentum variables will be governed by a set of first order differential equations. We would like to investigate the existence of integrating factors for such a system of differential equation and eventually define scaled momentum variables whose time evolution is of the form

$$\dot{\rho}^i = \dot{r}^T \Sigma^i(r)\dot{r}.$$

If such momentum governing equations exist, then we can use our intuitive dynamic phase shift evaluation to generate purely dynamic gaits as we explained in Section 6.2.2.

9.3 Body Versus Global Representation

At the core of our gait generation analysis is the integration of the reconstruction equation expressed in body coordinates. Thus, we are integrating a body representation, ξ, of the fiber velocity, $\dot{g}$. The two velocities are related to each other by the lifted action map, that is, $\xi = T_g L_{g^{-1}} \dot{g}$.

For commutative fiber spaces, the lifted action, $T_g L_{g^{-1}}$, is the identity map, thus only for this case, the position change in body representation, $\Delta\zeta$, and global coordinates, Δg, are identical. Recall that ζ is the integral of ξ, that is, $\Delta\zeta = \int \dot{\zeta} dt = \int \xi dt$. For non-commutative fiber spaces, $\Delta\zeta \neq \Delta g$, in general.

For example, for a system whose fiber space is $SE(2)$ designing a gait that ensures that $\Delta\zeta^1 \neq 0$ does not necessarily mean that $\Delta x \neq 0$. This is due to the non-commutativity of the special Euclidean group, $SE(2)$. In fact, for $SE(2)$ the relations between the global and body representations are given by

$$\begin{aligned}\Delta x &= \oint \left(\cos(\theta) d\zeta^1 - \sin(\theta) d\zeta^2\right), \\ \Delta y &= \oint \left(\sin(\theta) d\zeta^1 + \cos(\theta) d\zeta^2\right) \text{ , and} \\ \Delta\theta &= \Delta\zeta_3.\end{aligned}$$

Only the rotation variables θ and ζ^3 are identical. This explains why for most of the examples we presented in Chapter 7, even though the second height function was zero over the entire base space, that is, I^2_{GEO} must be identically zero, we were still able to design purely kinematic gaits, ($\Delta\zeta^2 = I^2_{GEO} = 0$) where $\Delta y \neq 0$. The gait ${}^{PK}\phi_2$ for the original snakeboard depicted in the second plot of Fig. 7.26 is an example of such a gait.

Another approach we used to overcome this discrepancy between body and global representation is by designing gaits that have at least $\Delta\zeta^1 \neq 0$ or $\Delta\zeta^2 \neq 0$. Then, by varying the starting position along these gaits, we were able to identify two starting positions where each of them yields a pure translation along either along the x or y directions. The two gaits ϕ_1 and ϕ_2 in Fig. 7.15 constitute such an approach. Note that by simply changing the initial position of the gait we were able to translate the kinematic snake along the x and y directions.

Another possible approach is to utilize different fiber space representation as was described by Tsakiris *et al.* in [56]. We would like to investigate how using different Lie groups to represent the fiber space, affect the expressions of the lifted action. Another approach we would like to investigate is by performing a local analysis of the gaits as we shall explain in the next section.

9.4 Localizing Volume Integration Analysis

Throughout this thesis, we generated gaits which ensure that the mechanical system moves along a specified direction after the proposed input gait is *completed*. Thus, we only know the robot location after the gait completed, however, we can not say anything about the set of locations that the robot traverses as it was performing the gait. For instance, for a designed gait that moves the robot along the x direction, the robot might have also moved along the y direction and counteracted this motion before the gait is completed.

Essentially, our approach is doing a "macro" Lie bracket motion. Recall that Lie bracket motions, as were described in the prior literature in [5, 13], are high frequency motions

that inefficiently locomote the mechanical system along unactuated fiber direction. Thus, one can argue that shrinking our gaits and performing them differentially, we could use our gait generation to move the robot along the specified directions. Nonetheless, there will still be infinitesimal motions along other directions.

Another approach, we would like to investigate is the local analysis of the height functions. We believe that the curvature of the height functions as the system flows along certain curves in the base space is related to how the system will move. So if we localize the height functions analysis, we could possible design gaits that minimize motions along the unspecified directions.

9.5 Optimal Magnitude Position Change

In this section we formulate a variational problem that maximizes the fiber motion magnitude for all gaits with a given length. For a detailed description of calculus of variations ideas used in this section, the reader is referred to [15].

Even though the variational problem for generating optimal gaits is well-defined in higher dimensions, we will formulate the problem in two dimensions for the sake of clarity and simplicity. Hence, the each row of $\mathbf{A}(r)dr$ is a two-dimensional one-form, that is, $(\mathbf{A}(r)dr)^i = f_1^i(r^1, r^2)dr^1 + f_2^i(r^1, r^2)dr^2$ where $r = (r^1, r^2)$ is the base variable. Then, the functional which we are maximizing is a one-form given by

$$J^i(\gamma) = \oint_\gamma f_1^i(r^1, r^2)dr^1 + f_2^i(r^1, r^2)dr^2. \tag{9.1}$$

For this problem it is convenient to parameterize the gait by its arc length, s. This yields a well-defined functional that we are trying to maximize, that is,

$$\max J^i(\gamma(s)) = \int_{s_0}^{s_1} \left(f_1^i(r^1, r^2)\frac{\partial r^1}{\partial s} + f_2^i(r^1, r^2)\frac{\partial r^2}{\partial s} \right) ds. \tag{9.2}$$

Next we enforce an essential fixed length requirement. This constraint on the length of the curves is represented by the following integral

$$L = \int_{s_0}^{s_1} \sqrt{\left(\left(\frac{\partial r^1}{\partial s} \right)^2 + \left(\frac{\partial r^2}{\partial s} \right)^2 \right)} ds \tag{9.3}$$

If such a bound is not enforced we can get unbounded volume for a gait with unbounded length. The above two integrals in (9.2) and (9.3) define a constrained calculus of variations

problem. We would like to solve this variational problem by first computing its Euler-Lagrange equations and then finding a maximizer solution which is an optimal gait.

Another flavor of this variational problem is to solve for a fixed magnitude fiber position change rather than an optimal one. This constraint will not affect the structure of the above variational problem, however, it will impose additional constraints. We would like to formulate and analyze such a problem which might be helpful in coupling the motion and path planning problems.

9.6 Purely Mechanical Systems with Non-zero Initial Momentum

One of the mechanical types of mechanical systems we analyzed in this thesis, was purely mechanical systems for which we assumed that momentum is zero for all time. This allowed us to relate the motion of this system solely to the geometric phase shift. Hence, we used the geometric gait analysis to design gaits for such systems.

Representing the reconstruction equation in body coordinates was essential for our analysis. However, this representation actually complicated the expression of the momentum evolution equations that prescribe the generalized momentum variables. To illustrate this point, we reconsider the floating three link snake robot presented in Section 7.1.1.

Since this system does not have any non-holonomic constraints acting on it and since the fiber space is three dimensional, we know that it will have three generalized momentum variables, that is, $p = \begin{pmatrix} p_1 & p_2 & p_3 \end{pmatrix}$. Computing the momentum evolution equations for this system in *body* representation we get

$$\begin{aligned}
\dot{p}_1^b &= \frac{(-5-3\cos(\alpha_1)-\cos(\alpha_1-\alpha_2))p_2\dot{\alpha}_1+(-5-3\cos(\alpha_2)-\cos(\alpha_1-\alpha_2))p_2\dot{\alpha}_2-\frac{3}{ML^2}p_1p_2}{19+6\cos(\alpha_1)+2\cos(\alpha_1-\alpha_2)+6\cos(\alpha_2)} = \tau_x^e \\
\dot{p}_2^b &= -\frac{(-5-3\cos(\alpha_1)-\cos(\alpha_1-\alpha_2))p_2\dot{\alpha}_1+(-5-3\cos(\alpha_2)-\cos(\alpha_1-\alpha_2))p_2\dot{\alpha}_2-\frac{3}{ML^2}p_1p_2}{19+6\cos(\alpha_1)+2\cos(\alpha_1-\alpha_2)+6\cos(\alpha_2)} = \tau_y^e \\
\dot{p}_3^b &= 0
\end{aligned}$$

where τ_x^e and τ_y^e are the generalized forces τ_x and τ_y, mapped to the group identity, e. Recall that $\tau_\theta = 0$ since we are dealing with an underactuated system. However, if we expressed the momentum variables in spacial coordinates, the above expressions will have the following simpler froms

$$
\begin{aligned}
\dot{p}_1^s &= \frac{\partial L}{\partial \dot{x}} = M\dot{x} = \tau_x \\
\dot{p}_2^s &= \frac{\partial L}{\partial \dot{y}} = M\dot{y} = \tau_y \\
\dot{p}_3^s &= \frac{\partial L}{\partial \dot{\theta}} = \frac{L^2 M}{3}\left((5 + 3\cos(\alpha_1) + \cos(\alpha_1 - \alpha_2))\,\dot{\alpha}_1 + (5 + \cos(\alpha_1 - \alpha_2) + 3\cos(\alpha_2))\,\dot{\alpha}_2\right) \\
&\quad + \frac{L^2 M}{3}\left(19 + 6\cos(\alpha_1) + 2\cos(\alpha_1 - \alpha_2) + 6\cos(\alpha_2)\right)\dot{\theta} = 0
\end{aligned}
$$

Thus, we propose to use the body representation to study how the three link snake robot rotates due to the body motion. Then if there were external forces acting on the system, we should use the spatial representation to compute how the position of the center of mass evolves with time. We believe that the above two motions are decoupled and the total motion of the system is a superposition of the two motions.

9.7 Time Scalability of Families of Gaits

Another interesting problem we would like to pursue, is the time scalability of the types of gaits we are proposing in this dissertation. We believe that the purely kinematic gaits are time scalable, that is, if the gaits is performed twice as fast, the magnitude of motion will be doubled in magnitude. The main reasoning behind this is due to the fact that purely kinematic gaits are related to the geometric phase shift which is in turn related to a line integral. Thus, if we do the gait twice as fast, we are effectively doing the same gait but tracing it twice. Thus, we expect the gait to yield exactly twice the volume under the height function which means that the magnitude of motion is doubled.

9.8 Path Planning Using Our Motion Planning Tools

Finally, we would like to use our gait analysis to design primitives of motion, that is, we can design families of gaits, each of which will move the robot using along a specified direction. Then by concatenating these primitives, we would like to drive the robotic system from a start to a goal configuration.

Some interesting sub-problems would be to choose which gait families to use in order to minimize a specified cost function. For example, we would like to partition our gait families by analyzing the volume swept by the robot. Thus, if we are in a tight location,

we should use gaits that correspond to the smallest swept volume possible.

Moreover, we would like to integrate obstacles into the base space, and thus are limited to designing gaits solely in the free base space. This will ensure that the robot will not hit the obstacles as it is performing a certain gait.

Chapter 10

Conclusion

The main goal of this dissertation was to present an intuitive gait generation technique that is applicable to several types of mechanical systems. We achieved this goal first by utilizing results from the mechanics of locomotion. In fact, we re-derived most of these results in what we believe to be more intuitive approaches which we later use to generate gaits. Secondly, we were able to relate position change, expressed in body coordinates, to two decoupled quantities: the geometric and dynamic phase shifts. Analyzing and intuitively evaluating both phase shifts constitute this dissertation's main contributions.

We were able to evaluate the geometric phase shift using Stokes' theorem by computing the volume integrals of two-forms on two-dimensional surfaces embedded in the base space. In the case of two-dimensional base spaces, we verified that the value of geometric phase shift along a specified fiber direction is equal to volume under the graph of a well-defined height function, the only component of the two-form, and bounded by a proposed gait, a closed base space curve. Analyzing these height functions, we prescribed rules to propose gaits for which the geometric phase shift is non-zero.

On the other hand, for computing the dynamic phase shift, we introduced a new scaled momentum variable. This new momentum variable not only simplified the expression of the dynamic phase shift where it was simply transformed into the product of another set of well-defined gamma function and the scaled momentum itself, but it also simplified the momentum evolution equation in such a way that we can intuitively analyze the sign-definiteness of this new scaled momentum variable. Then, by analyzing these gamma functions and the sign of the scaled momentum variable, we were able to propose gaits which ensure that the dynamic phase shift is non-zero along a specified fiber direction.

Both evaluation tools of the geometric and dynamic phase shifts were simple enough

that we actually utilize them to generate gaits. Moreover, the rules we devised to generate gaits are non-restrictive and allowed us to eliminate the requirement of sinusoidal inputs that was imposed in the prior work. The introduction of the height and gamma functions as well as the scaled momentum variable constitute other contributions of this dissertation.

A feature of our gait generation technique, beside its intuitiveness, is the generality of our approach. In fact, we unified the gait generation techniques for four types of mechanical systems: purely mechanical, principally kinematic, purely dynamic, and mixed systems. These types of systems span a spectrum where on one end are systems whose motion is governed solely by the laws of momentum conservation while the other end represents systems whose motion is governed solely by the existence of non-holonomic velocity constraints. This generality allowed us to generate gait for six robotic example systems that span the entire spectrum. Moreover, two of these example systems are complex enough that prior gait generation techniques were inadequate and the systems are unconventional enough that simple educated guesses of gaits was not possible.

Finally, utilizing our gait evaluation techniques we defined a partition on the space of allowable gaits. Specifically, we proposed three families of gaits: purely kinematic and purely dynamic gaits which respectively ensure that either the geometric phase shift or the dynamic phase shift is non-zero while the third type of gaits, kino-dynamic gaits, ensure that both the geometric and dynamic phase shifts are simultaneously non-zero. This partition allowed us to generate: purely kinematic gaits for both the purely mechanical and principally kinematic systems, purely dynamic gaits for purely dynamic systems, and the three typed of gaits for mixed systems.

As a conclusionary remark, we would like to highlight what we believe is the true value of this dissertation. Even though this thesis is closely related to the prior works of specifically Ostrowski *et al.* and Bullo *et al.* whose approaches to the motion planning problem are seemingly quite different, our work presents both approaches as being rather complementary components of one unifying theory. There still a long way ahead of us to develop this generalized motion planning theory for underactuated mechanical systems, however, the work presented here shows promising preliminary results geared towards not only assisting in devolving a unifying theory for the motion planning problem but also in forming a bigger picture that helps understanding this quite challenging research topic.

Bibliography

[1] R. Abraham and J. E. Marsden. *Foundation of Mechanics*. Addison Wesley, 1985.

[2] A. Baker. *Matrix Groups, An Introduction to Lie Group Theory*. Springer, 2003.

[3] R. Balasubramanian, A. Rizzi, and M. Mason. Legless Locomotion for Legged Robots. In *International Conference on Robotics and Intelligent Systems*, October 2003.

[4] R. Balasubramanian, A. Rizzi, and M. Mason. Kinematic Reduction and Planning using Symmetry for a Variable Inertia Mechanical System. In *IEEE/RSJ International Conference on Intelligent Robots and Systems*, 2004.

[5] A. Bloch. *Nonholonomic Mechanics and Control*. Springer Verlag, 2003.

[6] W. M. Boothby. *An Introduction to Differentiable Manifolds and Riemannian Geometry*. Academic Press, 2002.

[7] F. Bullo. *Nonlinear Control of Mechanical Systems: A Riemannian Geometry Approach*. Ph.D. thesis, California Institute of Technology, USA, 1998.

[8] F. Bullo and A. D. Lewis. Kinematic Controllability and Motion Planning for the Snakeboard. *IEEE Transactions on Robotics and Automation*, 19(3):494–498, 2003.

[9] F. Bullo and A. D. Lewis. *Geometric Control of Mechanical Systems*, volume 49. 2004.

[10] M. P. Do Carmo. *Riemannian Geometry*. Birkhauser Boston, 1994.

[11] S. Chitta, P. Cheng, E. Frazzoli, and V. Kumar. RoboTrikke: A Novel Undulatory Locomotion System. In *IEEE International Conference on Robotics and Automation*, 2005.

[12] H. Choset, J. Luntz, E. Shammas, T. Rached, D. Hull, and C. Dent. Design and Motion Planning for Serpentine Robots. In *Tokyo Institute of Technology Super Mechano Systems Workshop*, Tokyo, Japan, 2000.

[13] H. Choset, K.M. Lynch, S. Hutchinson, G. Kantor, W. Burgard, L.E. Kavraki, and S. Thrun. *Principles of Robot Motion: Theory, Algorithms, and Implementations*. The MIT Press, 2005.

[14] R. W.R. Darling. *Differential Forms and Connections*. Cambridge University Press, 1994.

[15] M. D. Foss and W. J. Hrusa. *Lecture Notes: Calculus of Variations*. 2004.

[16] I. M. Gelfant and S. V. Fomin. *Calculus of Variations*. Dover, 2000.

[17] H. Goldstein. *Classical Mechanics*. Addison Wesley, third edition, 2003.

[18] D. T. Greenwood. *Principles of Dynamics*. Printice Hall, 1988.

[19] B. C. Hall. *Lie Groups, Lie Algebras, and Representations*. Springer-Verlag, 2003.

[20] S. Hirose. *Biologically Inspired Robots (Snake-like Locomotor and Manipulator)*. Oxford University Press, 1993.

[21] H. Ikeda and N. Takanashi. Joint Assembly Movable Like a Human Arm. *U. S. Patent 4 683 406*, 1987.

[22] N. J. Hitchin J. E. Marsden. *Lectures on Mechanics*. Cambridge University Press, 1992.

[23] H. F. Jones. *Groups, Representations and Physics*. Institue of Physics Publishing Bristol and Philadelphia, 1998.

[24] S. Kelly. *The Mechanics and Control of Robotic Locomotion with Applications to Aquatic Vehicles*. Ph.D. thesis, California Institute of Technology, 1998.

[25] P.S. Krishnaprasad and D.P. Tsakiris. 2-module nonholonomic variable geometry truss assembly: Motion control. In *4th IFAC Symposium on Robot Control (SYROCO'94)*, Capri, Italy, September 1994.

[26] P.S. Krishnaprasad and D.P. Tsakiris. G-snakes: Nonholonomic kinematic chains on lie groups. In *33rd IEEE Conference on Decision and Control*, Lake Buena Vista, Florida, December 1994.

[27] P.S. Krishnaprasad and D.P. Tsakiris. Oscillations, se(2)-snakes and motion control. In *34rd IEEE Conference on Decision and Control*, New Orleans, Louisiana, December 1995.

[28] P.S. Krishnaprasad and D.P. Tsakiris. Oscillations, se(2)-snakes and motion control: A study of the roller racer. *Dynamical Systems*, 16(4):347–397, December 2001.

[29] V. Kumar and K. J. Waldron. *Robotics Review 1, A Review of Research on Walking Vehicles*, pages 243–266. MIT Press, Cambridge, Massachusetts, 1989.

[30] A. D. Lewis. Simple Mechanical Control Systems with Constraints. *IEEE Transactions on Automatic Control*, 45(8):1420–1436, 2000.

[31] G. Lugo. Differential Geometry in Physics. Technical report, University of North Carolina, 1998.

[32] J. E. Marsden and T. S. Ratiu. *Introduction to Mechanics and Symmetry*. Springer-Verlag, 1994.

[33] J.E. Marsden, R. Montgomery, and T.S. Ratiu. Reduction, Symmetry and Phases in Mechanics. *Memoirs of the American Mathematical Society*, 436, 1990.

[34] R. Mukherjee and D.P. Anderson. Nonholonomic Motion Planning Using Stokes' Theorem. In *IEEE International Conference on Robotics and Automation*, 1993.

[35] R. M. Murray and S. S. Sastry. Nonholonomic Motion Planning: Steering Using Sinusoids. *IEEE T. Automatic Control*, 38(5):700 – 716, May 1993.

[36] R.M. Murray, Z. Li, , and S.S. Sastry. *A Mathematical Introduction to Robotic Manipulation*. CRC Press, 1994.

[37] E. Muybridge. *Animals in Motion*. Dover Publications, 1957.

[38] Y. Nakamura and R. Mukherjee. Nonholonomic Path Planning of Space Robots. In *IEEE International Conference on Robotics and Automation*, 1989.

[39] Y. Nakamura and R. Mukherjee. Nonholonomic Path Planning of Space Robots via a Bidirectional Approach. In *IEEE Transactions on Robotics and Autmation*, volume 7, pages 500–514, 1991.

[40] J. Ostrowski. *The Mechanics of Control of Undulatory Robotic Locomotion*. Ph.D. thesis, California Institute of Technology, 1995.

[41] J. Ostrowski and J. Burdick. The Mechanics and Control of Undulatory Locomotion. *International Journal of Robotics Research*, 17(7):683 – 701, July 1998.

[42] J. Ostrowski, J. Desai, and V. Kumar. Optimal Gait Selection for Nonholonomic Locomotion Systems. *International Journal of Robotics Research*, 2000.

[43] J.P. Ostrowski. Reduced equations for nonholonomic mechanical systems with dissipation. *Journal of Mathematical Physics*, 1998.

[44] M. Raibert. *Legged Robots That Balance (Artificial Intelligence)*. The MIT Press, 1986.

[45] V. Kumar S. Chitta, F. Heger. Dynamics and Gait Control of a Rollerblading Robot. In *IEEE International Conference on Robotics and Automation*, 2004.

[46] E. Shammas, H. Choset, and A. Rizzi. Natural Gait Generation Techniques for Principally Kinematic Mechanical Systems. In *Proceedings of Robotics: Science and Systems*, Cambridge, USA, June 2005.

[47] E. Shammas, K. Schmidt, and H. Choset. Natural Gait Generation Techniques for Multi-bodied Isolated Mechanical Systems. In *IEEE International Conference on Robotics and Automation*, 2005.

[48] E. Shammas, A. Wolf, H.B. Brown, and H. Choset. New Joint Design for Three-dimensional Hyper Redundant Robots. In *IEEE/RSJ International Conference on Intelligent Robots and Systems*, volume 4, pages 3594 – 3599, Las Vegas, October 2003.

[49] E. Shammas, A. Wolf, and H. Choset. Three degrees-of-freedom joint for spatial hyper-redundant robots. *Mechanism and Machine Theory*, 41(2):170–190, February 2006.

[50] Elie Shammas and Howie Choset. Orientation preserving angular swivel joint. *United States Patent Application: 20020166403 (Filing Date: February 26, 2002)*, (US 083705), 2002.

[51] S. Smale. Topology and mechanics i. *Inventiones Mathematicae*, 10:305–331, 1970.

[52] S. Smale. Topology and mechanics ii. *Inventiones Mathematicae*, 11:45–64, 1970.

[53] S.M. Song. and K.J. Waldron. *Machines that walk: the Adaptive Suspension Vehicle*. The MIT Press, 1989.

[54] M. Tenenbaum and H. Pollard. *Ordinary Differential Equations*. Courier Dover Publications, 1985.

[55] J. A. Thorpe. *Elementary Topics in Differential Geometry*. Springer-Verlag, 2000.

[56] D.P. Tsakiris. *Motion Control and Planning for Nonholonomic Kinematic Chains*. Ph.D. thesis, Department of Electrical Engineering, University of Maryland, College Park, 1995.

[57] G. Walsh and S. Sastry. On reorienting linked rigid bodies using internal motions. *Robotics and Automation, IEEE Transactions on*, 11(1):139–146, January 1995.

[58] K. Yamada. Arm Path Planning for a Space Robot. In *IEEE/RSJ International Conference on Intelligent Robots and Systems*, 1993.